UNIVERSIDADE
LUSÓFONA

Performance Analysis of Optical Wireless Communication System

Mohammad Furqan Ali

Thesis to obtain the Degree of Doctor of Philosophy in

Informatics

Adviser: Prof. Dr. Jayakody Arachchilage Dushantha Nalin Kumara
Professor, Universidade Lusófona, Lisboa, Portugal

November, 2024

Performance Analysis of Optical Wireless Communication System

Mohammad Furqan Ali

Thesis to obtain the Degree of Doctor of Philosophy in

Informatics

Adviser: Prof. Dr. Jayakody Arachchilage Dushantha Nalin Kumara

Professor, Universidade Lusófona, Lisboa, Portugal

November, 2024

Performance Analysis of Optical Wireless Communication System

Acknowledgements

I would like to express my deepest gratitude to my doctoral adviser, Professor Dushantha Nalin Jayakody, for his invaluable guidance, constructive feedback, and supportive approach extended to me during the doctoral journey. I am also grateful to all professors and teachers: Prof. Marko Beko, Prof. Slavisa Tomic, Prof. Joel J. P. C. Rodrigues, and associate Professor Jaco Versfeld for their support and guidance in my research work, which also led to several publications.

I wish to acknowledge my colleagues at the Lusofona University, Stellenbosh University, South Africa, and the Universiti Sains Malaysia (USM), Malaysia - Chathuranga Madhushan Basnayaka, Urvahsi Rani, and Sajid Mumtaz Hassaan - who have made my time at these institutions memorable through their academic and personal support. I am deeply indebted to Universidade Lusófona - Centro Universitário de Lisboa (COPELABS) and University Autónoma de Lisboa (Autónoma TECHLAB) for hosting and supporting my research.

My work has been made possible through the financial support of several institutional projects from the Fundação para a Ciência e Tecnologia for their support through the AIEE-UAV project (No. 2022.03897.PTDC) and PortuLight (COFAC/ILIND/COPELABS/2/2023). I also extend my thanks to COFAC - Cooperativa de Formação e Animação Cultural, C.R.L. (University of Lusófona), for their backing via the European Research Executive Agency (REA) REMARKABLE (No. 101086387) project.

Last but not least, I want to express my heartfelt gratitude to my family. To my parents, grandparents, and siblings: Your unwavering love, support, and faith in me have been the cornerstone of my academic journey and success. Your sacrifices and unconditional love have not gone unnoticed, and I am profoundly grateful for everything you have done to support me throughout this endeavor.

Abstract

Optical Wireless Communication (OWC) has recently drawn significant interest for real-time data transfer in various terrestrial and underwater applications due to their extensive bandwidth, high data rates, low latency, and efficiency in terms of security, Energy Harvesting (EH), and cost efficiency. Despite these advantages, the optical communication is substantially impaired by absorption, scattering, and strong turbulence effects in various channels, which lead the optical scintillation and disrupt communication between connecting nodes.

In this thesis, the development of optical signaling focuses on novel mathematical expressions for new software tools that aimed to enhance spectral efficiency and communication reliability. It investigates the performance metrics of the proposed system models designed to improve data rate and throughput while accounting for moderate-to-strong optical turbulence between transceivers under diverse channel conditions. The OWC systems leverage advanced optical technologies for real-time monitoring and seamless communication towards advanced wireless networks. These systems support Ultra-Reliable Low Latency Communications (URLLC), increased network capacity, and high data rates. Therefore, optical communication in the visible light spectrum has opened new doors to explore unguided mediums such as devastating natural wildfire disasters and deep oceans through the Internet of Underwater Things (IoUTs).

Additionally, this thesis aims to evaluate various optical transmission arrangements to mitigate strong turbulence and misalignment phenomena amongst communication nodes. An optical-enabled Autonomous Underwater Vehicle (AUV) communication model is designed in mixed ocean water within varying vertical layers in real-time scenarios. Also, a proposed design introduces a generic hybrid Free Space Optics (FSO) and Visible Light Communication (VLC) system for underwater communication, extending the capabilities of optical-enabled wireless communication. This system is engineered to facilitate reliable communication over long-ranges in aqueous mediums. In addition to that a setup of Unmanned Aerial Vehicle (UAV)-assisted Wireless Sensor Network (WSN)s for wildfire communication towards 5G and Beyond (5GB) networks is investigated based on the real-time experimental data. It is noteworthy that the unified Gamma-Gamma Distribution (GG) distribution offers a promising solution to design optical turbulence and is evaluated to meet the current communication requirements in hostile channels. This thesis assesses the performance effects of optical impairments characterized by multiple transceivers in wildfire communication, IoUTs, and communication within varying vertical water layers by following the Monte Carlo (MC) simulation framework. The findings are anticipated to deepen understanding of optical communication within various wireless systems, including UAV and AUV-assisted WSNs. This

thesis aims to bridge the gap between the current optical-enabled Internet of Things (IoT) approaches and the existing communication infrastructures along with the future work can be laid to improve the hybrid optical communication in optimizing network connectivity, localization, optical EH, Re-Configurable Intelligent Surfaces (RIS) assisted UAV and AUV communication.

Keywords: Autonomous Underwater Vehicle (AUV), Internet of Underwater Things (IoUTs), Unmanned Aerial Vehicle (UAV), Underwater Wireless Optical Communications (UWOC), Wildfire Optical Networks.

Resumo

A comunicação ótica sem fios (OWC) atraiu recentemente um interesse significativo para a transferência de dados em tempo real em várias aplicações terrestres e subaquáticas, devido à sua grande largura de banda, elevados débitos de dados, baixa latência e eficiência em termos de segurança, recolha de energia (EH) e eficiência de custos. Apesar destas vantagens, a comunicação ótica é substancialmente prejudicada pela absorção, dispersão e fortes efeitos de turbulência em vários canais, que conduzem à cintilação ótica e perturbam a comunicação entre os nós de ligação.

Nesta tese, o desenvolvimento da sinalização ótica centra-se em novas expressões matemáticas para novas ferramentas de software que visam melhorar a eficiência espetral e a fiabilidade da comunicação. Investiga as métricas de desempenho dos modelos de sistema propostos, concebidos para melhorar a taxa de dados e o débito, tendo em conta a turbulência ótica moderada a forte entre transceptores em diversas condições de canal. Os sistemas OWC tiram partido de tecnologias ópticas avançadas para monitorização em tempo real e comunicação sem descontinuidades com redes sem fios avançadas. Estes sistemas suportam comunicações ultra fiáveis e de baixa latência (URLLC), maior capacidade de rede e elevados débitos de dados. Por conseguinte, a comunicação ótica no espetro de luz visível abriu novas portas para explorar meios não guiados, como catástrofes naturais devastadoras causadas por incêndios florestais e oceanos profundos, através da Internet das Coisas Subaquáticas (IoUTs).

Além disso, esta tese pretende avaliar várias disposições de transmissão ótica para mitigar a forte turbulência e os fenómenos de desalinhamento entre os nós de comunicação. Foi concebido um modelo de comunicação ótica para AUVs em águas oceânicas mistas em diferentes camadas verticais em cenários de tempo real. Além disso, uma proposta de conceção introduz um sistema híbrido genérico de ótica de espaço livre (Free Space Optics (FSO)) e de comunicação por luz visível (Visible Light Communication (VLC)) para comunicação subaquática, alargando as capacidades da comunicação sem fios com suporte ótico. Este sistema foi concebido para facilitar a comunicação fiável a longa distância em meios aquosos. Além disso, com base nos dados experimentais em tempo real, é investigada uma configuração de WSNs assistida por UAV para a comunicação de incêndios florestais com redes de 5GB. É de salientar que a distribuição unificada Gama-Gama (GG) oferece uma solução promissora para a conceção de turbulência ótica e é avaliada para satisfazer os actuais requisitos de comunicação em canais hostis. Esta tese avalia os efeitos de desempenho das deficiências ópticas caracterizadas por múltiplos transceptores na comunicação de incêndios florestais, IoUTs e comunicação em diferentes camadas verticais de água, seguindo a estrutura de simulação de Monte Carlo. Espera-se que os resultados aprofundem a compreensão da comunicação

ótica em vários sistemas sem fios, incluindo as WSNs assistidas por UAV e AUV. Esta tese tem como objetivo colmatar a lacuna entre as actuais abordagens IoT ópticas e as infra-estruturas de comunicação existentes, juntamente com o trabalho futuro que pode ser estabelecido para melhorar a comunicação ótica híbrida na otimização da conetividade da rede, localização, recolha de energia ótica e comunicação UAV e AUV assistida por superfície inteligente reconfigurável (RIS).

Palavras-chave: Veículo subaquático autónomo (AUV), Internet das coisas subaquáticas (IoUTs), Comunicações ópticas subaquáticas sem fios (UWOC), Veículo aéreo não tripulado (UAV), Rede ótica Incêndio florestal

Contents

List of Figures

List of Tables

Acronyms

5GB 5G and Beyond *(pp. v, vii, 1, 56, 57)*

AoP Apparent Optical Properties *(pp. 14, 18)*
AOUWSNs Acoustic-Optical Underwater Wireless Networks *(p. 73)*
AUV Autonomous Underwater Vehicle *(pp. v, vi, viii, xiii, 1, 2, 4–6, 9, 10, 14, 19, 22, 45, 46, 48, 52, 54, 70, 73)*
AWGN Additive White Gaussian Noise *(pp. 23, 35, 57, 58)*

BER Bit-Error-Rate *(pp. xiii–xv, xvii, 18, 23, 24, 26–29, 31, 33, 38–42, 46, 47, 50–54, 56, 60–65, 69, 70)*
BS Base Stations *(pp. xv, 2, 15, 22, 23, 45, 56, 57, 61, 63–65)*

CBFSK Coherent Binary Frequency Shift Keying *(pp. 39, 42)*
CBPSK Coherent Binary Shift Keying *(pp. 39, 42)*
CDF Cumulative Distribution Function *(pp. 25, 34, 36, 37, 47–49, 60, 67, 85)*
CH Cluster Head *(p. 71)*
CSI Channel State Information *(pp. xiii, 19, 23)*

DBPSK Differential Binary Phase Shift Keying *(p. 39)*
DF Decode-and-Forward *(pp. 33, 34, 44, 46, 48, 50, 54, 70)*

E2E End-to-End *(pp. 5, 17–19, 22, 26, 28, 31, 33, 34, 36, 37, 46, 47, 54, 56, 69, 70)*
EBGMGF Extended Bivariate Generalized Meijer-G Function *(pp. 5, 33, 34, 37, 47, 49, 54, 70, 85, 86)*
EH Energy Harvesting *(pp. v–vii, 72, 73)*

FOV Field of View *(p. 17)*
FSO Free Space Optics *(pp. vii, xv, 3, 4, 6, 14, 45–48, 50–54, 57, 62, 70)*

GG Gamma-Gamma Distribution *(pp. v, vii, xv, 1–3, 5, 6, 11, 12, 17, 19, 20, 25, 31, 33, 34, 36, 47, 54, 56, 58, 59, 67, 69, 70)*

IM/DD Intensity-Modulation/Direct-Detection *(pp. 3, 23, 25, 33, 37, 38, 56–58, 61, 67)*
IoP Inherent Optical Properties *(pp. 14, 18)*
IoT Internet of Things *(pp. vi, 1)*
IoUTs Internet of Underwater Things *(pp. v, vii, 5, 71, 72)*

LED Light Emitting Diode *(pp. xiii, xiv, 18, 19, 22, 24, 26, 28, 29, 31, 69)*
LEDs Light Emitting Diodes *(p. 5)*
LOS Line-of-Sight *(pp. 11, 15, 19, 35, 43)*

MC Monte Carlo *(pp. v, xv, 17, 18, 21, 22, 31, 33, 44, 52, 69, 70, 72)*
MIMO Multi-Input-Multi-Output *(pp. xv, 3, 4, 6, 55–57, 59–65, 67, 71)*
MISO Multi-Input-Single-Output *(pp. xv, 3, 6, 56, 61–65)*

NBFSK Non-Coherent Binary Frequency Shift Keying *(pp. 39, 42)*
NOMA Non-Orthogonal Multiple Access *(p. 71)*

OAM Optical Orbital Angular Momentum *(p. 72)*
OOK On-Off-Keying *(pp. 5, 23, 25, 31, 35, 56–58, 61, 67)*
OWC Optical Wireless Communication *(pp. v, vii, 1, 4–6, 9–15)*

P2P Point-to-Point *(pp. xiii, 10, 38)*
PAM Pulse Amplitude Modulation *(p. 50)*
PDF Probability Density Function *(pp. 12, 13, 20, 21, 25, 34–37, 47, 59–61, 67)*
PE Pointing Error *(p. 12)*
PSU Per Salinity Unit *(pp. xiv, 25, 26, 41, 42, 53)*

QoE Quality of Engineering *(pp. 4, 72)*
QoS Quality of Services *(pp. 1, 4, 34, 72, 73)*

RF Radio-Frequencies *(pp. 2, 9, 14, 15, 63)*
RIS Re-Configurable Intelligent Surfaces *(pp. vi, viii, 73)*
RSOA Reflective Semiconductor Optical Amplifier *(pp. 71, 72)*
RSS Received Signal Strength *(p. 73)*

SIM Sub-Carrier Intensity Modulation *(pp. 46, 54, 70)*
SIMO Single-Input-Multi-Output *(pp. xiii–xv, xvii, 3, 5, 6, 17–19, 22–31, 56, 61–65, 69, 71, 72)*
SIO Southern Indian Ocean *(pp. xiii, xiv, 5, 18, 25–31, 43, 69)*
SISO Single-Input-Single-Output *(pp. xv, 3, 6, 56, 61, 63–65)*
SLIPT Simultaneously Light-Wave Information and Power Transfer *(p. 72)*

SNR Signal-to-Noise Ratio *(pp. xv, 5, 12, 13, 17, 22–25, 27, 28, 34–37, 41, 47–49, 52, 53, 60, 61, 63, 64, 66)*

UAV Unmanned Aerial Vehicle *(pp. v–viii, xv, 1, 2, 4–6, 9, 10, 14, 15, 55–58, 60–67, 69, 71, 73)*

UEM Underwater Electromagnetic Waves *(pp. 2, 14)*

UOT Underwater Optical Turbulence *(pp. 3, 6, 17, 21, 34, 45, 54, 70, 83)*

UOWSNs Underwater Optical Wireless Sensor Networks *(pp. 46, 73)*

URLLC Ultra-Reliable Low Latency Communications *(pp. v, vii, 4, 6, 69)*

UVLC Underwater Visible Light Communication *(pp. xiii–xv, xvii, 5, 17–20, 22–31, 33–35, 43, 44, 50, 52–54, 69–72)*

UWC Underwater Wireless Communication *(p. 14)*

UWOC Underwater Wireless Optical Communication *(pp. 1, 4, 6, 14, 17, 19, 31, 71, 72)*

UWSN Underwater Wireless Sensor Network *(pp. 10, 14, 45, 71, 72)*

VLC Visible Light Communication *(pp. vii, xiii–xv, 3–6, 14, 17, 19–21, 36, 45–48, 50–53)*

WPE Without Pointing Error *(pp. xiii, xiv, 26–30)*

WSN Wireless Sensor Network *(pp. v, viii, 71)*

Symbols

ν_{mn}	Additive white Gaussian Noise *(p. 57)*
$a(\lambda)$	Absorption coefficient *(p. 11)*
h	Altitude of an individual UAV *(pp. 60, 64, 65)*
I_b	The ambient light intensity *(p. 23)*
ϕ	The angle between receiver plane and the transmitter *(p. 20)*
A	The aperture diameter *(pp. 35, 52)*
A_r	Receiver aperture area *(pp. 12, 52)*
ϕ_1	The arguement in G-meijer function *(p. 48)*
ϕ_2	The arguement in G-meijer function *(p. 48)*
a_p, b_q	The arguments of G-Meijer function *(p. 13)*
$I_l^{Terr}(\lambda, d)$	Terrestrial atmospheric attenuation *(pp. 11, 13)*
$I_l^{Water}(\lambda, L)$	Underwater attenuation *(p. 11)*
μ	The average signal to noise ratio *(pp. 13, 24)*
P_{avg}	The optical transmitted average power constraint between mn links *(pp. 57, 58)*
n_i	AWGN noise with zero mean *(p. 35)*
σ_{nm}^2	The AWGN noise variance *(p. 57)*
d	The optical beam factor *(p. 59)*
w_{zeq}^k	The optical beam-width *(p. 20)*
P_{error}	The conditional error rate *(p. 88)*
$P(1)_{e\|0}$	The conditional error rate while transmitting bit 1 *(p. 88)*
$P(0)_{e\|0}$	The conditional error rate while transmitting bit 0 *(p. 88)*
$K_{(\alpha-\beta)}$	The second kind of Bessel function *(p. 12)*
$b(\lambda)$	Scattering coefficient *(p. 11)*
D_r	Radial displacement of beam centroid *(pp. 12, 59)*
h_{rd}	Channel condition for r-d link *(p. 52)*
h_{sr}	Channel condition for s-r link *(p. 52)*
χ_T	The rate of dissipation of mean- square temperature *(pp. xiii, 26–28, 34, 41, 87)*
$c(\lambda)$	Extinction coefficient *(pp. 11, 19, 26)*
$c_{Terr}(\lambda)$	Extinction coefficient on varying terrestrial conditions *(p. 11)*

$c_{Water}(\lambda)$	Extinction coefficient of varying water types *(p. 11)*
z_{rd}	Coefficient for r-d hop *(p. 49)*
z_{sr}	Coefficient for s-r hop *(p. 49)*
I_K	The combined light intensity *(pp. 23, 24)*
a_k	The the resultant of the horizontal and vertical component of transceivers *(p. 20)*
r_x, r_y, r_z	The coordinate vector of each water layer *(p. 21)*
$z(t)$	The channel state information *(p. 23)*
δ	Size distribution coefficient of scattering) *(pp. 11, 52, 58)*
dt_K	The Verticle depth of underwater communication node *(pp. 19, 20)*
d	The receiver (destination) *(pp. 35, 39, 41)*
ψ	The detection technique *(pp. 36, 47)*
r_{mn}	The responsivity of photo-detectors *(p. 57)*
D_S	The molecular diffusivity of salinity *(p. 83)*
D_T	The molecular diffusivity of temperature *(p. 83)*
d_0	Distance between transceivers *(pp. 11, 12)*
PSU	Per salinity unit *(pp. 26–28, 63–65)*
d_t	Underwater depth for communication node *(pp. 26, 27, 41, 52)*
L	The communication link visiblity between mn links *(pp. 58, 59)*
ϕ	The beam divergence angle *(pp. 35, 52)*
η	The optical to electrical conversion efficiency *(pp. 23, 52, 57, 60)*
A_0	The optical energy collection at the receiver end *(pp. 12, 20)*
ϵ	Varying dissipation rate of turbulent kinetic energy per unit mass of fluid *(pp. xiii, 26–28, 41)*
γ	The instantaneous SNR *(pp. xv, 13, 22, 41, 64, 66)*
$\Gamma(\cdot)$	Gamma function *(p. 47)*
ω_0	The Gaussian beam wave *(p. 20)*
$D^2_{r_x}$	Horizontal component of random radial displacement *(p. 12)*
$a^2_{x_k}$	The horizontal component of deflection communication node *(p. 20)*
D	The The horizontal distance between communication nodes *(p. 41)*
m, n, p, q	The index of G-Meijer function *(p. 13)*
Υ	The instantaneous signal to noise ratio *(pp. 35–37)*
γ	The Instantaneous SNR at the transmitter end *(pp. 48, 49)*
I_k	The instantaneous light intensity *(p. 23)*
I^l_{mn}	The atmospheric optical pathloss irradiance *(p. 57)*
I	The optical irradiance for links *(pp. 25, 37)*

I_{mn}	The optical irradiance between mn links *(p. 57)*
I^{t}_{mn}	The atmospheric optical turbulence irradiance *(p. 57)*
I_{rd}	Optical irradiance for r-d link *(p. 50)*
I_{sr}	Optical irradiance for s-r link *(p. 50)*
λ	Wavelenght *(pp. 11, 20, 26, 52, 58, 59)*
α_k	The large scale factor in MIMO UVLC communication *(pp. 56, 59)*
α	The large scale parameter *(pp. 13, 18, 21, 22, 26–28, 34, 36, 63)*
k^{th}	The number of successive layers between mn links *(pp. 19–23, 31, 59)*
M	The number of LED array *(pp. 22, 24, 26, 28, 69)*
A	Level of refraction index *(p. 60)*
P_{enc}	The optical energy power level between mn links *(p. 57)*
I_{l^k}	The path loss coefficient in underwater environment *(p. 19)*
χ_T	The dissipation rate of mean-squared salinity *(p. 83)*
χ_T	The dissipation rate of mean-squared temperature *(pp. 83, 84)*
χ_{TS}	The correlation coefficient of mean-temperature and salinity *(p. 83)*
σ_i^2	The noise variance with zero mean *(p. 35)*
d_{min}	The maximum distance between nodes *(p. 35)*
P_{max}	The optical high energy constraint between mn links *(pp. 57, 58)*
P_1	The optical signal power assigned for 0 bit transmission *(p. 58)*
γ_{sc}	The signal to noise ratio *(pp. 23, 60)*
$n(t)$	The AWGN noise variance *(p. 23)*
v	The fixed parameters as kinematic viscosity *(pp. 26, 41)*
m	The number of base stations *(pp. xv, 56–59, 61, 63, 64)*
n	The number of UAVs *(pp. xv, 36, 39, 56–59, 61, 63, 64)*
$\omega_{d_{eq}}$	Equivalent optical beam width *(pp. 12, 41)*
ω_0	The ratio of temperature to salinity contributions to the refractive index *(pp. 26, 28)*
ω	The the relative strength of temperature and salinity *(pp. 34, 41)*
P_{out}	The outage probability *(p. 56)*
p	The modulation signal factor *(pp. 39, 42)*
q	The modulation signal factor *(pp. 39, 42)*
k	The path of the communication link *(p. 59)*
I_{p^k}	The pointing error between the underwater communication nodes *(p. 20)*
I_p	The pointing error attenuation coefficient *(p. 13)*
P_2	The optical signal power assigned for 1 bit transmission *(p. 58)*
P_E	The optical signal power level between mn links *(p. 57)*

P	Temperature of the channel *(p. 63)*
$P_{\alpha_{mn}\beta_{mn}}$	product of alpha and beta particle *(p. 47)*
ν_w	The ratio between aperture radius and beam-width *(p. 20)*
$\sigma^2_{I_{t_k}}$	The scintillation index *(p. 59)*
$\chi_{I_t^k}$	The underwater scintillation index *(p. 21)*
$y_k(t)$	The received signal *(p. 23)*
x	Recieved information symbol at the receiver *(pp. 35, 57)*
${C_n}^2(h)$	The refraction index *(pp. 52, 59, 60, 63)*
r_1	The regenerative relay-1 *(pp. 35, 39)*
r_2	The regenerative relay-2 *(pp. 35, 39)*
R	The photo-detector responsivity at the receiver end *(pp. 23, 52)*
PSU	Per salinity unit *(p. 25)*
S	The water salinity *(p. 41)*
P_c	The selecting optical signal power level between mn links *(p. 57)*
σ	The standard deviation *(pp. 12, 58)*
β_k	The small scale factor in MIMO UVLC communication *(pp. 56, 59)*
β	The large scale parameter *(pp. 13, 18, 21, 22, 26–28, 34, 36, 63)*
s	The optical transmitter *(pp. 35, 39)*
$x(t)$	The transmitted sysmbol through optical beam *(p. 23)*
τ	The correction coefficient *(p. 35)*
T	Temperature of the channel *(pp. 41, 63, 65)*
P_{min}	The optical thershold energy constraint between mn links *(pp. 57, 58)*
$\theta_{1/2}$	The half-beam width divergence angle *(p. 35)*
I_t	The turbulence attenuation coefficient *(p. 13)*
I_{t^k}	The underwater turbulence attenuation factor *(p. 21)*
σ^2_k	The AWGN variance with zero mean *(p. 23)*
$D^2_{r_x}$	Vertical component of random radial displacement *(p. 12)*
$a^2_{y_k}$	The vertical component of deflection communication node *(p. 20)*
z	The varying distance *(p. 20)*
ν	The kinematic viscosity *(p. 83)*
V_{nm}	The communication link visiblity between mn links *(p. 58)*
V	Atmospheric visiblity (Fog, dust, wind) *(p. 11)*
ϕ	The optical wave number *(p. 59)*
ρ_k	The weight factor *(p. 23)*
ν	The wind speed *(p. 60)*

ξ	The ratio between the equivalent beam radius at the receiver and the PE displacement standard deviation *(pp. 12, 26–28, 30, 41, 53, 54)*
ω_0	The Pointing error factor *(p. 28)*

Chapter 1

Introduction

1.1 Scope and Motivation

The continuous demand for high-speed data rate and large bandwidth in wireless communications is indeed driving significant advancements in technology [1]. This evolution of wireless communication is essential for accommodating the increasing number of Internet-connected devices IoT, enhancing mobile communications with technologies like 5GB, and supporting applications that require real-time data transfer, such as UAV wildfire communication, smart cities, AUV for underwater communication, and advanced hybrid communication transportation system in aqueous mediums [2, 3]. These innovative approaches facilitate data collection and communication from unguided mediums within the framework of large-scale mobile networks [4].

Optical communication has become a potential wireless candidate for robust communication rather than RF signaling in the context of high security, bandwidth, lower attenuation, and reduced interference [5–7]. With high signal quality and very cost-effective demand of optical communication, it is used for numerous indoor/outdoor applications [8]. However, there are several challenges while maintaining the Quality of Services (QoS) in inaccessible environments. Therefore, the necessity to design optical links for better connectivity and diminishing the fading factors through the best fit of the GG distribution function [9]. In this regard, the UAV wildfire communication system and AUV-enabled Underwater Wireless Optical Communication (UWOC) systems are developed based on the experimental data on terrestrial basis conditions as well in the mixed ocean waters [10, 11].

This comprehensive research explores the application of advanced optical and wireless communication technologies across multiple critical domains, including wildfire monitoring and long range of underwater communication. The research delves into innovative systems such as the OWC system and UWOC. By leveraging cutting-edge modulation schemes, performance metrics, and real-time data transmission, this thesis aims to enhance optical communication efficiency, accuracy, and reliability in both terrestrial and underwater environments. Additionally, it investigates the transformative impact of advanced wireless communication emphasizing real-time data transmission, and the development of smart transportation systems.

The motivation behind of this research stems from the critical need to improve quality of

communication systems in various challenging environments also supports the human interests in underwater environment exploration, such as military roaming areas for coastal securities, loading & unloading of goods at seaports, and to build up a connection between undersea nodes to the offshore/onshore BS. As wildfires pose a severe threat to ecosystems and human lives, necessitating advanced monitoring and communication solutions to detect and manage them effectively. Similarly, the growing interest in underwater applications requires robust communication media that capable of overcoming the challenges posed by optical turbulence and path loss in diverse water conditions. By addressing these challenges and exploring the potential of next-generation communication technologies, this study aims to contribute to the advancement of safety, sustainability, and efficiency in these vital areas.

1.2 Problem Statement

In underwater environment the acoustic waves offer limited bandwidth, high latency, and low propagation speed as 1500m/s [12, 13]. The traditional Underwater Electromagnetic Waves (UEM) propagate hardly in water only 8 to 10m [14, 15]. The water offers dielectric properties for UEM which causes high attenuation. The UEM waves in terms of Radio-Frequencies (RF) attenuate easily and require a large size of antenna [16]. These shortcomings in terrestrial and oceanic communication for real-time data streaming, a high speed, large bandwidth, and very cost-effective signaling approach is required such as optical communication.

On the other hand, the wildfires have become increasingly frequent events due to global warming and environmental changes, posing significant threats to ecosystems and endangering numerous wildlife species. These events often result from high-temperature heat waves that ignite forest areas, causing extensive damage to natural resources, the environment, and our ecosystem. To mitigate these threats and protect wildlife, developing an effective wildfire communication detection system is essential. Traditional monitoring and planetary imaging systems are limited by their passive nature and inability to provide real-time data monitoring [6, 17].

Therefore, enhancing the accuracy and efficiency of optical communication systems can be achieved through the integration of a UAV and AUV optical communication approach, which offers a promising solution for virtual real-time observation, monitoring, and data encryption/decryption of data collection.

1.3 Research Questions and Hypotheses

This thesis aims to address the following research-related questions and corresponding by the hypotheses as follows;

1. **Research Problem:** *What are the specific reasons for adopting the GG distribution fading model in optical wireless communication, and how does the GG distribution designed system models accurately represent the propagation effects observed in diversive environments?*

Hypothesis: The GG model factorizes the irradiance as a product of two random processes in strong turbulence channel conditions and is widely employed to model FSO and VLC links. Furthermore, the GG distribution is more fit for underwater VLC, also commonly used to characterize moderate-to-strong turbulence channel conditions. Additionally, the GG has less complexity and outperforms other traditional fading models. It is the reason that in this dissertation the GG distribution model has adopted.

2. **Research Problem:** *How does the Underwater Optical Turbulence (UOT) spectrum model has been used for under consideration plane wave model?*

   Hypothesis: The UOT spectrum model analyzes the light behaves in turbulent aqueous mediums and affecting plane wave signal propagation. It quantifies the refractive index fluctuations due to physio-chemical properties of water such as temperature, salinity, and pressure variations. This UOT model helps to predict the light diffusion, focusing, and intensity fluctuation, optimizing underwater optical systems for imaging and communication, ultimately enhancing performance and reliability in various underwater applications.

3. **Research Problem:** *How does MIMO, MISO, SIMO, and SISO, contribute to poliferate the diversity of optical communication?*

   Hypothesis: The diversity of optical communication within MIMO, MISO, SIMO, and SISO systems play a crucial role in enhancing the reliability of communication, particularly under challenging environmental conditions, such as strong turbulence in the channel. In the context of strong environmental turbulence, these diverse configurations especially MIMO enable the system to monitor and counteract unwanted events. The implementation of a diversive MIMO-enabled optical communication setup can be an advantageous approach for improving system reliability and maintaining communication quality even under harsh environmental conditions.

4. **Research Problem:** *Why is Intensity-Modulation/Direct-Detection (IM/DD) chosen for this system?*

   Hypothesis: IM/DD has chosen for this system because it enhances signal transmission reliability and improves the quality of real-time data streaming in challenging environments like wildfire detection. By utilizing the GG distribution under IM/DD, the system reduces noise and turbulence, leading to more precise signal detection. This approach not only captures high-resolution data but also improves the identification of fire events. The combination of IM/DD with the statistical model strengthens the system's capability for early detection and warning, making it an effective tool for timely wildfire intervention.

   By addressing these research questions and testing the proposed hypotheses, this thesis aims to advance the field of optical wireless communication and its integration into next-generation wireless networks, with the ultimate goal of enhancing the reliability and efficiency of time-sensitive communication systems.

1.4 Outline and Contributions

This thesis addresses critical research gaps in understanding of OWC systems. It consists of an introductory chapter and four technical chapters, each chapter focuses on a specific aspect of OWC towards the next generation of wireless networks. The following chapters are associated with the development of optical wireless information transmission and provide a comprehensive analysis and the utilization of optics in various wireless communication aspects. For a quick response in real-time data streaming the OWC has emerged as a crucial metric for information transmission in various harsh channel conditions such as in wildfire life rescue operations, underwater monitoring, observing marine lives, connecting human existence with the marine environments, and underwater smart transportation. As wireless communication evolves towards the advanced networks, the optical communication outperforms than the existing wireless communication approaches in very harsh channel conditions. However, several critical research gaps exist in the current understanding of optical wireless information transmission in an advance wireless networks. Therefore, this thesis addresses the gaps and provides the possible solution theoretically and practically implication of the proposed schemes.

The research presented in this thesis addresses the following key points are covered as follows;

- The traditional underwater optical communication techniques have limitations for low data rate and limited coverage ranges. An alternative communication media such as underwater optical communication in terms of VLC is proposed in this thesis for connecting small islands and naval tactical operations within in the mixed water mediums based on the experimental data recorded for the whole year. For over long coverage ranges an FSO-VLC underwater wireless communication system model is proposed in consideration of smart transportation.

- The research also focuses to improve the connectivity, QoS, Quality of Engineering (QoE) in estuaries where the fresh river water mix with the oceanic salt water. Therefore, the river-meets-ocean underwater VLC communication system is developed for various UWOC applications.

- The traditional wildfires communication techniques lack to support the real-time data streaming, compromise the video qualities, and lack of high-resolution imaging based on experimental data. However, this thesis proposes an innovative MIMO optical UAV-assisted communication system that improves the accuracy and data transmission within the URLLC aspect.

The following key points are covered in this thesis and provides a summary of the contributions of each chapter under consideration the objectives of this dissertation.

1.4.1 Chapter 2: Background of Optical Wireless Communication (OWC)

In this thesis, the chapter 2 presents a comprehensive literature review and background analysis on UAV and AUV-assisted optical in wireless communication systems. This chapter associated

with the advancement of optical communication and its possible applications that provides a strong background of optical signaling along with the deployment and consequences while information transmission. The foundational review of this chapter offers a deep understanding and mathematical formulation to support its applicability and compared with the traditional signaling approaches. The chapter proceeds with an assessment of different analytical approaches to the study of OWC, contrasting the integration of VLC.

The main focus of the chapter provides a critical review of the OWC enabled UAV and AUV-assisted communications, where the channel impairments and signal propagation challenges are widely discussed while information transmission. To mitigate the channel conditions, misalignment phenomena (pointing error), signal absorption, scattering, and scintillation index are widely reviewed and offering to diminish the channel effects throughout channel modeling. This chapter also examines the study on IoUTs to make smart ocean for better connectivity. Finally, the chapter proceeds the important research gaps and emerging trends in OWC development in diverse channel conditions. However, the research motivation and contributions are described in the following chapters of the thesis.

1.4.2 Chapter 3 : Single-Input-Multi-Output (SIMO)- Underwater Visible Light Communication (UVLC) System

The continuous extension of this dissertation, in chapter 3 a SIMO-UVLC system is developed towards the advance networking system in underwater environment. This chapter provides valuable insights into the trade-offs real-time information transmission in the resource-constrained networks. The SIMO-UVLC system model is investigated for the communication diversity amongst underwater sensor network nodes in SIO. In this chapter the SIMO-UVLC system model has potential benefits in mixed ocean water traits as in harsh channel conditions and misalignment of Light Emitting Diodes (LEDs) array mounted at the receiver end. Moreover, the system is designed by considering GG distribution following On-Off-Keying (OOK) modulation scheme. Consequently, the investigated performance metrics have given insight to simulate the results in varying channel parameters based on the experimental data.

1.4.3 Chapter 4 : Performance Analysis of Multi-Hop UVLC System: A River-meets-Ocean Scenario

Expanding the research is based on optical communication as AUV-assisted optical communication concepts introduce throughout this chapter. The contributions of this chapter lies in the development of a theoretical framework for analyzing multi-layers underwater optical communications where the river meets with ocean. Moreover, the closed-form expressions for the communication based on End-to-End (E2E) - SNR are derived in terms of G-Meijer function. Furthermore, for the accuracy of the technical work based on the real-tiem scenario, the analytical works further derived in the form of Extended Bivariate Generalized Meijer-G Function (EBGMGF), which provides an insight of the accuracy performance metrics of the proposed system model. The work determines of the optical beam propagation in varying vertical ans well as in horizontal layers of communication

nodes in harsh aqueous mediums. A key contribution of this chapter is the formulation of specifying optimal sensor activation probability for maintaining the pointing errors of the transceivers while the optical communication in varying water flow conditions. Therefore, this technical chapter provides the strong support for adoption of UWOC system. This chapter synthesises the concepts from the third chapter, applying them to a more complex multi-source network scenario, thus bridging the gap between theoretical AUV analysis and practical network deployments.

1.4.4 Chapter 5 : Dual-Hop Mixed FSO-VLC Underwater Wireless Communication Link

The continuation of the research extension, this chapter provides a development of dual-hop hybrid optical communication in mixed underwater environment. This chapter combines the two different optical spectrum beam ranges propagation over the longest distances in real-time scenario for a number of underwater applications. Throughout this investigated system model the main focus on achieving desired data rate within minimal delay response as well as enhance communication connectivity. The traditional wireless communication approaches have limitations while propagated in underwater environment. Therefore, the combination of FSO and VLC in underwater medium has considered a potential approach to full-fill the requirements of high quality of communication and security within low latency, very cost effective, and localization aspects. Additionally, this proposed communication system model is utilized the most updated spectrum model of UOT [18], that supports to calculate the exact value of suspended particles under the plane wave model on varying temperature and salinity parameters at different varying vertical depths. Furthermore, in this dual-hop hybrid optical communication system model both of the optical links are modeled by combined influence of alignment error and the strong turbulence effects.

1.4.5 Chapter 6: An UAV-based Optical Wildfire Communication System

This chapter provides the significant analysis of MIMO emerging optical communication by following URLLC-enabled UAV wildfire communication systems. A theoretical MIMO wildfire optical communication is proposed to analyse the performance metrics and closed-form expressions for UAV networks which are derived under consideration of channel properties. The work determines optimal UAV altitude, transmission power and performance comparison between MIMO, MISO, SIMO, and SISO in consideration of strong turbulence channel conditions. In this chapter the turbulence channels are designed by utilizing the GG distribution along with the large and small-scale channel parameters, which are calculated based on the real environmental data. However, the research in this chapter demonstrate advantages and the outer performances of UAV-assisted MIMO optical system that offers a valuable insights for the design of UAV-based optical communication networks. Additionally, this chapter lays the foundation for the subsequent chapters by introducing the concept of UAV-assisted OWC at the wildfire sites and analysis for the system performances, which is the further explored and expended throughout the later sections.

1.5 Publications Related to this Thesis

The results of this thesis work were published in **6** publications, including **3** Quartile-1 peer-reviewed journal papers, **2** Quartile-2 peer-reviewed journal paper, and **1** international conference paper. The list of publications produced during the Doctor of Philosophy in Informatics programme is as follows:

Journal articles

1. **Ali Mohammad Furqan**, Dushantha Nalin K. Jayakody†, Sahil Garg, Georges Kaddoum, and M. Shamim Hossain. "Dual-hop mixed FSO-VLC underwater wireless communication link." IEEE Transactions on Network and Service Management 19, no. 3 (2022): 3105-3120. **Q1, I.F. 4.7**

2. **Ali Mohammad Furqan**, and Dushantha Nalin K. Jayakody†. "SIMO-underwater visible light communication (UVLC) system." Computer Networks 232 (2023): 109750. doi.org/10.1016/j.comnet.2023.109750. **Q1, I.F. 4.4**

3. **Ali Mohammad Furqan**, Dushantha Nalin K. Jayakody†, and P. Muthuchidambaranathan. "Revolutionizing Firefighting: UAV-Based Optical Communication Systems for Wildfires." In Photonics, vol. 11, no. 7, p. 656. MDPI, 2024. doi.org/10.3390/photonics11070656. **Q2, I.F. 2.1**

4. **Ali Mohammad Furqan**, and Dushantha Nalink K. Jayakody†." Performance Analysis of SIMO-UVLC System in Mix-water Medium". (Accepted and in Printing process, Engineering Reports, Wiley. **Q2, I.F. 2.29**

5. Sajid Mumtaz†, **Ali Mohammad Furqan**, and Dushantha Nalink K. Jayakody†."Performance Analysis of M-ary Pulse Position Modulation on Varying Vertical Underwater System". (IEEE Access) (Under Review Process, IEEE Access). **Q1, I.F. 3.4**

Conference papers

1. **Ali Mohammad Furqan**, Dushantha Nalin K. Jayakody, Marko Beko, and Sérgio Correia. "Performance evaluation of vertical VLC link in mixed water mediums." In 2023 6th Conference on Cloud and Internet of Things (CIoT), pp. 195-199. IEEE, 2023

Chapter 2

Background of Optical Wireless Communication

2.1 Introduction of Optical Wireless Communication

OWC represents a promising frontier in wireless technology, combining innovation in physics and engineering to meet the ever-growing demand for high-speed communication. As research continues and technologies evolve, the potential applications for OWC are vast, underscoring the importance of understanding its principles and advancements for future developments [6]. Unlike conventional RF communication, the optical communication framework offers a secure, high-bandwidth, and interference-resistant alternative, enhancing situational awareness in various applications such as in firefighting strategies and underwater communications. An OWC system incorporates advanced optical sensors, high-resolution cameras, and laser communication devices mounted on UAV or AUV platforms [19, 20]. These state-of-the-art technologies enable the UAV and AUV nodes to navigate challenging terrains, collect the critical data swiftly, and communicate seamlessly with ground control centers to marine environments through the UAV and AUVs. This integration facilitates a rapid and coordinates response to unwanted incidents, significantly boosting the operational capabilities of scientific research teams in addressing the disasters with unprecedented efficiency.

The operational and deployment costs of terrestrial based optical enabled UAVs and underwater situated AUVs are as nominal as those of aircraft and submarine imagery of higher costs [21, 22]. An additional benefit of deploying hovering and floating UAVs and AUVs at effective sites is the real-time communication combined with high-resolution imaging at low altitudes and in shallow waters. It should be noted that the effective location and monitoring of affecting sites are facilitated by the flexible movement of unmanned/autonomous vehicles. The optical enabled communication devices are used for numerous application. At instant an UAV can apply for burning warnings as new fire confirmed emerge from affected wildfire locations [23]. On the other hand the AUV is useful for connecting the human existence with the marine lives virtually. However, the terrestrial and underwater channel conditions like temperature, wind speed, humidity, density, salinity, viscosity etc., are the main parameter to deal with OWC.

The optical communication devices further enhance the system capabilities by facilitating rapid and secure data transmission, fostering seamless communication and collaboration among multiple UAV and ground control centers [24][25]. An OWC not only overcomes the shortcomings of traditional firefighting methods but also users in a new era of innovation in reducing the impact of wildfires on communities and ecosystems. At a glance, the UAVs provide remote virtual access to observe the affected sites. The UAV recorded data could be in real time, highly accurate in positioning at the affected site, and provide an emergency call for safety purposes [26][27]. Moreover, the mobility of UAV allows for rapid and continuous video streaming of spreading wildfires in forests. The deployment of multiple UAVs can be more profitable by scanning the affected area in multiple passes and incorporating base stations (BS).

It should be noted that the oceans are typically challenging environments to deploy wireless communication setups as compared with the terrestrial-based communication links. A high quality, minimal delay, and high-speed enabled undersea communication is an essential approach for signal transmission to AUVs or to Underwater Wireless Sensor Network (UWSN)s [28, 29]. Additionally, the data collected from underwater must be transmitted to inland data fusion centers for further analysis. Operating instructions also need to be sent from the inland center to the AUV to ensure it operates according to real-time requirements. Therefore, the AUV-assisted OWC system can be more beneficial rather than the existing traditional communication media. Also, a dual-hop hybrid optical communication can be a promising solution for connecting UAVs or floating nodes with the underwater based AUVs.

2.1.1 An Optical Wireless Communication System Model

For the development of OWC, it is consider to understand a simple communication system containing a source-destination pair as illustrated in Figure. 2.1.

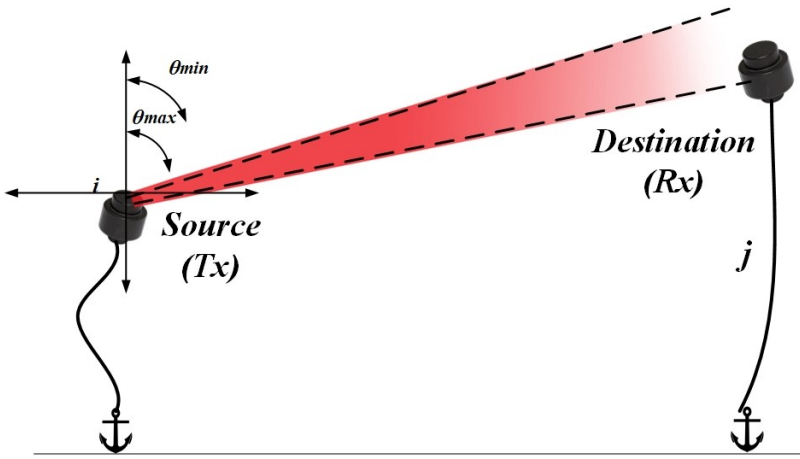

Figure 2.1: The P2P optical wireless communication, where the transmitter communicates with the optical receiver within the hars channel conditions.

As illustrated in Figure 2.1, the source communicates with the destination through an optical link in the presence of strong turbulence channel conditions while maintaining pointing error. The system

is designed under the Line-of-Sight (LOS) scenario where the transceivers are properly aligned and the misalignment phenomena (pointing error) should be optimize through the generalized exponential function. Despite the path-loss, pointing errors, and the turbulence phenomenon has been taken into account as a serious issue of designing optical communication system models. The best fit of GG distribution offers the most significant outcomes while dealing with OWC and utilized the Meijer-G function for the best fit to improve the efficiency of communication setup.

2.1.2 Channel Attenuation Coefficients for Optical Wireless Communication

The path loss in OWC depends on the vertical LOS that has distance d_0 between transceivers as well as at extinction coefficient $c(\lambda)$. In underwater environment, the extinction coefficient is the total sum of absorption $a(\lambda)$ and scattering $b(\lambda)$ phenomenon of the optical beam photons in the communication environment. Therefore, the extinction coefficient in underwater is defined in terms of scattering and absorption as $c_{Water}(\lambda) = a(\lambda) + b(\lambda)$. The typical values of $a(\lambda)$ and $b(\lambda)$ are the wavelength (λ) dependent in underwater channel are mentioned in Table 2.1. On terrestrial

Table 2.1: The typical values of absorption, scattering and extinction coefficients wavelength-dependent at 450nm blue light in different water mediums [30].

Description of water for UWC	**a**(λ)	**b**(λ)	**c**(λ)
Pure sea water	0.053	0.003	0.056
Clear Ocean water	0.069	0.08	0.15
Coastal Ocean water	0.088	0.216	0.305
Turbid Harbor water	0.295	1.875	2.17

basis communications the optical signals also affect by atmospheric conditions. The atmospheric extinction coefficient $c_{Terr}(\lambda) = \left(\frac{3.912}{V}\right)\left(\frac{\lambda}{550}\right)^{-\delta}$ is the function of the atmospheric visibility V (in km), transmission signal wavelength (λ), and the size distribution coefficient δ of scattering [31]. The typical values of terrestrial basis extinction coefficient are mentioned in Table 2.2.

Table 2.2: The typical values of terrestrial basis extinction coefficient on varying channel conditions [31].

Terrestrial weather conditions	**Extinction Coefficient** $c_{Terr}(\lambda)$
Clear air	0.43
Haze condition	4.2
Moderate rain (12.5 mm/h)	5.8
Heavy rain (25 mm/h)	9.2
Light fog	20
Moderate fog	42.2
Heavy fog	125

Therefore, the path loss coefficient $I_l^{Terr}(\lambda, d)$ on terrestrial basis optical link and the path loss coefficient in underwater environment $I_l^{Water}(\lambda, L)$ are designed by following Beer Lambert law that can be expressed as in (2.1) and (2.2)

$$I_l^{Terr}(\lambda, d_0) = \exp\Big(- c_{Terr}(\lambda) d_0 \Big). \tag{2.1}$$

$$I_l^{water}(\lambda, d_0) = \exp\Big(- c_{Water}(\lambda) d_0 \Big), \tag{2.2}$$

2.1.2.1 Pointing Error Model

The Pointing Error (PE) is also another fading source in OWC links. The PE occurs by the random movement of transceivers due to water currents. However, when a Gaussian beam propagates through distance d_0 from the transmitter to the circular detector with aperture area A_r, and the instantaneous radial displacement between the beam centroid D_r, the fraction of the collected power at the receiver end the coefficient of fading in lieu of PE can be approximated as follows;

$$I_p\left(D_r, d_0\right) \approx A_0 \exp\left(\frac{-2D_r^2}{\omega_{d_{eq}}^2}\right), \quad D_r \geq 0 \tag{2.3}$$

where the collected power factor $A_0 = [\mathrm{erfc}(\nu)]^2$ and the equivalent beam width is represented by $\omega_{d_{eq}}$. Also, the D_r presents the random radial displacement of communication nodes which is calculated by $D_r = \sqrt{D_{r_x}^2 + D_{r_x}^2}$ in terms of random horizontal and vertical components as $D_{r_x}^2$ and $D_{r_x}^2$. The Probability Density Function (PDF) of a uniform pointing error is expressed as follows [32];

$$f_{I_p}(I_p) = \frac{\xi^2}{A_0^{\xi^2}} I_p^{\xi^2 - 1}, \qquad 0 \leq I_p \leq A_0 \tag{2.4}$$

where $\xi = \omega_{d_{eq}}/2\sigma$ is the ratio between the equivalent beam radius at the receiver and the PE displacement standard deviation.

2.1.2.2 The Turbulence Channel Model

The turbulence conditions of different channels have considered in terms of GG distribution fading model as in [33]. The authors in [33] modeled the optical underwater channel conditions into successive vertical layers and the fading coefficient is associated with each distinct layer. The fading coefficient is modeled as independent but not identically distributed GG random variables. Thus, the GG probability distribution function for optical communication is written by (2.5) [34],

$$f_{I_t}(I_t) = 2\frac{(\alpha\beta)^{\frac{(\alpha+\beta)}{2}}}{\Gamma(\alpha)\Gamma(\beta)} (I_t)^{\frac{(\alpha+\beta)}{2} - 1} K_{\alpha-\beta}(2\sqrt{\alpha\beta I_t}), \tag{2.5}$$

where $K_{(\alpha-\beta)}(\cdot)$ is defined as the modified Bessel function of the second kind. The PDF of (2.5) in strong turbulence condition in terms of SNR is given as (2.6) [35];

$$f_\gamma(\gamma) = \frac{(\alpha\beta)}{\Gamma(\alpha)\Gamma(\beta)} G_{0,2}^{2,0}\left[\alpha\beta\sqrt{\frac{\gamma}{\mu}}\,\middle|\, \begin{matrix} \cdots \\ \alpha - 1, \beta - 1 \end{matrix}\right], \tag{2.6}$$

where $G(\cdot)$ is defined G-Meijer function as indexing numbers m, n, p, q along with the arguments a_p, b_q. The instantaneous and average electrical SNR are represented by γ and μ. The consideration of scattering process, the large scale cells and small scale cells in both of the links are defined by α and β, as in (6.7, 3.5), respectively [35] [36].

To investigate the multiple optical link layers the PDF in (2.6) is further derived by (2.7) as follows; [35];

$$f_{I_t}(I_{t^k}) = \frac{\prod_{k=1}^{K} \alpha_k \beta_k}{\prod_{k=1}^{K} \Gamma(\alpha_k)\Gamma(\beta_k)} G_{0,2K}^{2K,0}\left[\prod_{k=1}^{K} \alpha_k \beta_k I_{t^k} \middle| \begin{matrix} \cdots \\ \alpha_1 - 1, ..., \alpha_K - 1, \beta_1 - 1, ..., \beta_K - 1 \end{matrix} \right]. \quad (2.7)$$

2.1.2.3 Unified Channel Conditions for Optical Wireless Communication

The joint PDF of OWC are combined with the distance-dependant path loss $I_l^{Terr}(\lambda, d)$, channel turbulence I_t, and pointing errors I_p. It is noteworthy that the path-loss conditions are deterministic in nature. Therefore, the combined channel impairment $I = I_l^{Terr}(\lambda, d) I_p I_t$ of optical link can be expressed as follows in (2.8) [32];

$$f_I(I; \omega_{d_{eq}}) = \int f_{I|I_t}(I|I_t)\, f_{I_t}(I_t)\, dI_t, \quad (2.8)$$

where $f_{I|I_t}(I|I_t)$ is the conditional probability of the fading coefficient induced by cascaded turbulence which can be expressed as follows;

$$f_{I|I_t}(I|I_t) = \frac{1}{I_t I_l^{Terr}} f_{I_p}\left(\frac{I}{I_t I_l^{Terr}}\right) = \frac{\gamma^2}{(A_0 I_l^{Terr})^{\gamma^2}} \left(\frac{I}{I_t I_l^{Terr}}\right)^{\gamma^2 - 1}. \quad 0 \le I \le A_0 I_t I_l^{Terr} \quad (2.9)$$

Furthermore, substituting (2.9) into (2.8) and further utilizing the (2.7) for multiple layers communication links. The combined PDF of influenced channel conditions is written by (2.10) as follows;

$$f_I(I) = \frac{\prod_{n=1}^{N} (\alpha_n \beta_n)}{\prod_{n=1}^{N} \Gamma(\alpha_n)\Gamma(\beta_n)} \frac{\xi^2}{A_0 I_\ell} G_{1,2N+1}^{2N+1,0}\left(\prod_{n=1}^{N} (\alpha_n \beta_n) \frac{I}{A_0 I_\ell} \middle| \begin{matrix} \xi^2 \\ \xi^2 - 1, \alpha_1 - 1, ..., \alpha_n - 1, \beta_1 - 1, ..., \beta_n - 1 \end{matrix} \right). \quad (2.10)$$

2.2 AUV-assisted Underwater Wireless Optical Communication System

Our earth is a big blue planet, which occupies approximately two thirds of its surface by water. Unfortunately, the oceans are least explored mediums which necessitate to investigate for various underwater applications. Nevertheless, the scientific community is acquainted with oceans less than 5%, since having enough scientific and technological approaches to unveil the mysteries of

underwater bodies. The boisterous oceanic channels are highly accountable sectors for natural hazardous and adaptable the weather conditions cause of random physio-chemical properties of water. Therefore, a high quality of signaling approach requires to explore these aquatic environments. The Inherent Optical Properties (IoP)s and Apparent Optical Properties (AoP)s are the crucial requirements to deploy a high connectivity enabled UWOC system [37]. Alternatively, water offers dielectric properties for UEM which causes high attenuation [14]. The UEM waves in terms of RF attenuate easily and require a large size of antenna [38]. Due to the limitation of UEM waves, the traditional acoustic communications are used as a promising technology over long ranges communication coverage. Nonetheless, the acoustic waves offer limited bandwidth, high latency, and low propagation speed as 1500 m/s [12]. These traditional communication hindrances can be augmented by UWOC. The potential UWOC technology supports high speed of connectivity (in Gbps) among underwater wireless sensor networks UWSNs and builds up a connection between terrestrial environment with the underwater existence [39–41]. Thanks to the promising free licence spectrum, a very cost-effective, largely illuminating light sources, and large capacity enabled advantageous UWOC approach.

2.3 A Promising Solution for Long-Range Underwater Wireless Signal Transmission

Underwater Wireless Communication (UWC) has become a promising solution of exploration aquatic mediums through a diverse range for numerous underwater applications. It is noteworthy that the collected data from floating AUV has to transmit to inland data fusion centers for further investigation. Also, the operating instructions need to transmit from the inland center to floating nodes for further operation and control as per the real-time requirements. To facilitate these requirements, a dual-hop FSO-VLC hybrid underwater communication setup is essential, particularly in the context of naval tactical operations. The promising solution and implementation of dual-hop FSO-VLC hybrid underwater communication setup is to significantly enhances the capabilities of information transmission over extended distances. In order to operate and control unmanned AUVs, a high demand of dual-hop cooperative hybrid terrestrial and underwater communication system is required for numerous underwater applications.

2.4 A Revolutionary Approach of UAV-Assisted Optical Wireless Communication System

UAVs are one of the most promising approaches of their utilization for enhancing efficiency of OWC. The convergence of UAV technology with optical communication has opened new opportunity for high-speed, reliable data transmission and connectivity amongst a large number of communication nodes in various environmental channel conditions [42]. This innovative approach capitalizes on the mobility, flexibility, and efficiency of UAVs, offering an effective solution to the limitations faced

by conventional communication networks [43]. Generally, the UAVs full-fill the gap of traditional communication infrastructures where the signal transmission are impractical and impossible [44].

One of the most defining feature of UAV ability to operate using optical beam while the traditional RF communication enabled communication nodes are widely used within some limitations [45]. Therefore, the OWC overcomes of substantial benefits rather than RF in terms of high bandwidth, throughput, and data rate transmission. The OWC systems leverage UAVs can achieve significantly higher bandwidth, promoting faster data transfer rates. The UAV acts as a relay or communication node, flying at optimal altitudes to provide LOS connections between ground users or between ground BSs [46].

Moreover, the integration of UAVs into optical wireless communication networks addresses numerous challenges, including the dynamic nature of the environment and varying user demands. The mobility of UAVs allow for real-time adjustments to their position and orientation, ensuring optimal alignment with ground users, which is critical for maintaining a stable connection in OWC systems that rely on direct LOS. Additionally, the deployment of UAVs can be particularly beneficial in disaster recovery situations, remote area communications, or mass events where there may be sudden spikes in data traffic. Overall, UAV-assisted OWC represents a forward-thinking approach aimed at overcoming geographical limitations, enhancing connectivity, and providing versatile communication solutions in an increasingly mobile and data-driven world.

Chapter 3

SIMO-Underwater Visible Light Communication (UVLC) System

3.1 Introduction

The advent of VLC towards next generation of wireless networks has opened the doors to unveil the mysteries of unguided mediums such as ocean. Nevertheless, the bottleneck exists due to varying physio-chemical properties of water which leads UOT. In UWOC, the UOT and misalignment of optical transceivers are crucial factors which cause of random water flow patterns. Additionally, the performance analysis of UVLC system under consideration of combined influence fading in varying vertical depth is highly challenging. As, UWOC is complex approach and typically challenging to establish an advanced communication setups due to flow patterns, thermal expansions, and heavy winds, therefore, plenty of existing research works have dealt with the issues of UVLC as in [47–49]. The optical beam severs water turbidity due to the harsh aqueous channel conditions (irregular physiochemical water properties). The random propagation of optical beam by air bubbles influence the light fluctuation intensity, which is a big loss of light beam energy [50]. An estimation of statistical existing air-bubbles UWOC system model under GG distribution model is proposed as in [51]. To cope with turbulence induced fading factor and pointing error, a SIMO-UVLC system is proposed in this chapter to obtain the E2E performance metrics on averaging SNR conditions under consideration field of view Field of View (FOV) of UVLC link. It is noteworthy that the losses of underwater optical signaling are determined as average beam intensity. Further, this average beam intensity is used to investigate to obtain the better E2E performance of the proposed system [34]. Moreover, the MC approach is used to obtain the UOT effect and accuracy of the proposed analytical expressions throughout this research. Also, this work implies the multi-water layers to unify the turbulence effect along with the pointing error scenario. The proposed SIMO-UVLC system model is depicted by Fig. 3.1.

3.1.1 Motivations and Contributions

Motivated by this study, a SIMO-UVLC system model for real-time data streaming at sea port sites, better connectivity for coastal securities, various commercial applications, and naval tactical operations in oceanic environment is proposed. However, to the best of authors knowledge, there are very limited works are available where the performance evaluations are investigated through a set of LEDs at the receiver end within the boisterous channel medium under consideration strong underwater optical turbulence phenomena. In consideration of combined influence of channel conditions the investigated E2E performances are widely discussed and simulated based on the experimental data throughout this study. The MC validation is being used to obtain the analytical BER and outage performance of the proposed system. The main contributions of this research are summarized as follows:

- An observational study in successive vertical layers on varying temperature and salinity of mixing water is widely over-viewed through the experimental data in SIO during the whole year in strong turbulent oceanic environment;
- This study proposes the novel closed-form expressions in the form of G-meijer function on varying vertical water layers within the combined influence of channel conditions (turbulence and pointing error). Furthermore, E2E performance metrics (BER and outage probability) are obtained on arranging the set of LEDs at receiver end. The system is designed as a SIMO-UVLC where a sequential arrangement of LEDs is implied;
- Finally, the analytical findings are verified with the extensive simulation results at different channel parameters, such as varying temperature and salinity, transmission range, beam spreading angle, a number of arrangement of LEDs, successive varying vertical depth, and consisting pointing errors. Additionally, the IoPs and AoPs are also considered in this work.

3.1.2 Organization

This chapter is organized as follows; The combined influence of channel modeling coefficients are introduce by Section 3.2. Throughout Section 3.3, the system is designed by following SIMO-UVLC approach for the signal transmission methodologies between transceivers. Further the analytical work and E2E performances of closed-form expressions along with derivations are provided in Section 3.4. The simulations results are obtained by utilizing the MC approach as well as the numerical values of the provided real experimental data as in Section 3.5. The whole work is summarized and provided a brief summary of the proposed work in the Section 3.6 of this research.

3.2 Modeling Channel Conditions

In this proposed system model, firstly the channel conditions are designed individually then the large scale α and small scale β particles are measured based on the experimental data. Secondly, the SIMO-UVLC system design along with the signal transmission terminologies are presented.

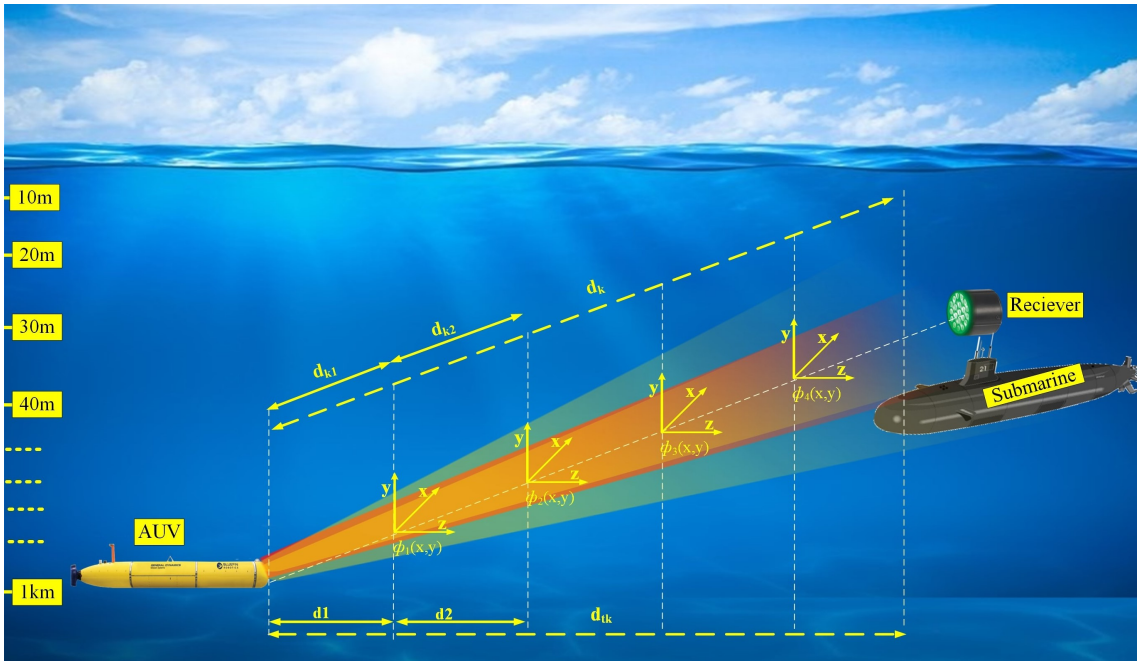

Figure 3.1: The proposed system model where the source as AUV communicates with the submarine (destination) and transmits the signal in VLC format through multiple water layers within varying strong turbulence channel conditions. The stimulated photons trajectories in random water layers analytically defined in all directions. It is noteworthy that the source transmits the signal through a single light beam and at the receiver end a multiple array of LEDs collect all possible signals for CSI.

Additionally, the closed-form expressions to obtain E2E performance analysis in the presence and absence of pointing error conditions are derived. However, the GG distribution is utilized to design the system model within the moderate-to-strong turbulence channel conditions. Most recently, in the literature GG fading model is introduced as the best fitting distribution for UWOC as in [9][52]. The GG distribution model factorizes irradiance as a product of two random processes in strong turbulence channel conditions and widely employed to model UVLC links in the literature [34]. An immense advantage is utilization of GG distribution, it has less complexity and outperforms among other traditional distribution models. Therefore, that is reason to adpot GG distribution to model SIMO-UVLC communication system in mixed ocean waters throughout this research.

3.2.1 Path Loss Channel Coefficient

The optical beam attenuates in underwater due to photon absorption and scattering phenomena. The absorption and scattering are wavelength dependent events and could be further summarized as extinction coefficient $c(\lambda)$. The extinction coefficient $c(\lambda)$ varies with type of waters such as pure, clear, coastal, and turbid harbor water According to the Beer's law, the path loss factor in LOS communication for k^{th} layers which is the deterministic in the nature and can be defined as follows [47];

$$I_{l^k} \approx \exp\left(-c(\lambda)\frac{dt_K}{cos(\phi)}\right), \tag{3.1}$$

where the distance apart transmitter and multiple receiver is denoted by dt_K, which is the total sum of distances for k^{th} horizontal layers, and ϕ is the angle between the receiver plane and the transmitter receiver trajectory. The total distance is defined as $dt_K = \sum_{k=1}^{K} d_{t_k}$ for varying water layers.

3.2.2 Pointing Error Coefficient

The pointing error phenomena is another signal fading factor in UVLC. Generally, the pointing error occurs because of transceivers misalignment due to wind loads and water current fluctuations. Therefore, the mathematical representation of pointing error fading coefficient is given as [34];

$$I_{p^k} = A_0 \exp\left(-\frac{2{a_k}^2}{w_{zeq}^k}\right), \tag{3.2}$$

where $A_0 = [erfc(\nu_w)]^2$ is defined as the fraction of received power collection, a_k denotes the resultant of the horizontal and vertical component of transceivers deflection due to water waves and w_{zeq}^k is optical beam-width, respectively. The random radial displacement a_k is defined as $a_k = \sqrt{a_{x_k}^2 + a_{y_k}^2}$ with the horizontal $a_{x_k}^2$ and vertical $a_{y_k}^2$ components. Further, the equivalent beam-width is defined as $w_{zeq}^k = \frac{w_z\sqrt{\sqrt{\pi}erf(\nu)}}{2\nu\exp(-\nu)^2}$. It is describe the ratio between aperture radius and beam-width $\nu_w = (\sqrt{\pi/2})D_r/2w_z$. The beam-width is formulated as $w_z \approx w_0\sqrt{1+(z\lambda/\pi w_0)^2}$ at varying distance z. The spot size of the Gaussian beam wave and optical beam wavelength are presented by ω_0 and λ, respectively. Therefore, the PDF of I_{p^k} is given as follows [32];

$$f_{I_p^k}(I_{p^k}) = \frac{\zeta^2}{A_0^{\zeta^2}} I_{p^k}^{\zeta^2-1}, \tag{3.3}$$

where $\zeta = w_{zeq}/2\sigma_s$ is the ratio between the equivalent beam radius and the pointing error displacement standard deviation.

3.2.3 Turbulence Channel Coefficient

Despite of the path-loss and pointing error, the most considerable phenomenon of signal fading factor is turbulence which occurs due to random variation of scintillation index. The continuously changing depth dependent water temperature, pressure, density, and salinity leads scintillation index. In this study, we consider the optical beam propagates according to the water flow. The water flow is categorized into two main categories as 1) Lagrangian fluid flow and 2) Eulerian method of fluid flow [53]. As considering the laminar flow the optical beam propagates in well smooth path with straight stream-line. On the other hand in turbulence phenomena, the high probability of photon scatterrance or absorption cause of random flow pattern of water streams. Due to this, the optical beam experiences a huge loss in propagation of signal intensity. Hence, the necessity to model the strong turbulence channel conditions under consideration of GG distribution. Throughout this study, a VLC system model is designed within the strong turbulence channel conditions regardless

of water types [34]. Therefore, the PDF of turbulence induced fading I_{t^k} for k^{th}-layers is obtained by (3.4) as follow,

$$f_{I_t}(I_{t^k}) = \frac{\prod_{k=1}^{K} \Phi_{\alpha_k\beta_k}}{\prod_{k=1}^{K} \Phi_{\Gamma(\alpha_k)\Gamma(\beta_k)}} G_{0,2K}^{2K,0}\left[\prod_{k=1}^{K} \Phi_{\alpha_k\beta_k} I_{t^k} \middle| \begin{matrix} \cdots \\ \mathbf{a}_{arg} \end{matrix}\right], \tag{3.4}$$

where $\Phi_{\alpha_k\beta_k} = \alpha_k\beta_k$ and $\Phi_{\Gamma(\alpha_k)\Gamma(\beta_k)} = \Gamma(\alpha_k)\Gamma(\beta_k)$ along with the argument $\mathbf{a}_{arg} = [\alpha_1 - 1, ..., \alpha_K - 1, \beta_1 - 1, ..., \beta_K - 1]$ can be written respectively.

In (3.4), the large-scale (α_k) and small-scale (β_k) factors for k^{th} layers are modeled under consideration of spherical Gaussian wave models as in (3.5) [35],

$$\alpha_k = \left[\exp\left(\frac{0.17\chi_{I_{tk}}^2}{\left(1 + 0.167\chi_{I_{tk}}^{\frac{12}{5}}\right)}\right)^{\frac{7}{6}} - 1\right]^{-1}, \beta_k = \left[\exp\left(\frac{0.225}{\left(1 + 0.259\chi_{I_{tk}}^{\frac{12}{5}}\right)}\right)^{\frac{5}{6}} - 1\right]^{-1}. \tag{3.5}$$

In (3.5) the scintillation index for k^{th} layer is denoted by $\chi_{I_t^k}$ which is known as Rytov variance. The proof of Rytov variance is mentioned in Appendix A. However, the Rytov variance is determined under consideration of UOT [18][Eq. (22)] as follows,

$$\chi_{I_t^k}^2 = \frac{2\pi^2 k_0^2 d_0 C_0 \alpha^2 \chi_T}{\omega^2 \sqrt[3]{\epsilon} \int_0^1 \int_0^\infty \frac{1}{\sqrt[3]{\kappa^8}}} \left\{1 - cos\left[\frac{d_0\kappa^2}{k_0}(\xi - \xi^2)\right]\right\} \times [1 + C_1(\kappa\eta)^{\frac{2}{3}}]\Big(\omega^2 \exp(-A_T\delta) + d_r \exp(-A_S\delta)$$
$$- \omega(d_r + 1)\exp(-A_{TS}\delta)\Big) d\kappa d\xi. \tag{3.6}$$

It also considers that the optical beam effects by the water layers in the corresponding propagation of photons. If the coordination vectors for VLC beam spreading in each of layer are denoted as (r_x, r_y, r_z). Therefore, the direction vector of passes VLC beam through MC approach which could be defined as follows [54];

$$r_{\hat{x}} = r_x + \frac{1}{k}\frac{\partial\phi(x,y)}{\partial x}, r_{\hat{y}} = r_y + \frac{1}{k}\frac{\partial\phi(x,y)}{\partial y}, r_{\hat{z}} = \sqrt{1 - r_{\hat{x}}^2 - r_{\hat{y}}^2}.$$

As a result, the random variation of VLC beam passes through each water layer. The updated Rytov variance from (3.7) for UOT could be written as follows;

$$\chi^2_{I_t^k}(\kappa_x,\kappa_y) = Z_{coef}\int_0^1\int_0^\infty \frac{1}{\left(\sqrt{\kappa_x^2+\kappa_y^2}\right)^{\frac{8}{3}}}\left\{1-cos\left[\frac{d_0\kappa^2}{k_0}(\xi-\xi^2)\right]\right\}$$
$$\times\left[1+C_1\left(\eta\sqrt{\kappa_x^2+\kappa_y^2}\right)^{\frac{2}{3}}\right]\left(\omega^2\exp(-A_T\delta)+d_r\exp(-A_S\delta)-\omega(d_r+1)\exp(-A_{TS}\delta)\right)d\kappa d\xi. \tag{3.7}$$

The coefficient as $Z_{coef} = \frac{2\pi^2 k_0^2 d_0 C_0 \alpha^2 \chi_T}{\omega^2\sqrt[3]{\epsilon}}$, and the variables used in (3.7) are defined in Table 3.1.

Table 3.1: The parameters are used to design the scintillation index in the proposed SIMO-UVLC system model.

Parameters	**Variable Definition**
$k_0 = 2\pi/\lambda$	Wave number
d_0	Link length parameter
κ	The magnitude of the spatial frequency in UOT spectrum model
χ_T	The dissipation rate of mean squared temperature of refractive index
χ_S	The dissipation rate of mean squared salinity of refractive index
ω	Relative Strength of temperature and salinity
ϵ	The dissipation rate of turbulent kinetic energy per unit mass of fluid
η	The Kolmogorov micro-scale length
A_T	$A_T = C_0 C_1^{-2} P_T^{-1}$
A_S	$A_S = C_0 C_1^{-2} P_S^{-1}$
A_{TS}	$A_{TS} = 0.5 C_0 C_1^{-2} P_{TS}^{-1}$
P_T	Prandtl Number for temperature
P_S	Prandtl Number for sanity
C_0	Constant
C_1	Constant

Throughout the expression in (3.7), the α_k and β_k factors for k^{th} layers are calculated for the given temperature and salinity by as in [55], and further used to investigate the closed-form expressions to obtain E2E performance metrics of the proposed system model.

3.3 SIMO-UVLC System Design

In this chapter, the system model considers an AUV as a source which is situated at a particular depth in underwater environment, transmits the collected oceanographical data to fixed BS through successive k^{th} vertical water layers with a laser diode. It is noteworthy that the receiver has mounted a consecutive number 2^M of LEDs at the receiver aperture. The number of LEDs are denoted by M, where the received SNR can be written by γ_k. However, in this study the MC simulation is used to simulate the photon trajectories in random water flow towards the destination. The proposed schematic diagram of the proposed system model is depicted by Fig. 3.1, where AUV

communicates with the fixed BS in harsh channel conditions. Therefore, the received signal at the BS can be written as,

$$y_k(t) = R\eta_e(I_k + I_b)x(t) + n_k(t), \tag{3.8}$$

where I_k is an instantaneous intensity gain with an ambient light intensity I_b, which could be optimize by using filter at the receiver end. Moreover, an optical to electrical conversion efficiency and photo-detector responsivity are denoted by η, and R, respectively. The transmitted information symbol $x(t)$, the Additive White Gaussian Noise (AWGN) with zero mean and σ_k^2 variance is represented by $n(t)$.

Remarkably, in this research the received light intensity experiences by the total sum of multiplicative factors of path-loss, pointing error, and turbulence channel conditions for k^{th} vertical layers. Therefore, the multiplicative factor is defined by $I_K = \sum_{k=1}^{K}\left[\prod_{k=1}^{K} I_{l^k} I_{p^k} I_{t^k}\right]$. However, the propagation signal wavelength of optical beam strongly depends on water quality, misalignment of transceivers, turbulence, and water currents flow.

Additionally, the instantaneous electrical SNR for k^{th} layers under IM/DD within OOK scheme is written as $\gamma_k \triangleq (R\eta)^2|I_k|^2/\sigma_k^2$ in this proposed system model. The received intensity of light I_k could be defined as $I_K = \max(I_1, I_2, I_3, ..., I_n)$. Furthermore, the selection combining SNR (γ_{sc}) at the destination within SIMO scenario can be expressed as,

$$\gamma_{SC} = \max_{k=1,...,K}(\gamma_K). \tag{3.9}$$

The instantaneous average electrical SNR for k^{th} layer is defined as $\overline{\mu}=\gamma_{SC}/|I_k|^2$. In contrast the CSI of the proposed system model mathematically is written as,

$$z(t) = \sum \rho_k y_k(t), \tag{3.10}$$

where ρ_k is the wight factor of the received signal for k^{th} layers and can be defined as follows

$$\rho_k = \begin{cases} 1, & \text{if } \gamma_{SC} \leq \gamma_{th} \\ 0, & \text{otherwise.} \end{cases}$$

3.4 End-to-End (E2E) Performance Analysis

In this section, the average BER and outage probability of the proposed SIMO-UVLC system based on the experimental data are investigated. The performance metrics are further analyzed with and without pointing error conditions.

3.4.1 Average Bit Error Rate (BER) Performance

In this research, the vertical UVLC system under consideration of IM/DD-OOK modulation and selection combining method is considered. Therefore, the average BER for an individual layer of the proposed system is obtained as follows [12];

$$\overline{BER} = \frac{1}{2}\int_{0}^{\infty} erfc\left(\sqrt{\frac{\mu I_K}{2M}}\right) \times f_{I_t}(I_{t^k}) f_{I_p}(I_{p^k}) dI_t dI_p. \tag{3.11}$$

where, μ represents the average SNR, the light irradiance, and the number of LEDs at the receiver end are denoted by I_K and M, respectively. Furthermore, replacing (3.4) into (3.11) after converting erfc function into Meijer-G function by utilizing equation [56, p. 06.27.26.0006.01]. Further, utilizing the properties of Wolfram Mathematica [56, Eq. 07.34.21.00013.01] to the complex integration expression are obtained as (3.12) and (3.13) as follows;

$$\overline{BER} = \frac{\prod_{k=1}^{K} \Phi_{\alpha_k\beta_k}}{2\sqrt{\pi}\prod_{k=1}^{K} \Phi_{\Gamma(\alpha_k)\Gamma(\beta_k)}} \int_{-\infty}^{\infty}\int_{0}^{\infty} G_{0,2K}^{2K,0}\left[\prod_{k=1}^{K} \Phi_{\alpha_k\beta_k} I_{t^k} \middle| \begin{matrix} \cdots \\ \mathbf{a}_{arg} \end{matrix}\right] G_{1,2}^{2,0}\left[\frac{\mu I_{p^k}^2}{2M} I_{t^k}^2 \middle| \begin{matrix} 1 \\ 0, \frac{1}{2} \end{matrix}\right] dI_{t^k} dI_{p^k}. \tag{3.12}$$

$$\overline{BER} = \frac{2^{\sum_{k=1}^{K}(\alpha_k+\beta_k)-2K}\zeta^2}{2\pi^{(\frac{2K+1}{2})} A \prod_{k=1}^{K} \Phi_{\Gamma(\alpha_k)\Gamma(\beta_k)}} \int_{0}^{A} I_{p^k}^{\zeta^2-1} G_{4K+1,2}^{2,4K}\left[\frac{2^{4K}\mu I_{p^k}^2}{2M\left(\prod_{k=1}^{K} \Phi_{\alpha_k\beta_k}\right)^2} \middle| \begin{matrix} \frac{1-\alpha_1}{2}, \ldots \frac{1-\alpha_k}{2}, \frac{2-\alpha_1}{2}, \ldots \frac{2-\beta_k}{2}, 1 \\ 0, \frac{1}{2} \end{matrix}\right] dI_{p^k}. \tag{3.13}$$

The expressions in (3.14) is a complex integration in term of pointing error. To solve the expression in (3.13) plugin (3.3) and integrates by using the properties as in [56, Eq. 07.34.21.0084.01].

$$\overline{BER} = \frac{2^{\sum_{k=1}^{K}(\alpha_k+\beta_k)-2K-1}\zeta^2}{2\pi^{(\frac{2K+1}{2})} \prod_{k=1}^{K} \Phi_{\Gamma(\alpha_k)\Gamma(\beta_k)}} G_{4K+2,3}^{2,4K+1}\left[\frac{2^{(4K-1)}\mu A^2}{M\left(\prod_{k=1}^{K} \Phi_{\alpha_k\beta_k}\right)^2} \middle| \begin{matrix} \frac{2-\zeta^2}{2}, \frac{1-\alpha_1}{2} \ldots, \frac{2-\alpha_1}{2}, \ldots \frac{1-\beta_1}{2}, \ldots \frac{2-\beta_k}{2}, 1 \\ 0, \frac{1}{2}, \frac{-\zeta^2}{2} \end{matrix}\right]. \tag{3.14}$$

Additionally, for simplifying the expression complexity as in (3.14) by utilizing the properties of G-meijer function [56, Eq. 07.34.03.0001.01]. The final expression is obtained by (3.15), which is the total BER analytical performance metrics of the proposed SIMO-UVLC system.

$$\overline{BER} = \frac{2^{\sum_{k=1}^{K}(\alpha_k+\beta_k)-2K}}{2\pi^{(\frac{2K+1}{2})} \prod_{k=1}^{K} \Phi_{\Gamma(\alpha_k)\Gamma(\beta_k)}} G_{4K+1,2}^{2,4K}\left[\frac{2^{(4K-1)}\mu}{M\left(\prod_{k=1}^{K} \Phi_{\alpha_k\beta_k}\right)^2} \middle| \begin{matrix} \frac{1-\alpha_1}{2} \ldots \frac{1-\alpha_k}{2}, \frac{2-\alpha_1}{2}, \ldots \frac{1-\beta_1}{2}, \ldots \frac{2-\beta_k}{2}, 1 \\ 0, \frac{1}{2} \end{matrix}\right]. \tag{3.15}$$

3.4.2 The Outage Performance

In this section the outage probability of UVLC-SIMO system model on the basis of the real experiment data is investigated. The PDF of aggregated channel conditions are considering in combined influences of all channel parameters as formulated by (3.16). The combined PDF of channel conditions are given as follows;

$$f_{I_K}(I_{k,th}) = \frac{\prod_{k=1}^{K} \Phi_{\alpha_k\beta_k}}{AMI_{l_k} \prod_{k=1}^{K} \Phi_{\Gamma(\alpha_k)\Gamma(\beta_k)}} G_{1,3}^{3,0}\left[\left(\frac{\prod_{k=1}^{K} \Phi_{\alpha_k\beta_k}}{AMI_{l_k}}\right) I_{K,th} \middle| \begin{matrix} \zeta^2 \\ \zeta^2 - 1, \alpha_k - 1, \beta_k - 1 \end{matrix}\right]. \tag{3.16}$$

For obtaining outage performance of the system, the Cumulative Distribution Function (CDF) should be less than or equal to the threshold of combined channel conditions ($I_{k,th}$). The analytical formulation for outage performance of investigated SIMO-UVLC system in terms of CDF by integrating (3.16) as follows,

$$P_{out} = F_I(I_K \leq I_{K,th}) = \int_0^{I_{K,th}} f_I(I_{K,th}) dI_{K,th}. \tag{3.17}$$

Furthermore, the combined influences of channel conditions in terms of SNR are obtained by replacing $I_K = \sqrt{\gamma_{th}/\mu}$ in (3.17). The combined channel conditions of CDF is derived by (3.18), which is the outage probability of the whole system.

$$P_{out} = \frac{\left(\prod_{k=1}^{K} \Phi_{\alpha_k\beta_k}\right) \zeta^2}{AMI_{l_k} \prod_{k=1}^{K} \Phi_{\Gamma(\alpha_k)\Gamma(\beta_k)}} \sqrt{\frac{\gamma_{th}}{\mu}} G_{2,4}^{3,1}\left[\left(\frac{\prod_{k=1}^{K} \Phi_{\alpha_k\beta_k}}{AMI_{l_k}}\right) \sqrt{\frac{\gamma_{th}}{\mu}} \middle| \begin{matrix} \zeta^2, 0 \\ \zeta^2 - 1, \alpha_k - 1, \beta_k - 1, 0 \end{matrix}\right]. \tag{3.18}$$

3.5 Numerical Results

In this section the analytical and simulation results for a variety of performance metrics of the proposed UVLC-SIMO system model in SIO under strong turbulence channel conditions (GG distribution) following IM/DD-OOK modulation scheme are investigated. The average seawater temperature is about 28^0C with the mean salinity 33.75 *PSU* has been recorded in this vast acrimonious ocean environment throughout the year in 2016 in SIO. More specifically, the surface mixed layer temperature is registered as 22.5^0C to 30^0C while the monthly changes in average temperature of mixed layer was recorded as 27.5^0C. The salinity profile is directly related to the temperature variation and varies 34 PSU to 35.5 PSU. Even though, the Indonesian sea changes water pattern due to fluctuation in water temperature (20^0C to 25^0C) in mixed SIO. During this

occasion, the salinity ranges vicissitude approximately 34.2 PSU to 34.7 PSU. It is noticeable that during mid-year in the eastern ocean of Australia the strong salinity fronts are recorded 31 PSU to 35.8 PSU while the average temperature is recorded approximately 30^0C.

Following all above facts, we are considered the water quality as clear ocean water with the extinction coefficient $c(\lambda)$ = 0.15, and the distance apart the transceivers has taken as PSU = 100m. We also obtain the E2E performances underneath consecutive multiple layers as d_t = 10m, 20m, 30m, and 40m along with the fixed pointing error ξ = 1.5. The corresponding physio-chemical properties such as temperature, pressure, salinity, and density are varying with depth. Due to varying physio-chemical water properties, α and β particles are calculated based on every individual depth, temperature, and salinity for the whole year during 2016. It is noteworthy that the fixed varying arrangement of LEDs array is fixed at the receiver end for improving system performance and efficiency along with the green light spectrum wavelength λ = 532nm. The arrangement of LEDs are arranged in 2^M sequential structure, where M is the number of LEDs at the receiver end.

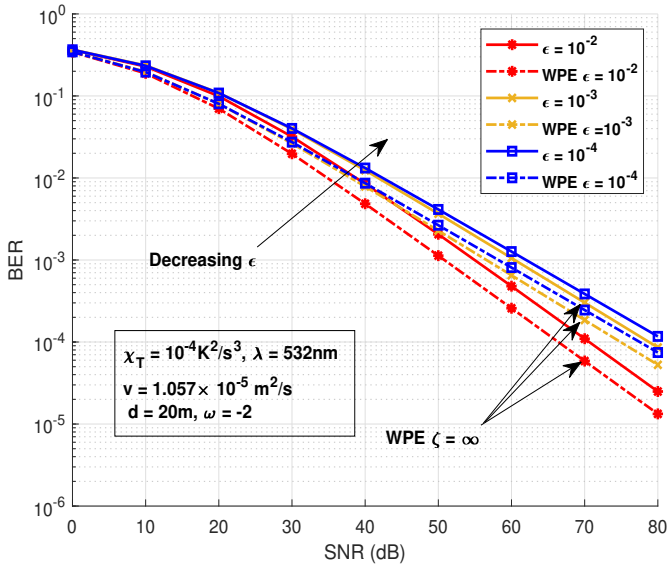

Figure 3.2: The BER performance of SIMO-UVLC system model is depicted and comprised in the presence of pointing error and WPE under strong turbulence channel conditions in SIO. The performance metrics are obtained on varying dissipation rate of turbulent kinetic energy per unit mass of fluid (ϵ), when the setup is below 20m of water surface and other parameters are fixed.

The BER performances of the experimental data on varying dissipation rate of turbulent kinetic energy per unit mass of fluid (ϵ) with pointing error WPE are simulated in Fig. 3.2. It is clearly seen that the higher value of ϵ shows the superior performances while the minimum has the poorer performance at the fixed parameters as kinematic viscosity (v), unit less parameter (ω_0) (the ratio of temperature to salinity contributions to the refractive index), and rate of dissipation of mean-square temperature (χ_T), and the distance between transceivers has taken 20m. The dotted lines are showing the performances in WPE while the straight lines show the BER performances are obtained in presence of pointing errors within strong turbulence channel conditions. If targeting 10^{-4} BER, it reaches 70dB and 67dB at 1×10^{-2} of ϵ in the presence of pointing and WPE conditions. An

interesting point could be made here that the BER is almost the same at 40dB while it achieve 10^{-2} at $\epsilon = 1 \times 10^{-3}$ and $(\epsilon) = 1 \times 10^{-4}$ in the presence of pointing and WPE withing strong turbulence channel conditions. The reason is that the slightly changes of temperature and salinity, due to this α and β particles are changed. The worst performance is obtained at ϵ=10^{-4} in high SNR regime.

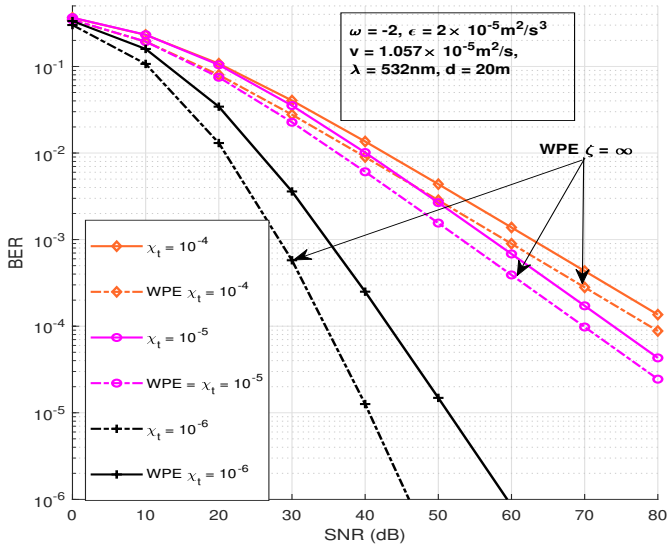

Figure 3.3: The BER performance of the SIMO-UVLC system model is depicted and comprised with pointing error and WPE under strong turbulence channel conditions in SIO. The performance metrics are obtained on varying dissipation rate of temperature (χ_T), when the setup is below 20m of water surface and other parameters are fixed.

The BER performances are also obtained on varying χ_T to depict the variation of water temperature of the proposed UVLC-SIMO system model in SIO. The whole affecting scenario of BER on varying χ_T is depicted by Fig. 3.3. The performances are plotted within strong turbulence based experimental data with fixed parameters when the depth of setup has taken d_t = 20m below the water surface. It seems that on decreasing χ_T the performance is improving at fixed pointing error ξ = 1.5. The superior performance can be depicted at $\chi_T = 1 \times 10^{-6}$ in low SNR regime. On the other hand, when the χ_T improves then BER decrease simultaneously, within presence of pointing errors and in WPE conditions. A huge gape could be found the performances in varying χ_T values. It is because the sudden falls of temperature from upper layer to lower layer of water in corresponding depth. In the absence of pointing error, it shows the best performance within SNR regime at 46dB while with pointing error at 59.5dB. The comparison is also getting the best insight to observe the BER performance of SIMO-UVLC system model within the strong turbulence channel conditions.

The most significant observation is obtained the BER performance at varying distance underwater withing in SIO. As stated that the temperature decrease and pressure rises proportionally to increasing depth. The comparison of the BER performance metrics with and WPE conditions in strong turbulence based on experimental data are depicted by Fig. 3.4. The best BER performance is obtained at PSU = 10m below the water surface because of corresponding temperature and

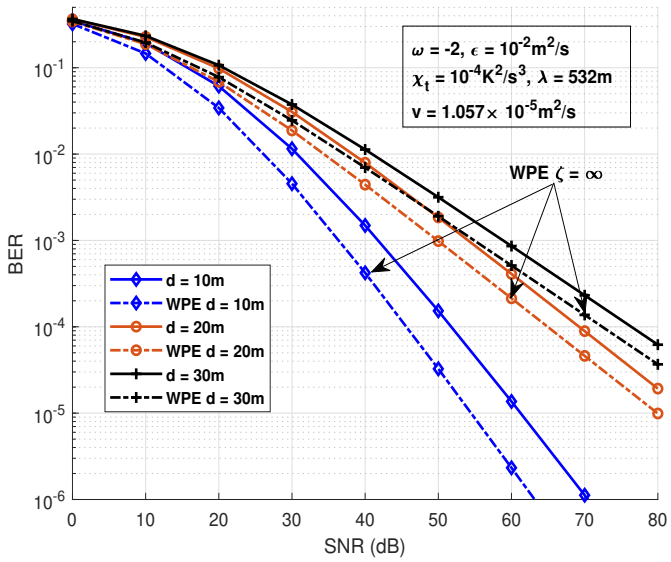

Figure 3.4: The BER performance of SIMO-UVLC system model is depicted and comprised with pointing error and WPE under strong turbulence channel conditions in SIO. The performance metrics are obtained on increasing vertical depth from water surface in affection of varying temperature, pressure, density, salinity, while the other parameters are fixed.

salinity while the performances of the proposed system model reduce by varying depth because of the physio-chemical properties of the water. The α and β particles increase due to increasing depth, it means the high turbulence and pressure occurs at increasing depth. Due to the reason, the performance decrease with increasing vertical depth of communication node or setup. As compared the performance of the proposed system model with no pointing error, the superior performance at each depth is also depicted in Fig. 3.4.

The impact of the pointing error on the BER of the proposed system is illustrated by Fig 3.5. Expectedly, the BER decreases when ω_0 decreases from 1.60 to 1.20 in the average SNR regimes. There is a huge gap while pointing error changes from 1.20 to 1.40 when average SNR $\geq$ 30dB. It could be explain as the large pointing error impairment has high accuracy at the high SNR regimes. It is noteworthy that the BER performance is obtained at infinite value of ξ=∞, which corresponds to the no pointing error at fix vertical distance PSU = 20m. Following the same pattern in Fig. 3.4 the other parameters ϵ, χ_T, and ω_0 are fixed.

Fig.3.6 shows the varying LEDs arrangement at the receiver end that affect the BER performance within the strong turbulence channel and misalignment of the transceivers. It could be depicted that the better performance is obtained of the system in without pointing error scenario. The best performance is depicted at M = 2, while increasing M values performance reduces simultaneously. It can be stated that the intensity of the optical beam distributes and received average SNR decreases. In other means, reducing M supports to improve the system performance in both of the misalignment phenomena in highly turbulence channel conditions.

The outage performance of the proposed system is the most significant approach to obtain the E2E performance for the purpose of real-time monitoring. In Fig. 3.7, we obtained the SIMO-UVLC

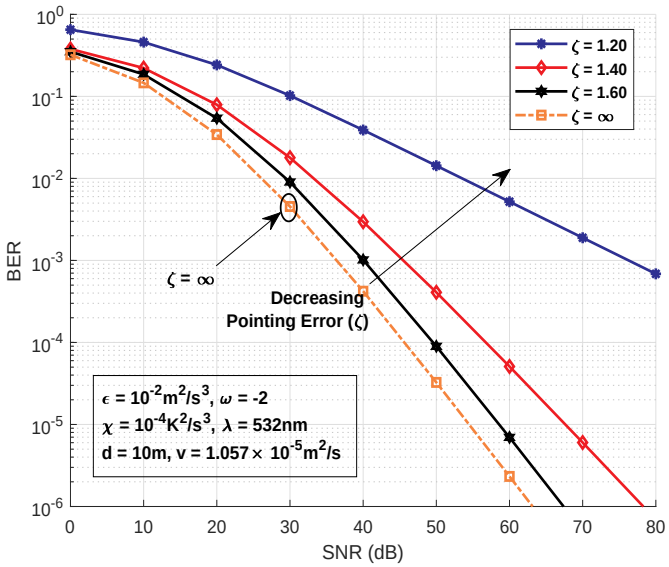

Figure 3.5: The BER performance of SIMO-UVLC system model is depicted and comprised with and without misalignment phenomena of transceivers due to water current, water flow, and physio-chemical properties in SIO. The performance metrics are obtained on varying pointing error that affect the corresponding BER performance of the system. The performances are depicted when the setup is situated at 10m below the water surface while other physio-chemical properties of water are remain fixed.

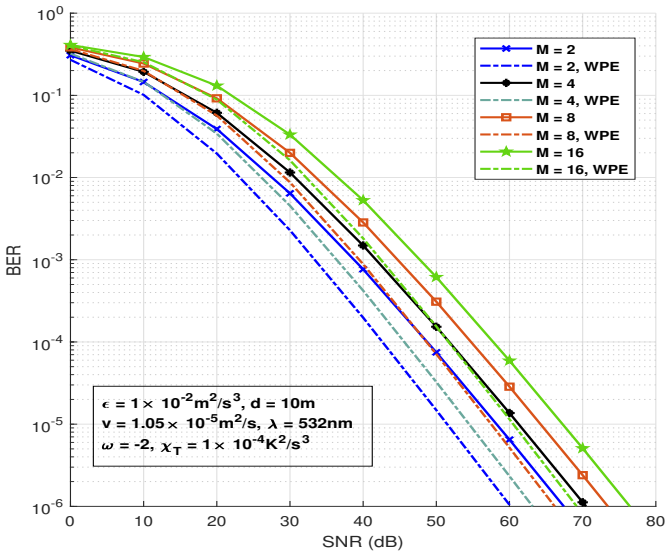

Figure 3.6: The BER performances of SIMO-UVLC system model are obtained on varying number of receiver LEDs at receiver end. The performances are depicted as square or spherical 2, 4, 8, and 16 LEDs array arrangement along with the comparison of with and WPE scenario of transceivers due to water current, and physio-chemical properties in SIO. The performances are depicted when the setup is situated at 10m below the water surface while other physio-chemical properties of water are remain fixed.

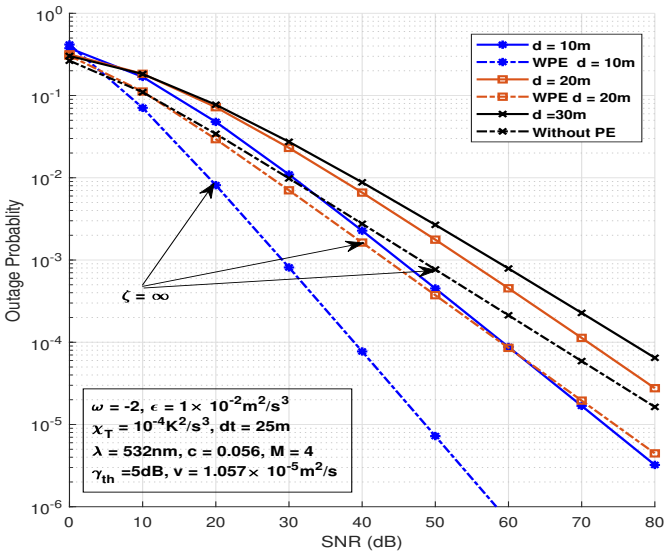

Figure 3.7: The outage performance of SIMO-UVLC system model is obtained on varying vertical depth with and without pointing error phenomenon. It is noteworthy that on varying vertical distance the performance reduces because of the physio-chemical properties of water while the other parameters are kept constant in SIO. The performance are obtained on the basis of the experimental data and the distance is measured from the water surface.

outage performance within pointing error and WPE scenarios. Even though, the water currents and physio-chemical properties directly affect the performance. To obtain the outage performance on the experimental data provided is challenging and taken on varying vertical distances while the transceivers are kept fix distance 25m. The best performance is obtained at 10m, when the transceivers consider properly aligned. An interesting insight could be seen as huge gap between the performance at 10m and 20m within & WPE scenario. It can be explain that the upper layer of the ocean is kept contact of sunlight and the temperature and salinity are higher in quantity. In existing literature it is recorded that on increasing temperature and salinity the performance raises. As a result, if we target 10^{-5} the outage performance at 10m is achieved at 73dB rather than the corresponding outage performances at 20m and 30m vertical distances. So far, it seems that superior outage performances are obtained in WPE conditions regardless of the water types.

Aforementioned that misalignment phenomena is an affecting factor on the system performances. However, in no pointing error scenario the performance metrics show on the superiority over considering with pointing error. Due to this, in Fig. 3.8 depicts the outage performances on varying ξ factor. The corresponding outcomes of the system are obtained on varying ξ parameter. It is depicted that the decreasing ξ factor the outage performance of the system improves. The outage performances are obtained while the other parameters are fixed and the system is considered at 20m below the water level.

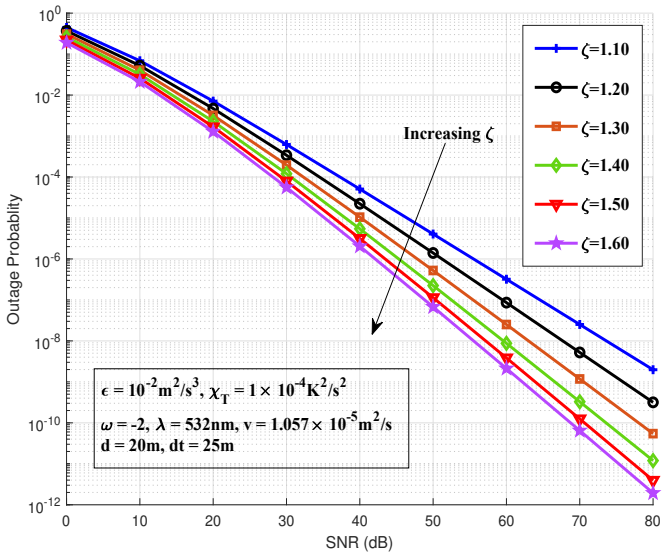

Figure 3.8: The outage performance of SIMO-UVLC system model is depicted on varying pointing error. It is clearly seen that on decreasing pointing error the outage performance of the system increases. The performance are obtained at fix vertical distance 20m while the transceivers apart 25m in strong turbulence channel conditions.

3.6 Conclusions

In this research the average BER and outage probability are widely investigated of SIMO-UVLC system. The whole system is model LED through GG distribution following OOK modulation scheme in consideration of misalignment phenomena as well as within the strong turbulence conditions in SIO. Throughout this study, the simulated performance metrics are obtained for the first time based on the experimental data available during the whole year during 2016 in SIO. The analytical works are simulated with various physio-chemical properties of the water at different vertical depth and multiple k^{th} horizontal water layers along with 2^M arrangement of LEDs at the receiver end. Additionally, we provide an updated closed form expression for infinite pointing error and the results are compared with no pointing error conditions, respectively. The simulation results are validated by derived expressions also analytically verifies by MC approach throughout this study. Attentively, it founds that the performance metrics deteriorate when the physio-chemical properties vary. So far, it is obtained that without pointing error the E2E performances are superior in the proposed SIMO-UVLC system model regardless of the water type. It would be interesting to extend the proposed system model in multi-hop energy harvesting hybrid communication for the support of high quality UWOC and localization.

The contributed chapter is published in **one Q1** and **one** Q2 Journal as follows;

1. **Ali Mohammad Furqan**, and Dushantha Nalin K. Jayakody†. "SIMO-underwater visible light communication (UVLC) system." Computer Networks 232 (2023): 109750. doi.org/10.1016/j.comnet.2023.109750 **Q1, IF 4.4**.

2. **Ali Mohammad Furqan**, and Dushantha Nalink K. Jayakody†." Performance Analysis of SIMO-UVLC System in Mix-water Medium". (Accepted and in Printing process, Engineering Reports, Wiley. **Q2, IF 2.29**.

Chapter 4

Performance Analysis of Multi-Hop UVLC System: A River meets Ocean Scenario

4.1 Introduction

The extension of the previous chapter, this research work presents a unified E2E performance of the UVLC system within estuaries (fresh river water mixed with sea salt water). In this regard, a full-duplex data encryption/decryption UVLC system model is investigated, which is subjected to heterodyne detection and IM/DD schemes in the presence of transceivers misalignment within moderate-to-strong turbulence channel conditions. More specifically, the novel closed-form expressions are derived by utilizing both of the probability distribution function and cumulative distribution function in terms of the generalized Meijer-G function as a continuation of the EBGMGF. In this work, the two consecutive Decode-and-Forward (DF) relay protocols are used to assist information within three different aqueous mediums such as river, estuary, and ocean. It is noteworthy that the transceiver's pointing error is designed by exponential distribution while the GG distribution is used to model turbulence channel conditions. Further, the performance metrics in the presence and absence of pointing error i.e., BER, outage performance, and the channel capacity for an individual channel. For the accuracy of the proposed system, the MC simulation approach is used for proper curve fittings. Finally, all simulation results are verified by analytically derived expressions.

4.1.1 Motivation and Contribution

Motivated by this research, the river-meets-ocean UVLC system model for the purpose of various shallow-deep underwater wireless applications is investigated. Currently, time there are plenty of natural hazards such as floods, earthquakes, submerging landscapes, and effectiveness marine lives event are the most significantly observed. Along with plenty of applications such as goods transportation, connecting small islands, and data collection of aqueous mediums are extensively

required for further analyses, also the necessity is to develop a high capacity and real-time data monitoring system in highly critical channel conditions. However, to the best of authors knowledge, there are very limited work available in existing literature, where the E2E performance metrics in mixed waters specially including estuaries estimation are well studied and investigated based on experimental data within the river-meets-ocean scenario. The major contributions of this research are as follows;

- This study is mainly focused on the behaviour of UVLC communication in mixed water for various underwater applications such as water pollution, marine life, land decay, irrigation, crops harvesting, water quality, fishing industry, connecting small islands, and exploration of water reservoirs. This research emphasizes to improve the UVLC link efficiency, QoS of the system over long ranges coverage in a particular aqueous sectors. However, most of the studies are based on an independent channel conditions and mainly focused inherent properties.

- Throughout this research, an advanced framework to analyze the performance metrics in moderate-strong turbulence channel conditions of triple-Hops UVLC system followed by EBGMGF function. By utilizing the two consecutive DF relay protocols with fixed gain the performance metrics are derived analytically under different modulation techniques, and further verified through simulation outcomes. However, the turbulence and misalignment of transceivers are strongly considered to obtain the E2E SNR for the proposed system model.

- More specifically, the derived expressions are the extended form of our previous study Chapter 3. The main cause of signal impairments such as the impurity, water flow, suspended particles, absorption, and scattering of the beam are the source of fading. Therefore, we have included all of these aspects of signal fading and modeled the large (α) and small scale (β) parameters through spherical wave model consideration. Further, the PDF and CDF are analytically derived for the closed-form expression with combining each and individual hop. The simulation results are verified the analytical expressions.

- As a benchmark, throughout this chapter an updated spectrum model for UOT and simulated the results on varying dissipation rate of the mean squared temperature of refractive index χ_T, the relative strength of temperature and salinity ω, the dissipation rate of turbulent kinetic energy per unit mass of fluid dissipation. In summary, the E2E performances are depicted and verified by analytically as well as simulating the physio-chemical properties of water.

4.1.2 Chapter Organization

The chapter 4 is structured as follows: The statistical channel model within the strong channel conditions (GG distribution), pointing error (Exponential distribution), and the path-loss (Beer's Law) channel coefficients are modeled in Section 4.2. Subsequently, the analytical expressions of E2E performances by following the G-Meijer function and DF relay protocol analysis are

summarized in Section 4.3. Furthermore, the numerical and simulation results are recorded in Section 4.4. Finally, the whole work is concluded in Section 4.5.

4.2 System Model

The schematic diagram of the proposed system model is depicted in Fig.4.1, where the river-based source (s) communicates through UVLC link via the two consecutive regenerative relay protocols (r_1 and r_2 are situated at the boundary of the estuary) with the fixed destination (d) located in the ocean. Each communication node is implied by the two directional antennas for signal encryption/decryption in full duplex mode. Therefore, the received signal at the destination is expressed as follows;

$$y_d(t) = R_i \eta_i I x(t) + n_i(t), \tag{4.1}$$

where the optical to electrical conversion efficiency and photo-detector responsivity for each hop is denoted by η_i, and R_i, with $i \in \{s{-}r_1, r_1{-}r_2, r_2{-}d\}$ respectively. The transmitted information symbol x(t) under the OOK modulation scheme under the AWGN with zero mean and σ_i^2 variance is represented by $n_i(t)$. Moreover, the instantaneous intensity light gain I is the combined influence of each channel condition is considered as $I{=}\prod_{i=1}^{n}(I_l I_p I_t)_i$. The channel conditions are modeled individually in further sections of this study. In this study the authors consider the transceivers are communicating in bi-directional fashion, where an each of individual node is capable of adapting beam divergence angle (ϕ), $\forall \phi \in [0 \leq \phi \leq \phi_{max}]$. Naturally, the optical beam attenuates in underwater due to photons absorption and scattering phenomena which are the wavelength dependent.

As Fig . 4.1, poses a fundamental trade off among communication range and divergence angle. It means the large angle can reach the nearby node while the narrow divergence angle is used for farthest destination. Therefore, the Beer's law, the path loss factor in LOS communication including geometric loss is given as;

$$I_l \approx \left(\frac{A cos(\phi)}{\theta_{1/2}}\right)^2 \exp\left[-\frac{c(\lambda) d_{max}}{cos(\phi)}\left(\frac{A cos(\phi)}{\theta_{1/2} d_{max}}\right)^{\tau}\right], \tag{4.2}$$

where A, $\theta_{1/2}$, τ, and d_{min} are defined as the aperture diameter, half-beam width divergence angle, the correction coefficient, and the maximum distance between nodes.

The pointing error phenomena is another signal fading factor in line of sight LOS-UVLC, which occurs because of transceivers misalignment due to water currents and random deflection of communication nodes. Therefore, in this work the pointing error impairments in terms of PDF of optical irradiance is given as [32];

$$f_{I_p}(I_p) = \frac{\zeta^2}{A_0^{\zeta^2}} I_p^{\zeta^2 - 1} 0 \leq I_p \leq A_0, \tag{4.3}$$

Additionally, the instantaneous SNR (Υ) of combined channel conditions could be written as $\Upsilon = (R_i \eta_i)^2 \{I\}^2 / \sigma_i^2$. More explicitly, the equivalent SNR of the system for N^{th} channels/hops could be written as follows [57];

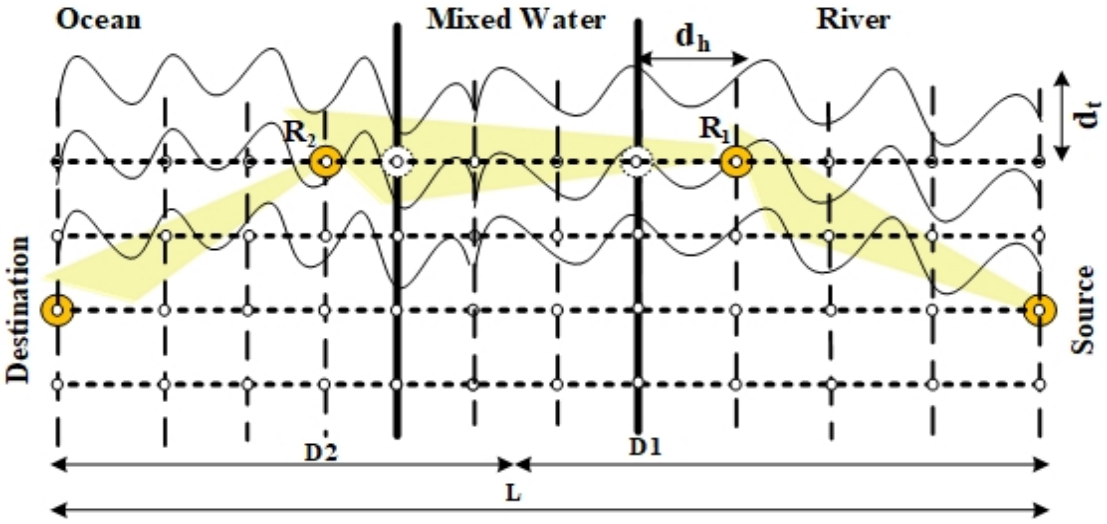

Figure 4.1: The proposed river-meets-ocean VLC system model. The system model is designed by implying two regenerative relay protocols for assisting optical signal transmission.

$$\Upsilon_{eq} = \left[\prod_{n=0}^{N}\left(1+\frac{1}{\Upsilon_n}\right)-1\right]^{-1}, \tag{4.4}$$

where n is the number of relays and according to the system model Υ_{eq} is the E2E SNR of the three consecutive relay-hops expressed as,

$$\frac{1}{\Upsilon_{eq}} = \frac{1}{\Upsilon_{sr_1}} + \frac{1}{\Upsilon_{r_1r_2}} + \frac{1}{\Upsilon_{r_2d}} + \frac{1}{\Upsilon_{sr_1}\Upsilon_{r_1r_2}} + \frac{1}{\Upsilon_{r_1r_2}\Upsilon_{r_1d}} + \frac{1}{\Upsilon_{r_2d}\Upsilon_{sr_1}}. \tag{4.5}$$

The most influencing phenomena of optical signal impairment is turbulence which occurs due to random variation of physio-chemical properties of water and further leads scintillation index. Since the turbulence fading follows the GG distribution fading model and probability PDF can be expressed as follow [58];

$$f_{\Upsilon_i}(\Upsilon_i) = \frac{\zeta_i^2}{\psi_i \Upsilon \Gamma\alpha_i \Gamma\beta_i} G_{1,3}^{3,0}\left(\frac{\zeta_i^2\alpha_i\beta_i}{\zeta_i^2+1}\left(\frac{\Upsilon}{\mu}\right)^{\frac{1}{\psi_i}}\middle| \begin{matrix}\zeta_i^2+1\\ \zeta_i^2,\alpha_i,\beta_i\end{matrix}\right), \tag{4.6}$$

where α_i and β_i are the large and small scale suspended particles in underwater environment for an individual hop. The parameter ψ is indicating the type of detection technique ($\psi = 1$ for heterodyne detection and $\psi = 2$ for direct detection technique). Furthermore, integrating (4.6) as $F_{\Upsilon_i}(\Upsilon_i) = \int_0^{\Upsilon_i} f_{\Upsilon_i}(\Upsilon_i)d\Upsilon_i$, and utilizing the properties of wolfarm mathematica [56, p. 07.34.21.0084.01] to obtain outage probability of an individual hop in terms of the CDF by (4.7) as follows;

$$F_{\Upsilon_i}(\Upsilon_i) = \frac{\psi_i^{(\alpha_i+\beta_i-2)}\zeta_i^2}{(2\pi)^{\psi_i-1}\Gamma\alpha_i\Gamma\beta_i} \times G_{\psi_i+1,3\psi_i+1}^{3\psi_i,1}\left(\left(\frac{\zeta_i^2\alpha_i\beta_i}{\psi_i^2(\zeta_i^2+1)}\right)^{\psi_i}\left(\frac{\Upsilon_i}{\mu_{\psi_i}}\right)\middle| \begin{matrix} 1, \frac{\zeta_i^2+1}{\psi_i}, ..., \frac{\zeta_i^2+\psi_i}{\psi_i} \\ \frac{\zeta_i^2}{\psi_i}, ..., \frac{\zeta_i^2+\psi_i-1}{\psi_i}, \frac{\alpha_i}{\psi_i}, ... \frac{\alpha_i+\psi_i-1}{\psi_i}, \frac{\beta_i}{\psi_i}, ... \frac{\beta_i+\psi_i-1}{\psi_i}, 0 \end{matrix}\right). \tag{4.7}$$

4.3 The End-End (E2E) Performance Analysis

In this section, the optical performance metrics are analytically derived of the proposed system and widely discussed based on the channel characteristics. Besides of it, the performance metrics in terms of closed-form expressions are provided by utilizing the PDF and CDF in the presence and absence of pointing error in harsh turbulence channel conditions.

4.3.1 Outage Performance

The outage performance is defined as the probability that should be less than or equal to the received threshold SNR. An exact closed-form expression for outage performance of the system by following EBGMGF in both of heterodyne and IM/DD schemes in the presence and absence of misalignment of transceivers is written by (4.12), (4.13) and (4.14). Therefore, the E2E outage probability in this proposed system model can be expresses as follows [59];

$$P_{out}(\Upsilon_{th}) = Pr[min(\Upsilon_{sr_1}, \Upsilon_{r_1r_2}, \Upsilon_{r_2d}) \leq \Upsilon_{th}], \tag{4.8}$$

where Υ_{sr_1}, $\Upsilon_{r_1r_2}$, and Υ_{r_2d} are the instantaneous SNR of each link, respectively. Furthermore, the equivalent CDF in terms of outage probability of the system can be written as (4.9) and extend by (4.10) as follows;

$$F_{\Upsilon_{eq}}(\Upsilon) = 1 - [(1 - F_{\Upsilon_{sr_1}}(\Upsilon))(1 - F_{\Upsilon_{r_1r_2}}(\Upsilon))(1 - F_{\Upsilon_{r_2d}}(\Upsilon)]. \tag{4.9}$$

Expanding the expression in (4.9) into (4.10), the outage probability of the proposed system is expressed by (4.11) that refers to (4.12), where the terms I_1, I_2, and I_3 are showing outage performances analytically for an individual link.

$$\begin{aligned} P_{out}(\Upsilon_{th}) &= F_{\Upsilon_{eq}}(\Upsilon_{th}) = Pr(\Upsilon_{eq} \leq \Upsilon_{th}) = 1 - [(1 - F_{\Upsilon_{sr_1}}(\Upsilon_{th}))(1 - F_{\Upsilon_{r_1r_2}}(\Upsilon_{th}))(1 - F_{\Upsilon_{r_2d}}(\Upsilon_{th})] \\ &= \underbrace{F_{\Upsilon_{sr_1}}(\Upsilon_{th}) + F_{\Upsilon_{r_1r_2}}(\Upsilon_{th}) + F_{\Upsilon_{r_2d}}(\Upsilon_{th})}_{I_1} + \underbrace{F_{\Upsilon_{sr_1}}(\Upsilon_{th})F_{\Upsilon_{r_1r_2}}(\Upsilon_{th})F_{\Upsilon_{r_2d}}(\Upsilon_{th})}_{I_3} \\ &\underbrace{- F_{\Upsilon_{sr_1}}(\Upsilon_{th})F_{\Upsilon_{r_1r_2}}(\Upsilon_{th}) - F_{\Upsilon_{r_1r_2}}(\Upsilon_{th})F_{\Upsilon_{r_2d}}(\Upsilon_{th}) - F_{\Upsilon_{r_2d}}(\Upsilon_{th})F_{\Upsilon_{sr_1}}(\Upsilon_{th})}_{I_2}, \end{aligned} \tag{4.10}$$

$$P_{out}(\Upsilon_{th}) = I_1 - I_2 + I_3 = \sum_{j=1}^{3}\left[F_{\Upsilon_j}(\Upsilon_j)\right] - \sum_{j=1}^{3}\left[\prod_{k=1}^{3}F_{\Upsilon_{j,k}}(\Upsilon_j)\right] + \prod_{j=1}^{3}(F_{\Upsilon_j}(\Upsilon_j)), \tag{4.11}$$

$$P_{out} = \frac{1}{C_\psi^3}\Bigg[C_\psi^2\Bigg\{\Xi_1 G_{\psi+1,3\psi+1}^{3\psi,1}\left(\frac{D_1\Upsilon_{th}}{\mu_{\psi_{sr_1}}}\middle|\begin{matrix}1,\varkappa_1\\ \varkappa_2,0\end{matrix}\right)+\Xi_2 G_{\psi+1,3\psi+1}^{3\psi,1}\left(\frac{D_2\Upsilon_{th}}{\mu_{\psi_{r_1r_2}}}\middle|\begin{matrix}1,\varkappa_3\\ \varkappa_4,0\end{matrix}\right)$$
$$+\Xi_3 G_{\psi+1,3\psi+1}^{3\psi,1}\left(\frac{D_3\Upsilon_{th}}{\mu_{\psi_{r_2d}}}\middle|\begin{matrix}1,\varkappa_5\\ \varkappa_6,0\end{matrix}\right)\Bigg\}$$

$$-C_\psi\Bigg\{\Xi_1\Xi_2 G_{0,0:\psi+1,3\psi+1:\psi+1,3\psi+1}^{0,0:3\psi,1:3\psi,1}\left(\frac{D_1\Upsilon_{th}}{\mu_{\psi_{sr_1}}},\frac{D_2\Upsilon_{th}}{\mu_{\psi_{r_1r_2}}}\middle|\begin{matrix}1,\varkappa_1\\ \varkappa_2,0\end{matrix}\middle|\begin{matrix}1,\varkappa_3\\ \varkappa_4,0\end{matrix}\right)$$
$$+\Xi_2\Xi_3 G_{0,0:\psi+1,3\psi+1:\psi+1,3\psi+1}^{0,0:3\psi,1:3\psi,1}\left(\frac{D_2\Upsilon_{th}}{\mu_{\psi_{sr_1}}},\frac{D_3\Upsilon_{th}}{\mu_{\psi_{r_1r_2}}}\middle|\begin{matrix}1,\varkappa_3\\ \varkappa_4,0\end{matrix}\middle|\begin{matrix}1,\varkappa_5\\ \varkappa_6,0\end{matrix}\right)$$
$$+\Xi_3\Xi_1 G_{0,0:\psi+1,3\psi+1:\psi+1,3\psi+1}^{0,0:3\psi,1:3\psi,1}\left(\frac{D_3\Upsilon_{th}}{\mu_{\psi_{r_2d}}},\frac{D_1\Upsilon_{th}}{\mu_{\psi_{sr_1}}}\middle|\begin{matrix}1,\varkappa_5\\ \varkappa_6,0\end{matrix}\middle|\begin{matrix}1,\varkappa_1\\ \varkappa_2,0\end{matrix}\right)\Bigg\}$$
$$+\Bigg\{\Xi_1\Xi_2\Xi_3 G_{\psi+1,3\psi+1}^{3\psi,1}\left(\frac{D_1\Upsilon_{th}}{\mu_{\psi_{sr_1}}}\middle|\begin{matrix}1,\varkappa_1\\ \varkappa_2,0\end{matrix}\right)G_{\psi+1,3\psi+1}^{3\psi,1}\left(\frac{D_2\Upsilon_{th}}{\mu_{\psi_{r_1r_2}}}\middle|\begin{matrix}1,\varkappa_3\\ \varkappa_4,0\end{matrix}\right)G_{\psi+1,3\psi+1}^{3\psi,1}\left(\frac{D_3\Upsilon_{th}}{\mu_{\psi_{r_2d}}}\middle|\begin{matrix}1,\varkappa_5\\ \varkappa_6,0\end{matrix}\right)\Bigg\}\Bigg]. \tag{4.12}$$

where $C_\psi = (2\pi)^{\psi-1}$ and the parameters are used in (4.12) to obtain the closed-form expression of outage performance of the system are written as follows;

$$\Xi_1 = \frac{\psi_{sr_1}^{(\alpha_{sr_1}+\beta_{sr_1}-2)}\zeta_{sr_1}^2}{\Gamma\alpha_{sr_1}\Gamma\beta_{sr_1}}, \Xi_2 = \frac{\psi_{r_1r_2}^{(\alpha_{r_1r_2}+\beta_{r_1r_2}-2)}\zeta_{r_1r_2}^2}{\Gamma\alpha_{r_1r_2}\Gamma\beta_{r_1r_2}}, \Xi_3 = \frac{\psi_{r_2d}^{(\alpha_{r_2d}+\beta_{r_2d}-2)}\zeta_{r_2d}^2}{\Gamma\alpha_{r_2d}\Gamma\beta_{r_2d}},$$

$$D_1 = \left(\frac{\zeta_{sr_1}^2\alpha_{sr_1}\beta_{sr_1}}{\psi_{sr_1}^2(\zeta_{sr_1}^2+1)}\right)^{\psi_{sr_1}}, D_2 = \left(\frac{\zeta_{r_1r_2}^2\alpha_{r_1r_2}\beta_{r_1r_2}}{\psi_{r_1r_2}^2(\zeta_{r_1r_2}^2+1)}\right)^{\psi_{r_1r_2}}, D_3 = \left(\frac{\zeta_{r_2d}^2\alpha_{r_2d}\beta_{r_2d}}{\psi_{r_2d}^2(\zeta_{r_2d}^2+1)}\right)^{\psi_{r_2d}},$$

If it is considered that both of the relays are in idle state, and only the source directly communicates with the destination (P2P Communication System). Therefore the outage performance of P2P system could be obtain by (4.13) and (4.14) in hetrodyne and IM/DD detection scenarios.

$$P_{out} = \frac{\psi^{(\alpha+\beta-2)}\zeta^2}{(2\pi)^{\psi-1}\Gamma\alpha\Gamma\beta}G_{\psi+1,3\psi+1}^{3\psi,1}\left(\frac{(\zeta^2\alpha\beta)^\psi}{(\zeta^2+1)^\psi\psi^{2\psi}}\left(\frac{\Upsilon_{th}}{\mu_\psi}\right)\middle|\begin{matrix}1,\frac{\zeta^2+1}{\psi},\ldots,\frac{\zeta^2+1}{\psi}\\ \frac{\zeta^2}{\psi},\ldots,\frac{\zeta^2+\psi-1}{\psi},\frac{\alpha}{\psi},\ldots\frac{\alpha+r-1}{\psi},\frac{\beta}{\psi},\ldots\frac{\beta+\psi-1}{\psi},0\end{matrix}\right). \tag{4.13}$$

$$P_{out_{(IM/DD)}} = \frac{2^{(\alpha+\beta-2)}\zeta^2}{2\pi\Gamma\alpha\Gamma\beta}G_{3,7}^{6,1}\left(\left(\frac{\zeta^2\alpha\beta}{4(\zeta^2+1)}\right)^2\left(\frac{\Upsilon_{th}}{\mu_r}\right)\middle|\begin{matrix}1,\frac{\zeta^2+1}{2},\frac{\zeta^2+2}{2}\\ \frac{\zeta^2}{2},\frac{\zeta^2+1}{2},\frac{\alpha}{2},\frac{\alpha+1}{2},\frac{\beta}{2},\frac{\beta+1}{2},0\end{matrix}\right). \tag{4.14}$$

4.3.2 The Average Bit-Error Rate (ABER) Performance

In this section, the closed-form analytical expressions of BER performances in river-meets-ocean mixed water system is provided. Additionally, the BER performance metrics are analytically derived

within and without the pointing error scenarios. Following the equation [60, Eq. 12] for different modulation schemes, the BER performance of the system for an individual hop could be find by the equation (4.15). Therefore, for an individual hop an analytical BER expression is written by (4.15) where the modulation parameters p and q are defined in the Table 4.1 as followings;

$$BER_i = \frac{q^p}{2\Gamma(p)} \int_0^\infty \exp(-q\Upsilon_i)\Upsilon_i^{p-1} F_\Upsilon(\Upsilon_i) d\Upsilon_i \tag{4.15}$$

Table 4.1: The parameter in expression (4.15) are used to obtain the analytical expression for BER performance metrics in different optical modulation techniques.

Modulation Scheme	**p**	**q**
Coherent Binary Frequency Shift Keying (CBFSK)	0.5	0.5
Coherent Binary Shift Keying (CBPSK)	0.5	1
Non-Coherent Binary Frequency Shift Keying (NBFSK)	1	0.5
Differential Binary Phase Shift Keying (DBPSK)	1	1

Further plug (4.7) into (4.15) for sr_1 link and utilizing the properties of G-meijer function [56, Eq. 07.34.21.0088.01] for integration and get the expressions (4.17) and (4.18) for an individual hop. Similarly, for $r_1 - r_2$ and $r_2 - d$ hops, the BER could be written by (4.19) and (4.20). Therefore, the unified BER expression for for N^{th} hops/channel is given as [33, 61];

$$BER = 1 - \prod_{n=0}^{N}(1 - BER_n), \tag{4.16}$$

where n is the number of relays. In this work the two consecutive relays are used. It should be noted that for triple hop putting $n = 2$ as in (4.16).

$$\begin{aligned} BER_{sys} &= 1 - \Big[(1 - BER_{sr_1})(1 - BER_{r_1r_2})(1 - BER_{r_2d})\Big] \\ &= BER_{sr_1} + BER_{r_1r_2} + BER_{r_2d} - BER_{sr_1}BER_{r_1r_2} \\ &- BER_{r_1r_2}BER_{r_2d} - BER_{r_2d}BER_{sr_1} + BER_{sr_1}BER_{r_1r_2}BER_{r_2d}. \end{aligned} \tag{4.17}$$

In (4.17), the BER for an individual link is mentioned. The performance metrics of an individual link is complex integration in the form of G-Meijer function. Therefore, utilizing the properties of [56, Eq. 07.34.21.0082.01] and integrating (4.15) by replacing (4.7). The BER for the sr_1 link is obtained by (4.19). Similarly, for the r_1r_2, and r_2d links, the BER expressions are derived by (4.20) and (4.21), respectively.

$$\begin{aligned} BER_{sr_1} &= \frac{q^p \psi^{(\alpha_{sr_1}+\beta_{sr_1}-2)} \zeta_{sr_1}^2}{2C_\psi \Gamma(p)\Gamma(\alpha_{sr_1})\Gamma(\beta_{sr_1})} \\ &\times \int_0^\infty \frac{\Upsilon_{sr_1}^{p-1}}{e^{(q\Upsilon_{sr_1})}} G_{\psi+1,3\psi+1}^{3\psi,1}\left(\left(\frac{\zeta_{sr_1}^2 \alpha_{sr_1}\beta_{sr_1}}{\psi^2(\zeta_{sr_1}^2+1)}\right)^\psi \frac{\Upsilon_{sr_1}}{\mu_{sr_1}}\middle| \begin{matrix} 1, \frac{\zeta_{sr_1}^2+1}{\psi}, \ldots \frac{\zeta_{sr_1}^2+\psi}{\psi} \\ \frac{\zeta_{sr_1}^2}{\psi}, \ldots \frac{\zeta_{sr_1}^2+\psi-1}{\psi}, \frac{\alpha_{sr_1}}{\psi}, \ldots \frac{\alpha_{sr_1}+\psi-1}{\psi}, \ldots \frac{\beta_{sr_1}+\psi-1}{\psi}, 0 \end{matrix}\right) d\Upsilon_{sr_1} \end{aligned} \tag{4.18}$$

$$BER_{sr_1} = \underbrace{\frac{z_1}{2C_\psi \Gamma(p)} G^{3\psi,2}_{\psi+2,3\psi+1}\left(\frac{D_{sr_1}}{q\mu_{sr_{sr_1}}}\middle| \begin{matrix} 1-p,1,\kappa_{sr_1} \\ \Phi_{sr_1},0 \end{matrix}\right)}_{A_1} \tag{4.19}$$

$$BER_{r_1r_2} = \underbrace{\frac{z_2}{2C_\psi \Gamma(p)} G^{3\psi,2}_{\psi+2,3\psi+1}\left(\frac{D_{r_1r_2}}{q\mu_{r_1r_2}}\middle| \begin{matrix} 1-p,1,\kappa_{r_1r_2} \\ \Phi_{r_1r_2},0 \end{matrix}\right)}_{A_2} \tag{4.20}$$

$$BER_{r_2d} = \underbrace{\frac{z_3}{2C_\psi \Gamma(p)} G^{3\psi,2}_{\psi+2,3\psi+1}\left(\frac{D_{r_2d}}{q\mu_{r_2d}}\middle| \begin{matrix} 1-p,1,\kappa_{r_2d} \\ \Phi_{r_2d},0 \end{matrix}\right)}_{A_3} \tag{4.21}$$

Similarly, to obtain the closed-form expression of average BER for the whole proposed system, the expressions in (4.19), (4.20), and (4.21) plug in to (4.17). The expression (4.22) is the final closed-form expression of the average BER for the whole system.

$$\begin{aligned}
\overline{BER} = \frac{1}{8C_\psi^3\Gamma(p)^3}\Bigg[& 4C_\psi^2\Gamma(p^2)\Bigg\{ z_1 \underbrace{G^{3\psi,2}_{\psi+2,3\psi+1}\left(\frac{D_{sr_1}}{q\mu_{sr_1}}\middle| \begin{matrix} 1-p,1,\kappa_{sr_1} \\ \Phi_{sr_1},0 \end{matrix}\right)}_{I_{sr1}} \\
& + z_2 \underbrace{G^{3\psi,2}_{\psi+2,3\psi+1}\left(\frac{D_{r_1r_2}}{q\mu_{r_1r_2}}\middle| \begin{matrix} 1-p,1,\kappa_{r_1r_2} \\ \Phi_{r_1r_2},0 \end{matrix}\right)}_{I_{r1r2}} + z_3 \underbrace{G^{3\psi,2}_{\psi+2,3\psi+1}\left(\frac{D_{r_2d}}{q\mu_{r_2d}}\middle| \begin{matrix} 1-p,1,\kappa_{r_2d} \\ \Phi_{r_2d},0 \end{matrix}\right)}_{I_{r2d}} \Bigg\} \\
& - 2C_\psi\Gamma(p)\Bigg\{ P_{z_1z_2} G^{0:0:3\psi,2:3\psi,2}_{0,0:\psi+2,3\psi+1:\psi+2,3\psi+1}\left(\frac{D_{sr_1}}{q\mu_{sr_1}}\middle|\frac{D_{r_1r_2}}{q\mu_{r_1r_2}}\middle| \begin{matrix} 1-p,1,\kappa_{sr_1} \\ \Phi_{sr_1},0 \end{matrix}\middle| \begin{matrix} 1-p,1,\kappa_{r_1r_2} \\ \Phi_{r_1r_2},0 \end{matrix}\right) \\
& + P_{z_2z_3} G^{0:0:3\psi,2:3\psi,2}_{0,0:\psi+2,3\psi+1:\psi+2,3\psi+1}\left(\frac{D_{r_1r_2}}{q\mu_{r_1r_2}}\middle|\frac{D_{r_2d}}{q\mu_{r_2d}}\middle| \begin{matrix} 1-p,1,\kappa_{r_1r_2} \\ \Phi_{r_1r_2},0 \end{matrix}\middle| \begin{matrix} 1-p,1,\kappa_{r_2d} \\ \Phi_{r_2d},0 \end{matrix}\right) \\
& + P_{z_3z_1} G^{0:0:3\psi,2:3\psi,2}_{0,0:\psi+2,3\psi+1:\psi+2,3\psi+1}\left(\frac{D_{r_2d}}{q\mu_{r_2d}}\middle|\frac{D_{sr_1}}{q\mu_{sr_1}}\middle| \begin{matrix} 1-p,1,\kappa_{r_2d} \\ \Phi_{r_2d},0 \end{matrix}\middle| \begin{matrix} 1-p,1,\kappa_{sr_1} \\ \Phi_{sr_1},0 \end{matrix}\right)\Bigg\} \\
& + \Big\{ P_{z_1z_2z_3} I_{sr_1} I_{r_1r_2} I_{r_2d} \Big\}\Bigg]
\end{aligned} \tag{4.22}$$

$$BER_{P2P} = \frac{\psi^{(\alpha+\beta-2)}\zeta^2}{2C_\psi\Gamma(p)\Gamma(\alpha)\Gamma(\beta)} G^{3\psi,2}_{\psi+2,3\psi+1}\left(\frac{D}{q\mu}\middle| \begin{matrix} 1-p,1,\kappa \\ \Phi,0 \end{matrix}\right) \tag{4.23}$$

4.4 Numerical Results

Throughout this section, the analytical performance metrics are presenting based on the numerical results and obtained the simulation outcomes of the proposed system model in three distinctive water mediums. In this research, it is considered that the fixed horizontal distance between

communication nodes as ($d_{s-r_1} = d_{r_1-r_2} = d_{r_2-d} = 30m$) while the vertical distance ($d_{ts} = 9m, d_{tr_1} = 14.07m, d_{r_2} = 16m$) has taken according to provided data in river, estuary, and ocean reservoir, respectively. The temperature and salinity of each water medium has taken at varying vertical depth. However, the average temperature $T = 23.92^0C$, and salinity $S = 23.04$PSU are considered at fixed vertical depth in mixed estuary water at $d_{tr_1-r_2} = 2.04m$ along with fixed pointing error $\xi = 6.5$ amongst transceivers.

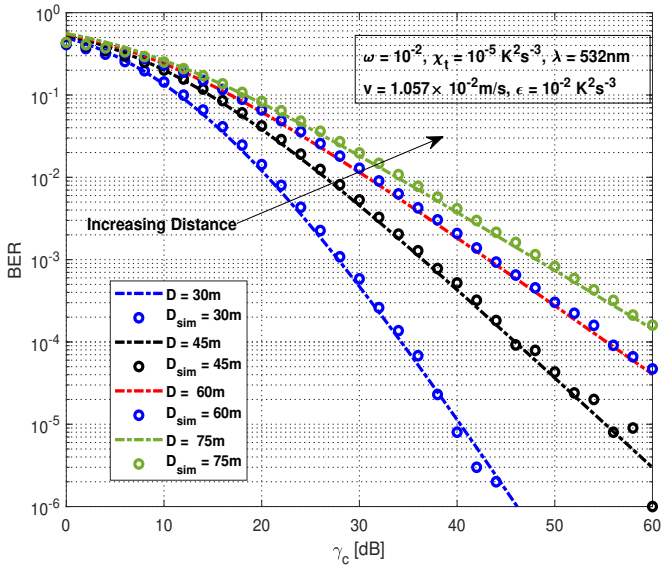

Figure 4.2: The average BER performance of the system is depicted on varying distance between the transceivers. However, the other physio-chemical parameters of water are kept constant. It is noteworthy that the performance are taken in river meets ocean scenario where the estuary has considered the mixed water mediums.

The BER performance of the system on varying distance is depicted by Fig. 4.2. It is noteworthy each node are placed equal distance from each other. It means an individual hop has equiv-distance. The eddy diffusivity (ω), the rate of dissipation of mean-square temperature χ_T, dissipation rate of turbulent kinetic energy per unit mass of fluid (ϵ), and kinematic viscosity (v) are kept constants. It is clearly seen that the BER performance is degrading on increasing distance in harsh channel conditions. The best performance of the system can be depicted at the minimum distance of nodes in low SNR regimes. If targeting BER 10^{-5}, the performance is the maximum at 40dB while it is achieved 55dB at $D = 45$m horizontal distance. However, the poorest performance is obtained at the maximum distance $D = 75$m.

The BER performance on varying eddy diffusivity ($\omega_{d_{eq}}$) are simulated in the Fig.4.3, while the other parameters are kept constant. It is noteworthy that the system offers the maximum performance at low value of eddy diffusivity and maximum performance is depicted at $\omega_{d_{eq}} = -2$. However, at low SNR conditions $\gamma = 0$ to 12dB, the triple hop investigated system has almost the same performances. On the other hand increasing SNR the simulated BER curve shows poorest outcomes. To obtain the maximum performance, the system system should be design on the lowest eddy diffusivity factor.

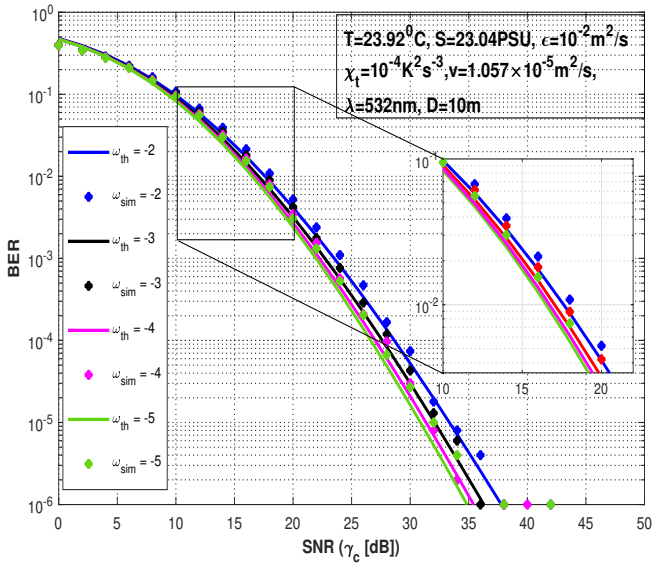

Figure 4.3: The BER performance metrics are simulated on varying ω parameters within the proposed system model. The other parameters are kept constant as T = 23.9^{0}C and S = 23.04 PSU.

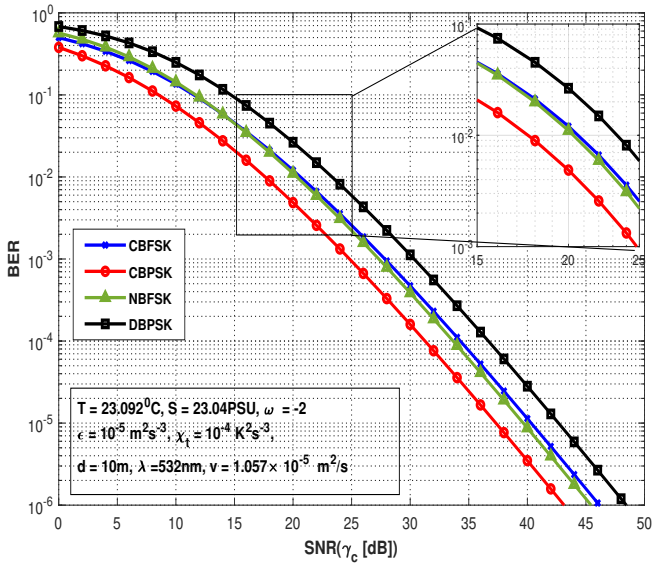

Figure 4.4: The BER performance metrics are simulated and comprised amongst various optical modulation techniques. The performances are simulated on varying channel conditions while other channel parameters are kept constant.

Throughout the Fig.4.4, the average BER performances in different higher modulation techniques are simulated and compared. The simulated results in CBPSK are offered the maximum performances while kept p = 0.5 and q = 1 values. The CBFSK and NBFSK modulation schemes show the similar performances because of the quantifying p and q parameters in expression (4.15). Therefore, it can be concluded that on the minimum p factor in phase shift keying the investigated system outperform. However, the equalizing the factors in modulation schemes shows the poorest

performances. It should be noted that other channel parameters are kept constant while dealing the performance of the proposed river-meets-ocean UVLC system.

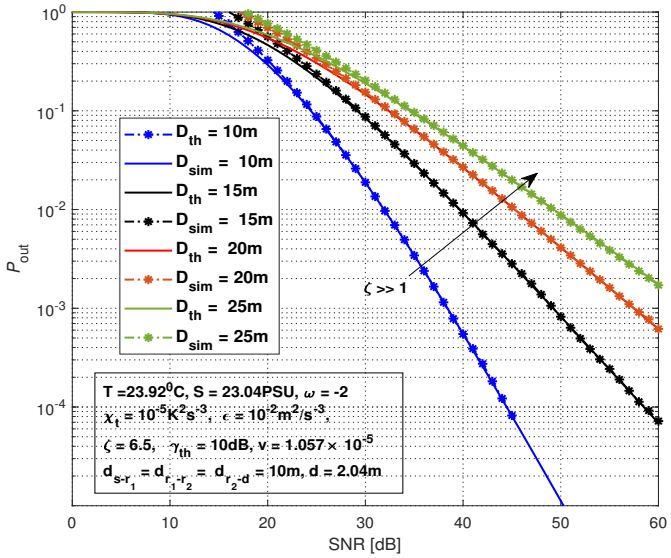

Figure 4.5: The outage performance metrics of the proposed system model are simulated on varying vertical depth in underwater environments. It is noteworthy that the vertical distance has taken for all communication nodes in fresh and salt waters. It is clearly seen that on varying vertical distance the performance curves shows poor performance. The pointing error is minimally considered and the other channel parameters kept constants.

An important insight of the system is the outage performance on varying vertical consecutive depth of the communication nodes from the water surface. The outage performances of the proposed system model are depicted on varying vertical depth in Fig. 4.5. The simulation results are based on the experimental data has taken in the SIO. The experimental data has taken on 10m to 40m and utilize to simulate the results to validate the performance metrics. The simulation results are obtained on approximately LOS scenario and the maximum performance depicts the minimum vertical depth on communication nodes. While increasing the vertical depth the performances reduce and the worst performance depicts on 25m below the water surface. An interesting huge gap between the curves is seen. It is because instantly change the physio-chemical properties of water such as reducing temperature and in increasing salinity on depth. However, the other channel parameters are kept constant and the horizontal distance between communication nodes has taken 10m.

4.5 Conclusions

In conclusion, this study successfully establishes a comprehensive understanding of the performance of UVLC system within estuaries environments, revealing the significant impact of various factors such as transceiver misalignment and channel turbulence on communication efficacy. By employing a full-duplex model tied to advanced detection and modulation schemes, and employing

innovative mathematical frameworks through the Meijer-G function, the research provides valuable insights into the dynamics of underwater communication. The incorporation of DF relay protocols across different aquatic mediums underscores the versatility of the system, while the use of MC simulations ensures the robustness of the findings. Overall, this work not only enhances the understanding of UVLC systems in challenging underwater conditions but also lays a foundation for future studies aimed at improving data transmission reliability in complex aquatic environments.

The contributed chapter is published in **two Q1** Journal and **one** international IEEE conference as follows;

1. Sajid Mumtaz, **Ali Mohammad Furqan**, and Dushantha Nalink K.Jayakody."Performance Analysis of M-ary Pulse Position Modulation on Varying Vertical Underwater System". (IEEE Access) (Under Review Process, IEEE Access). **Q2, IF 3.4**.

   Q1, I.F. 3.4.

2. **Ali Mohammad Furqan**, Dushantha Nalin K. Jayakody, Marko Beko, and Sérgio Correia. "Performance evaluation of vertical VLC link in mixed water mediums." In 2023 6^{th} Conference on Cloud and Internet of Things (CIoT), pp. 195-199. IEEE, 2023.

Chapter 5

Dual-Hop Mixed FSO-VLC Underwater Wireless Communication Link

5.1 Introduction

Optical signaling are considered as an alternative potential wireless carriers in various hybrid communication scenarios, such as indoor/outdoor signaling [62], satellite communication[63], air-to-ground base station [64], and onshore/offshore underwater hybrid cooperative communications [65]. The most significant advantages of optical communications are low in cost, unlicensed spectrum, easy to deploy in harsh channels, and play an ample role as a high connectivity wireless carriers with low latency [66]. Nevertheless, the channel impairments due to strong turbulence and misalignment of transceivers are crucial factors of signal fading in optical communications. As, FSO and VLC are the complementary links which are utilized for oceanic exploration and various underwater applications throughout this study. Thanks for highly qualitative and advantageous optical signaling as a promising communication media in wireless domain. It is noteworthy that numerous variations and fluctuations occur mainly in aqueous mediums such as oceans. Oceans are extremely deep and extensive aqueous reservoirs with random physiochemical properties of water molecules. These distinctive random properties make oceans unique and more complex channels. Therefore, oceans are typically challenging environments to deploy wireless communication setups as compared with the terrestrial-based communication links. A high quality, minimal delay, and high-speed enabled undersea communication is an essential approach for signal transmission to an underwater based AUVs or UWSNs.

To full-fill the requirement of high quality communication, optical signaling is received an impressive attention as a high speed wireless carrier with higher achievable rates (in Gbps), low latency, enhanced security, and very cost effective links for nodes connectivity and localization aspects [38]. UWSNs or AUVs connectivity with onshore/offshore BS is quiet significant approach for long ranges communication through an intermediate node (relay node). As a benchmark, in our investigated communication system, we use the spectrum model of UOT [18] to calculate the exact value suspended particles under the plane wave model on varying temperature and salinity parameters at different depth. The proposed dual-hop hybrid FSO-VLC underwater wireless

communication system model is depicted by Fig. 5.1.

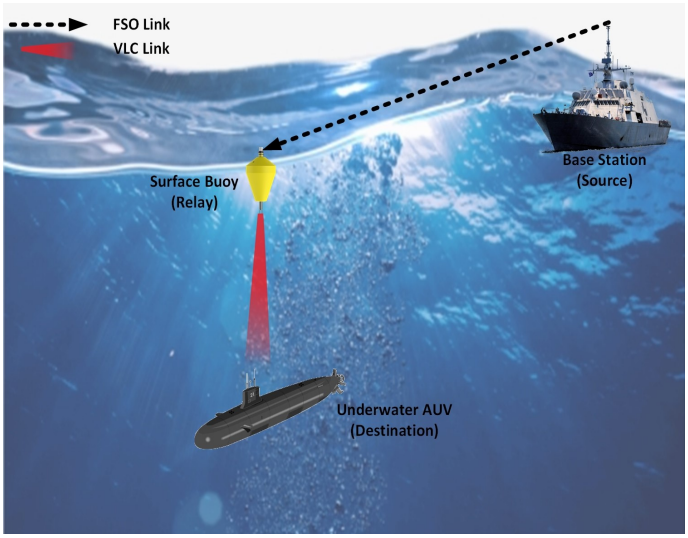

Figure 5.1: An investigated mixed dual-hop FSO-UVLC regenerative relayed communication setup, where a floating vessel (onshore BS) communicates with an autonomous underwater vehicle (AUV). It is depicted that the BS shared information with floating node through FSO link, while the relay forwards the received signals to AUV in VLC format.

5.1.1 Motivation and Contribution

In this chapter, a mixed dual-hop hybrid optical communication system under strong turbulence channel conditions is investigated and presented the outage and average BER performances of the corresponding links. Motivated by this research, the proposed system model supports human interests in various underwater applications. In summary, the below factual points are the major contribution of the study as follows:

- The corresponding dual-hop hybrid FSO-VLC system model is mainly developed to support the signal extraction terminology in various underwater mediums. Additionally, the investigated solutions emphasize to enhance the efficiency of underwater optical links. Throughout this research, the performances of a hybrid cooperative optical communication system to connect onshore/offshore nodes with AUVs in facilitating geographical mapping or bathymetrical data collection for shallow and coastal water reservoirs are observed. Therefore, the proposed system model is applicable and profitable for seaports, connecting small islands, and naval tactical operations in real-time data streaming;

- A vital role of this research work incorporates better insight of higher modulation technique following various Underwater Optical Wireless Sensor Networks (UOWSNs) architecture. Therefore, the E2E performance metrics average BER and outage probability of FSO-VLC system within the combined channel impairments are widely derived analytically;

- The proposed FSO-VLC system model is considered with a Sub-Carrier Intensity Modulation (SIM)-based DF-relay protocol for optical signaling. Moreover, the channels are modeled

under consideration of independent but not necessarily identically distributed GG signal fading distribution;

- Absorption, scattering, and physio-chemical properties of the two distinctive channels are the main influencing factors to contribute scintillation index. Due to this, the variation of scintillation index cause strong turbulence, the small scale, and large scale parameters influence is quite different in both channels and considered as a plane wave model by using turbulence spectrum model;

- A novel analytical expression of statistical characteristics for E2E SNR of the proposed system is presented. A closed-form expression is also investigated for FSO-VLC channel conditions in terms of PDF and CDF through the E2E SNR. Additionally, the outage performance and average BER of the whole system are derived by using channel statistics. Further, the simulation results are performed and verified with the theoretical results through analytical EBGMGF.

5.1.2 Chapter Organization

The rest of the paper is structured as follows: In Section 5.2, a dual-hop hybrid optical underwater wireless communication is analytical proposed for various underwater applications. The E2E performance matrics of investigated communication system are widely discussed and presented in Section 5.3. Furthermore, the numerical and simulation results are obtained in Section 5.4 and finally, the whole work is concluded by Section 5.5.

5.2 Analytical System Model

The combined influence of signal fading of the proposed system model is discussed in previous sections. Moreover, the PDF of aggregated channel conditions is expressed in [67] as follows,

$$f_{\gamma_{mn}}(\gamma_{mn}) = \frac{\zeta_{mn}^2}{\psi \gamma_{mn} P_{\Gamma\alpha_{mn}\Gamma\beta_{mn}}} G_{1,3}^{3,0}\left[P_{\alpha_{mn}\beta_{mn}} \left(\frac{\gamma_{mn}}{\overline{\gamma}_{mn}}\right)^{\frac{1}{\psi}} \middle| \begin{matrix} \zeta_{mn}^2 + 1 \\ \zeta_{mn}^2, \alpha_{mn}, \beta_{mn} \end{matrix} \right], \tag{5.1}$$

where $\Gamma(\cdot)$ and $G_{\cdot,\cdot}^{\cdot,\cdot}(\cdot|\cdot)$ are denoted as the double Gamma function and generalized Meijer-G function, while $P_{\alpha_{mn}\beta_{mn}}$ is the product of the large and small scale factors in both of the links. The parameter for detection technique is denoted by ψ. The detection parameter has taken $\psi = 1$ for hetrodyne detection while, $\psi = 2$ for direct detection and $\overline{\gamma}_{mn}$ is represented the average electrical SNR. It is noteworthy that the whole work is considered in this study under direct detection technique. Therefor, $\psi = 2$ has been taken for analytical and simulation results. However, the average SNR for both of the links is described as, $\bar{\gamma}_{mn} = \gamma_{mn} / |I_{p_{mn}} I_{t_{mn}}|^2$.

As a result, the CDF of instantaneous SNR for each link is obtained by integrating (5.1), as $F_{\gamma_{mn}}(\gamma) = \int_0^{\gamma} f_{\gamma_{mn}}(\gamma)d\gamma$ by using [68, Eq. 26] as follows,

$$F_{\gamma_{mn}}(\gamma_{mn}) = \frac{\zeta_{mn}^2}{P_{\Gamma\alpha_{mn}\Gamma\beta_{mn}}} G_{2,4}^{3,1}\left[P_{\alpha_{mn}\beta_{mn}} \sqrt{\frac{\gamma_{mn}}{\overline{\gamma}_{mn}}} \middle| \begin{matrix} 1, \zeta_{mn}^2 + 1 \\ \zeta_{mn}^2, \alpha_{mn}, \beta_{mn}, 0 \end{matrix} \right]. \tag{5.2}$$

To simplify (5.2), the above expression is modified by utilizing Meijer-G function [56, Eq. 07.34.17.0013.01], then we obtained (5.3) as,

$$F_{\gamma_{mn}}(\gamma_{mn}) = \frac{2^{\alpha_{mn}+\beta_{mn}-2}\zeta_{mn}^2}{2\pi P_{\Gamma\alpha_{mn}\Gamma\beta_{mn}}} G_{4,8}^{6,2}\left[\frac{P_{\alpha_{mn}\beta_{mn}}^2}{16\overline{\gamma}_{mn}} \gamma_{mn} \middle| \begin{matrix} \phi_1 \\ \phi_2 \end{matrix} \right]. \tag{5.3}$$

The arguments ϕ_1 and ϕ_2 are utilized in (5.3) given as follows,

$$\phi_1 = \left[\frac{\zeta_{mn}^2 + 1}{2}, \frac{\zeta_{mn}^2 + 2}{2}, \frac{1}{2}, 1 \right],$$

$$\phi_2 = \left[\frac{\zeta_{mn}^2}{2}, \frac{\zeta_{mn}^2 + 1}{2}, \frac{\alpha_{mn}}{2}, \frac{\alpha_{mn} + 1}{2}, \frac{\beta_{mn}}{2}, \frac{\beta_{mn} + 1}{2}, 0, \frac{1}{2} \right].$$

The above expression in (5.3) is complex and difficult to integrate. In addition to that for further simplification again using the properties of generalized Meijer-G function [56, Eq.07.34.03.0001.01], the expression in (5.3) is modified and obtaining CDF expression for an individual link, the expression is derives by (5.4) as follows,

$$F_{\gamma_{mn}}(\gamma_{mn}) = z_{mn} G_{3,7}^{6,1}\left[\frac{B_{mn}\gamma_{mn}}{\overline{\gamma}_{mn}} \middle| \begin{matrix} \phi_{mn} \\ \kappa_{mn} \end{matrix} \right]. \tag{5.4}$$

Adhering, the parameters were used in (5.4), are describe as follows,

$$z_{mn} = \frac{2^{\alpha_{mn}+\beta_{mn}-3}\zeta_{mn}^2}{\pi P_{\Gamma\alpha_{mn}\Gamma\beta_{mn}}}, B_{mn} = \left(\frac{P_{\alpha_{mn}\beta_{mn}}}{4} \right)^2, \phi_{mn} = \left[\frac{\zeta_{mn}^2 + 2}{2}, \frac{1}{2}, 1 \right],$$

$$\kappa_{mn} = \left[\frac{\zeta_{mn}^2 + 1}{2}, \frac{\alpha_{mn}}{2}, \frac{\alpha_{mn} + 1}{2}, \frac{\beta_{mn}}{2}, \frac{\beta_{mn} + 1}{2}, 0, \frac{1}{2} \right].$$

5.2.1 Decode-and-Forward (DF) Relay Protocol Analysis

In this proposed dual-hop cooperative communication system, a DF relay protocol is used to assist information transmission to AUV. The instantaneous SNR for FSO link $(s - r)$ and VLC link $(r - d)$ are represented by γ_{sr} and γ_{rd}, respectively. Furthermore, the equivalent instantaneous SNR (γ_{DF}) for the whole system could be expressed as follows [69],

$$\gamma_{DF} = min(\gamma_{sr}, \gamma_{rd}). \tag{5.5}$$

For efficient decoding signal at relay and receiver end, the CDF $F_{DF}(\gamma_{DF})$ of equivalent instantaneous SNR γ_{DF} should be less than or equal to the threshold SNR (γ_{th}), which can be derived as,

$$F_{DF}(\gamma_{DF}) = P_r(\gamma_{DF} \leq \gamma_{th}) = P_r[min(\gamma_{sr}, \gamma_{rd} \leq \gamma_{th})]. \tag{5.6}$$

Consequently, the independency of the instantaneous SNR for each of link is defined as the above expression in (5.7), which can be further expand and rewritten as,

$$\begin{aligned} F_{\gamma_{DF}}(\gamma_{DF}) &= Pr(\gamma_{sr} \leq \gamma_{th}) + Pr(\gamma_{rd} \leq \gamma_{th}) - Pr(\gamma_{sr} \leq \gamma_{th})Pr(\gamma_{rd} \leq \gamma_{th}), \\ &= F_{\gamma_{sr}}(\gamma_{sr}) + F_{\gamma_{rd}}(\gamma_{rd}) - F_{\gamma_{sr}}(\gamma_{sr})F_{\gamma_{rd}}(\gamma_{rd}). \end{aligned} \tag{5.7}$$

The CDF of instantaneous SNR for $s-r$ and $r-d$ links, $F_{\gamma_{sr}}(\gamma_{sr})$ and $F_{\gamma_{rd}}(\gamma_{rd})$ for each individual hop already calculated by (5.4), which could be replace in (5.6) to obtain the outage probability, of the system.

5.3 Performance Analysis of Outage Probability

The analytical expressions of outage probability performance for the corresponding system are derived in this section. Additionally, the outage performances of the system are formulated and analysed in the presence of pointing error and without pointing error scenarios, respectively. Adequately, we sub-divided this section in two parts; firstly we derive the expression of outage performance in consideration of pointing errors. Secondly, the expressions are provided by excluding misalignment phenomena of the transceivers.

5.3.1 The Outage Performance with and without Pointing Error

The outage probability of the system is formulated when the instantaneous SNR should equal or below the threshold SNR conditions. Thus, the outage performance of the system could be defined as follows,

$$P_{out} = F_{\gamma}(\gamma) = Pr[min(\gamma_{sr}, \gamma_{rd}) < \gamma_{th}]. \tag{5.8}$$

Subsequently to calculate the outage performance, replacing $F_{\gamma_{sr}}(\gamma_{th})$ and $F_{\gamma_{rd}}(\gamma_{th})$ in (5.8) by using (5.4). The above mathematical expression (5.9) could be expended as,

$$P_{out} = 1 - (1 - F_{\gamma_{sr}}(\gamma_{th}))(1 - F_{\gamma_{rd}}(\gamma_{th})) = F_{\gamma_{sr}}(\gamma_{th}) + F_{\gamma_{rd}}(\gamma_{th}) - \underbrace{F_{\gamma_{sr}}(\gamma_{th})F_{\gamma_{rd}}(\gamma_{th})}_{\phi(\gamma)}. \tag{5.9}$$

It is noteworthy that the term $\phi(\gamma)$ involves the two CDFs which is the product of two independent Meijer-G functions and can be expressed in terms of EBGMGF. The product representation of the two Meijer-G functions is derived by following the same concept as in [60, 70, 71]. The steps are following in Appendix B to formulate EBGMGF for outage performance of the investigated system. Therefore, the product of CDFs $\phi(\gamma)$ is calculated by applying Meijer-G function in [56, Eq. 07.34.16.0003.01] and obtained by (5.10) as follows,

$$\phi(\gamma) = P_{z_{sr}z_{rd}} G^{0,0:6,1:6,1}_{0,0:3,7:3,7} \left[\begin{matrix} - \\ - \end{matrix} \middle| \begin{matrix} \phi_{sr} \\ \kappa_{sr} \end{matrix} \middle| \begin{matrix} \phi_{rd} \\ \kappa_{rd} \end{matrix} \middle| B_{sr}\left(\frac{\gamma_{th}}{\overline{\gamma}_{sr}}\right), B_{rd}\left(\frac{\gamma_{th}}{\overline{\gamma}_{rd}}\right) \right], \tag{5.10}$$

where $G^{\cdot,\cdot:\cdot,\cdot:\cdot,\cdot}_{\cdot,\cdot:\cdot,\cdot:\cdot,\cdot}(\cdot|\cdot|\cdot|\cdot,\cdot)$ is denoted as EBGMGF and $P_{z_{sr}z_{rd}}$ is the product of z_{sr} and z_{rd} that are mentioned in (5.10). The product of the CDFs is obtained by (5.10), further substituting (5.10) and

(5.4) into (5.9) and derived the expression (5.11). In (5.11), the obtained closed-form expression of outage performance for the overall DF relay-based FSO-UVLC system. Thus, the closed form expression of (5.11) is used to obtain the outage performance of the overall proposed system in the presence of strong turbulence channel conditions and pointing error scenarios.

$$\begin{aligned} P_{out} &= z_{sr} G_{3,7}^{6,1}\left[\frac{B_{sr}\gamma_{th}}{\overline{\gamma}_{sr}}\middle| \begin{matrix}\phi_{sr}\\ \kappa_{sr}\end{matrix}\right] + z_{rd} G_{3,7}^{6,1}\left[\frac{B_{rd}\gamma_{th}}{\overline{\gamma}_{rd}}\middle| \begin{matrix}\phi_{rd}\\ \kappa_{rd}\end{matrix}\right] \\ &- P_{z_{sr}z_{rd}} G_{0,0:3,7:3,7}^{0,0:6,1:6,1}\left[\begin{matrix}-\\ -\end{matrix}\middle| \begin{matrix}\phi_{sr}\\ \kappa_{sr}\end{matrix}\middle| \begin{matrix}\phi_{rd}\\ \kappa_{rd}\end{matrix}\middle| B_{sr}\left(\frac{\gamma_{th}}{\overline{\gamma}_{sr}}\right), B_{rd}\left(\frac{\gamma_{th}}{\overline{\gamma}_{rd}}\right)\right]. \end{aligned} \tag{5.11}$$

Similarly, the outage analytical outage performance of the proposed hybrid FSO-VLC system within j^{th} vertical water layers in the absence of pointing error is derived by (5.12) as follows;

$$\begin{aligned} P'_{out} &= z'_{sr} G_{2,6}^{4,2}\left[\frac{P^2_{\alpha_{rd}\beta_{rd}}\gamma_{th}}{16\bar{\gamma}_{sr}}\middle| \begin{matrix}\frac{1}{2}\\ \kappa'_{sr}\end{matrix}\right] + z'_{rd} G_{1,4J+1}^{4J,1}\left[\prod_{j=1}^{J}(\alpha_{rd}^{j}\beta_{rd}^{j})^2\left(\frac{\gamma_{rd}}{2^{4j}\bar{\gamma}_{rd}}\right)\middle| \begin{matrix}\frac{1}{2}\\ \kappa'_{rd}\end{matrix}\right] \\ &- z'_{sr}z'_{rd} G_{0,0:2,6:1,4J+1}^{0,0:4,2:4J,1}\left[\begin{matrix}-\\ -\end{matrix}\middle| \begin{matrix}\frac{1}{2}\\ \kappa'_{sr}\end{matrix}\middle| \begin{matrix}\frac{1}{2}\\ \kappa'_{rd}\end{matrix}\middle| \left(\frac{P^2_{\alpha_{sr}\beta_{sr}}}{16\overline{\gamma}_{sr}}\gamma_{th}\right), \left(\prod_{j=1}^{J}(\alpha_{rd}^{j}\beta_{rd}^{j})^2\left(\frac{\gamma_{rd}}{2^{4j}\bar{\gamma}_{rd}}\right)\right)\right]. \end{aligned} \tag{5.12}$$

5.3.2 Pointing Error Effect on Average BER

The average BER analytical expression in the presence of pointing error effect on the proposed system model is derived in this sub-section. Alternatively, in this research the DF relay protocol is considered as a sub-carrier intensity modulator and is being used to regenerate the information into VLC format. For an individual hop, the average BER denoted by I_{sr}, I_{rd}, and the product of $I_{sr}I_{rd}$ is represented by $\phi_{I_{sys}}$ which has been followed in Appendix B.

To calculate the average BER for an individual hop of each of link, we used [35, Eq.16] under-consideration of M-ary Pulse Amplitude Modulation (PAM) modulation scheme in (5.13).

$$I_{mn} = K\int_{0}^{\infty} erfc\sqrt{D\gamma_{mn}} \times f_{h_t}(h_{t_{mn}}) f_{h_p}(h_{p_{mn}}) dh_{t_{mn}} dh_{p_{mn}}, \tag{5.13}$$

where $K = (M-1)/(M\log_2(M))$ and $D = 3/(2(M-1)(2M-1))$ for PAM scheme. In addition to that utilizing the properties of [56, Eq. 06.27.26.0006.01], and conversion error function into G-Meijer function. Further, replacing the value of $f_{h_t}(h_{t_{rd}})$ from [34, Eq. 3] into (5.13) and obtained (5.14). To integrate the product of the two G-Meijer functions in (5.13) by utilizing the properties in [56, Eq.07.34.21.0013.01], and substituting the values from (5.1) into (5.13). To calculating the average BER performance for UVLC link, again utilizing Meijer-G function as in [56, Eq. 07.34.03.0001.01], it is obtained (5.14). For FSO link it is considered as single layer, the average BER expressed by (5.15)) through (5.16).

$$z_1 = \frac{KP_{\alpha_{sr}^j\beta_{sr}^j}}{\sqrt{\pi}P_{\Gamma\alpha_{sr}^j\Gamma\beta_{sr}^j}}, \rho_1 = \sum_{j=1}^{J}(\alpha_{rd}^j + \beta_{rd}^j - 2J), C_{rd} = \left(\frac{2^{2J}}{P_{\alpha_{rd}^j\beta_{rd}^j}}\right)^2,$$

$$C_{sr} = \left(\frac{4}{\alpha_{sr}\beta_{sr}}\right)^2, z_2 = \frac{2^{\rho_1-1}K\zeta_{rd}^2}{\pi^{\frac{2J+1}{2}}\prod_{j=1}^{J}\Gamma\alpha_{rd}^j\Gamma\beta_{rd}^j}, \rho_2 = (\alpha_{rd}+\beta_{rd}-3),$$

$$z_3 = \frac{2^{\rho_2}K\zeta_{sr}^2}{\pi^{3/2}P_{\Gamma\alpha_{sr}\Gamma\beta_{sr}}}, \phi_{I_{sr}} = \left[\frac{2-\zeta_{sr}^2}{2}, \frac{1-\alpha_{sr}}{2}, \frac{2-\alpha_{sr}}{2}, \frac{1-\beta_{sr}}{2}, \frac{2-\beta_{sr}}{2}, 1\right],$$

$$\phi_{I_{rd}} = \left[\frac{2-\zeta_{rd}^2}{2}, \frac{1-\alpha_{rd}^1}{2}, \ldots\frac{1-\alpha_{rd}^J}{2}, \frac{2-\alpha_{rd}^1}{2}, ..\frac{2-\alpha_{rd}^J}{2}, \frac{1-\beta_{rd}^1}{2}, \ldots\frac{1-\beta_{rd}^J}{2}, \frac{2-\beta_{rd}^1}{2}\ldots, \frac{2-\beta_{rd}^J}{2}, 1\right].$$

$$\begin{aligned} I_{rd} = z_1 \int_{-\infty}^{\infty}\int_{0}^{\infty} G_{0,2J}^{2J,0}\left[P_{\alpha_{rd}^j\beta_{rd}^j} h_{t_{rd}} \;\middle|\; \begin{matrix} \cdots \\ \alpha_{rd}^1-1, ..\alpha_{rd}^J-1, \beta_{rd}^1-1, ...\beta_{rd}^J-1 \end{matrix} \right] \\ \times G_{1,2}^{2,0}\left[D\bar{\gamma}_{rd}h_{p_{rd}}^2 h_{t_{rd}}^2 \;\middle|\; \begin{matrix} 1 \\ 0, \frac{1}{2} \end{matrix} \right] f_{h_p}(h_{p_{rd}})dh_{p_{rd}}dh_{t_{rd}}, \end{aligned} \tag{5.14}$$

$$I_{rd} = \frac{2^{\rho_1-1}K\zeta_{rd}^2}{\pi^{\frac{2J+1}{2}}\prod_{j=1}^{J}\Gamma\alpha_{rd}^j\Gamma\beta_{rd}^j} G_{4J+2,3}^{2,4J+1}\left[\left(A_{rd}^2 C_{rd} D\bar{\gamma}_{rd}\right) \;\middle|\; \begin{matrix} \phi_{I_{rd}} \\ 0, \frac{1}{2}, \frac{-\zeta_{rd}^2}{2} \end{matrix} \right], \tag{5.15}$$

$$I_{sr} = \frac{2^{\rho_2}K\zeta_{sr}^2}{\pi^{3/2}P_{\Gamma\alpha_{sr}\Gamma\beta_{sr}}} G_{6,3}^{2,5}\left[\left(A_{sr}^2 C_{sr} D\bar{\gamma}_{sr}\right) \;\middle|\; \begin{matrix} \phi_{I_{sr}} \\ 0, \frac{1}{2}, \frac{-\zeta_{sr}^2}{2} \end{matrix} \right], \tag{5.16}$$

$$\overline{BER} = I_{sr} + I_{rd} - 2P_{z_2z_3} G_{0,0:6,3:4J+2,3}^{0,0:2,5:2,4J+1}\left[\begin{matrix} - \\ - \end{matrix} \;\middle|\; \begin{matrix} \phi_{I_{sr}} \\ 0, \frac{1}{2}, \frac{-\zeta_{sr}}{2} \end{matrix} \;\middle|\; \begin{matrix} \phi_{I_{rd}} \\ 0, \frac{1}{2}, \frac{-\zeta_{rd}}{2} \end{matrix} \;\middle|\; \left(A_{sr}^2 C_{sr} D\bar{\gamma}_{sr}\right), \left(A_{rd}^2 C_{rd} D\bar{\gamma}_{rd}\right) \right]. \tag{5.17}$$

Similarly, the analytical average BER performance metrics of the proposed hybrid FSO-VLC system within j^{th} vertical water layers in the absence of pointing error is derived by (5.18) as follows;

$$\overline{BER'} = I'_{sr} + I'_{rd} - 2P_{z_4z_5} G_{0,0:4,1:4J+1,2}^{0,0:2,3:2,4J}\left[\begin{matrix} - \\ - \end{matrix} \;\middle|\; \begin{matrix} \phi'_{I_{sr}} \\ \frac{1}{2} \end{matrix} \;\middle|\; \begin{matrix} \phi'_{I_{rd}} \\ 0, \frac{1}{2} \end{matrix} \;\middle|\; \left(DC_{sr}\bar{\gamma}_{sr}\right), \left(DC_{rd}\bar{\gamma}_{rd}\right) \right]. \tag{5.18}$$

. The arguments in (5.18) are used as follows;

$$\phi'_{I_{sr}} = \left[\frac{2-\alpha_{sr}}{2}, \frac{1-\beta_{sr}}{2}, \frac{2-\beta_{sr}}{2}, 1\right], \phi'_{I_{rd}} = \left[\frac{1-\alpha_{rd}^1}{2}, \ldots\frac{1-\alpha_{rd}^J}{2}, \frac{2-\alpha_{rd}^1}{2}, ..\frac{1-\beta_{rd}^1}{2}, ..\frac{2-\beta_{rd}^1}{2}, ..1\right].$$

5.4 Numerical and Simulation Results

In this section, we have investigated the outage probability and average BER performance of the whole system with combined influences of channel impairments in both of the hops. For FSO link the path-loss channel conditions the beam wavelength λ = 1550 nm and path-loss exponent has been taken δ = 0.46 while the refraction index ${C_n}^2(h) = 1 \times 10^{-13}$ being used to model strong turbulence channel coefficient. The fixed-length apart source and relay is used as 0.5 km. For UVLC the optical wavelength $\lambda = 532nm$, and extinction coefficient $c(\lambda) = 0.0566$ has been taken, respectively. The receiver aperture area and diameter at the relay and AUV has been taken A_r = 1cm, A = 0.5cm respectively. The vertical distance between relay and destination has taken d_t = 100m. The photo-detector efficiency for both of the hops is equally assumed as η_{mn} = 0.5 while, the photo-detector responsivity R_{mn} = 0.28, respectively. The beam divergence angle is used as $\phi = 6^0$ to 18^0 for the VLC link. Additionally, we use independent but not necessarily identically strong channel fading conditions with pointing errors to simulate all-over system outage performance.

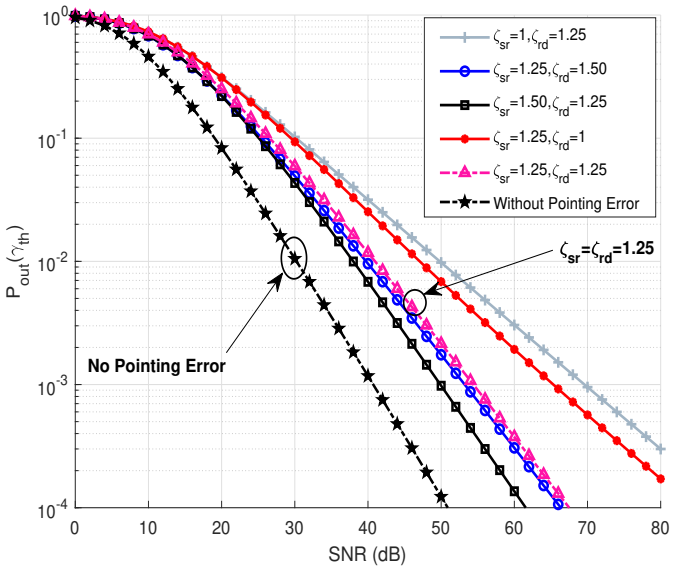

Figure 5.2: The outage probability performance with varying pointing error in dual-hop hybrid cooperative relay-based FSO-VLC underwater wireless communication links are depicted within moderate-strong turbid channels. The experimental setup parameters and the threshold SNR are fixed. For the proper matching curves, the MC approach taken place.

In Fig. 5.2, we obtained the system outage performance in strong channel conditions due to varying pointing errors in both of the links at fixed underwater channel parameters. However, the path loss coefficients are deterministic and have been taken constant as h_{sr} = 0.9998, and h_{rd} = 0.2466, respectively. The distance apart source to relay is kept 0.5 km and relay to destination 25m has been taken for the purpose of simulation results. The performances are demonstrated of the proposed system on varying pointing errors in both links. It is clearly depicted that the outage performance of the system is decreased by decreasing pointing error in both of the links. On the

other hand, it is dramatically disfigured while reduction of pointing errors in an individual hop. In another expectation, if equal pointing error, the system performance shows reliable achievement in performances. It is noticeable here that the pointing error is the most significant factor to affect the system performance and lesser pointing error transceiver supports to improve system efficiency. However, under consideration of no-pointing error, the outage performance is superior so far in the proposed FSO-VLC system model.

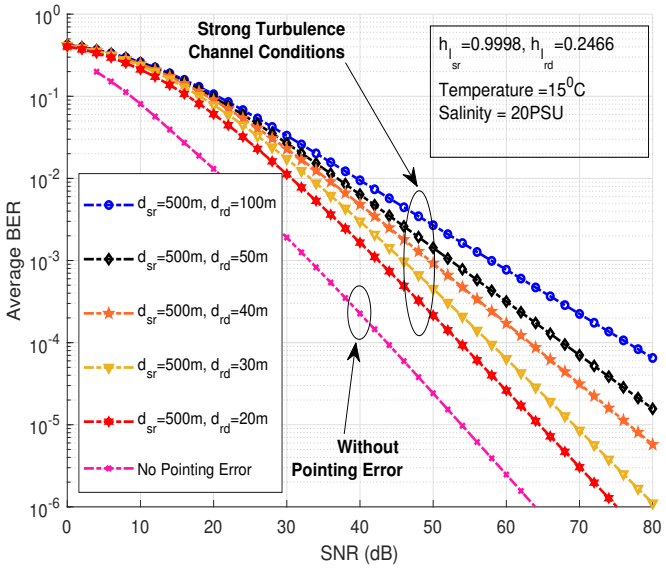

Figure 5.3: The average BER performance of the proposed system model with varying depths of the underwater destination while the distance between source and relay is kept fix. The average BER performance is observed in moderate-to-strong channel conditions and comprised with no-pointing errors scenario.

The Fig. 5.3 demonstrates the average BER performances at fix distance (0.5km) apart source relay, however, the distance between relay and destination is varied. The BER performance is also observed at 100m distance apart relay and destination. The varying distance in underwater considered as j^{th} successive vertical layers (10m each) in water mediums at the fixed water temperature 20^0C and salinity 20 PSU. The simulation results are shown the continuously poor performance due to increasing the vertical distance in the underwater medium. If approaching 20m in underwater the BER 10^{-3} is achieved in low SNR regime. The average BER observes poorer performance in successive layers within high SNR conditions. The superior performance is achieved with no-pointing error at underwater vertical distance 20m.

In the Fig. 5.4, the average BER performance of the system is observed on varying pointing error in UVLC link while the fixed pointing error has been kept in FSO link within heavy turbulence channel conditions. A big impact of the system performance can be seen if varying the pointing error. The worst performance is obtained at ξ_{rd} = 1.10 while ξ_{sr} = 1.40. If targeting the average BER performance of 10^{-4}, which is obtained at ξ_{rd} = 1.30 and ξ_{rd} = 1.40 within 60dB and 54.5 dB SNR regime. The other channel parameters are taken as fixed value such as temperature 15^0C and salinity 20 PSU. It is clearly observed as the best performance in combined influence channel

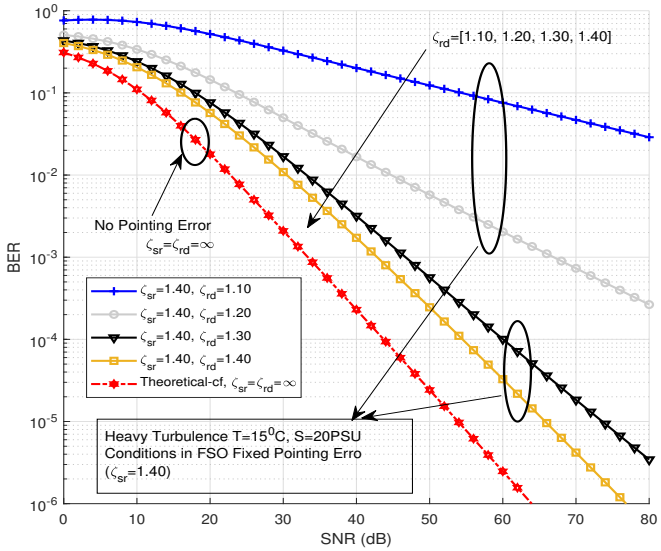

Figure 5.4: The average BER performances are depicted of the proposed FSO-UVLC system model with variable pointing errors in UVLC link at fixed water temperature and salinity.

conditions achieved at $\xi_{sr} = \xi_{rd} = 1.40$. The dotted line shows the average BER performance of the system within no-pointing error in both of the hops, which is the superior performance achieved as compare with combined channel conditions.

5.5 Conclusion

This research is proposed a new approach to obtain the E2E performance metrics; outage probability and average BER of FSO-UVLC system towards the next generation of wireless networks. The proposed system operates in full-duplex mode, where the source communicates with underwater based AUV through the DF-relay protocol. The DF relay protocol is considered as SIM to decode the signals and forwards in different channel. The GG distribution is also used to model moderate-to-strong turbulence channel conditions. The UOT spectrum model is utilized to compute the large and small eddy variances under-consideration of plane wave model. The pointing error effects are also widely summarized and carried out the performances as affecting factors in signal processing per hop. The EBGMGF is used for the accuracy of the proposed work as a new mathematical foundation to obtain the system performance.

The contributed chapter is published in **one Q1** Journal as follows;

1. **Ali Mohammad Furqan**, Dushantha Nalin K. Jayakody, Sahil Garg, Georges Kaddoum, and M. Shamim Hossain. "Dual-hop mixed FSO-VLC underwater wireless communication link." IEEE Transactions on Network and Service Management 19, no. 3 (2022): 3105-3120. **Q1. I.F. 4.7**

Chapter 6

An UAV-based Optical Wildfire Communication System

6.1 Introduction

In recent times, wildfires have become increasingly frequent events due to global warming and environmental changes, posing significant threats to ecosystems and endangering numerous wildlife species. These events often result from high-temperature heat waves that ignite forest areas, causing extensive damage to natural resources, the environment, and our ecosystem. To mitigate these threats and protect wildlife, it is essential to develop an effective wildfire communication detection system. Traditional monitoring and planetary imaging systems are limited by their passive nature and inability to provide real-time data monitoring [17]. Enhancing the accuracy and efficiency of such systems can be achieved through the integration of an UAV optical communication technique, which offers a promising solution for real-time observation and monitoring. Therefore, an immediate call was required to find the wildfire sites before the events happened to save lives. Throughout this study, a wildfire UAV-enabled communication system is proposed as depicted Fig. 6.1.

6.1.1 Contributions

Throughout this research work, an optical UAV-assisted wildfire communication system is developed for affecting site monitoring and rescue operations in various environmental channel conditions. The main contributions of this research are as follows:

- In this research, the development of the traditional wildfire communication technique is proposed to support real-time data streaming, rescue operations, improving video quality, and high-resolution imaging in wildfire sites. The existing literature primarily lacks experimental data-driven approaches utilizing optical MIMO technology for the rapid real-time monitoring of wildfires. Therefore, this proposed research scheme is extended the existing wildfire approaches in real-time scenarios based on the experimental data. In addition to that UAV-based wildfire communications are beneficial for sensing and capturing real-time data such as moisture, temperature, wind speed, etc., which could be further useful for the accurate

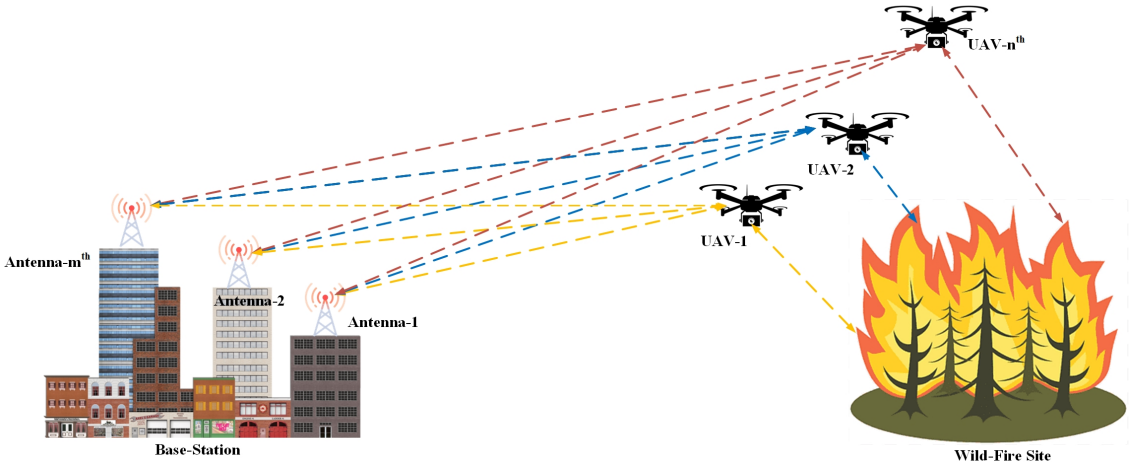

Figure 6.1: The proposed optical wildfire communication system model, where the n^{th} number of UAVs shared the recorded data with the m^{th} number of the BSs. The system is designed by the GG distribution model to optimize channel turbulence.

prediction of fire spreading rate. Therefore, the main contribution of this study is significantly important in the sphere of the provision in perspective of datasets;

- This research proposes the diversity of optical communication within MIMO, MISO, SIMO, and SISO proposed communication models under the strong turbulence channel conditions towards 5GB wireless networking systems. It should be noted that the strong turbulence channel is designed taking into account the GG distribution and the channel parameters α_k and β_k are calculated based on the experimental data;

- The novel closed-form analytical expressions are derived from and comprised of existing models. It is noteworthy, that the path loss is deterministic, whereas the turbulence channel conditions are modeled by considering the random variables. Consequently, the proposed system is designed under IM/DD following the OOK modulation/demodulation scheme;

- The evaluation of performance metrics the average BER and outage probability (P_{out}) of the proposed system models are well investigated and further simulated based on real-time experimental data. The performance metrics are simulated at different altitudes of UAVs. For the simulation, the experimental data is used based on the temperature, humidity, wind speed, and other environmental factors.

6.1.2 Organization

The chapter is organized as follows: Section 6.1 includes the introduction and main contribution. The Section 6.3 presents the system design, managing power of UAV, and the approximated channel coefficients. The end-to-end (E2E) performance metrics are analytically derived in Section 6.3. Section 6.4 is presented the some numerical results and the system performance analysis. Finally, the work is concluded in Section 6.5.

6.2 Wildfire Communication System Design

In this research, it is considered the n number of UAVs communicate with the m number of monitoring base stations BSs through optical links within the harsh channel conditions. This chapter considers the multiple UAVs transmit captured data from the affected site to the BS. It is obvious that the UAVs capture the wildfire data and transfer it to the BS enabling combining methodology. Additionally, It should be noted that each of UAV can share information with an individual BS for a high probability of communication. The received signal at the BS within MIMO approach in full-duplex mode communication scenario in the framework of 5GB wireless network is given as follows;

$$y_{nm} = r_{nm}\eta x \sum_{m=1}^{M} I_{nm} + \nu_{nm}, \tag{6.1}$$

where the parameters n and m represent the number of transmitter and receiver within the IM/DD technique by following the OOK modulation/demodulation scheme. However, in this research the parameters are considered as $m = n$ for equalization, where $n, m = 1, 2, 3, ...N, M$. The responsivity of the photo-detector r_{mn}, the optical-to-electric conversion efficiency η, the transmitted information symbol x and ν_{mn} is represented as the AWGN amongst nm links of UAVs with zero means and the variance σ^2_{nm}, respectively. The normalized optical beam irradiance of n transmitter to m receiver is denoted by I_{mn}. It should be noted that I_{mn} is considered by implying the signal among nm communication nodes, where the path loss I^l_{mn} and atmospheric turbulence I^t_{mn} conditions are determined. Therefore, the combined channel conditions in terms of optical beam irradiance could be written as I_{mn}=$I^l_{mn}I^t_{mn}$, where, I^l_{mn} is considered deterministic values.

6.2.1 Managing Signal Power of UAV

Generally, optical communication links are widely defined based on IM/DD approach and the simplicity of OOK modulation provides quite a significant suitability for UAV platforms, where the communication nodes consume high-energy constraints P_{max}. However, it is necessary to maintain the linear relationship among the UAV nodes in their operational flight times. The optical powers received must not go beyond the threshold power P_{min} that produces a nonlinear effect. It is noteworthy that the transmitted average power P_{avg} is defined as $P_{min} \leq P_{avg} \leq P_{max}$.

In OOK modulation, the power level (P_{enc}) of the encoding FSO signal which maintain the linearity $[P_{max}, P_{min}]$ for constellation purpose, the selecting signal power level $\{P_c\}^C_{c=1}$ is written as $P_{min} \leq P_1, < P_2 ... < P_E \leq P_{max}$. Furthermore, in this proposed optical wildfire communication system model designed by utilizing the IM/DD-OOK scheme, the selection of power levels (P_c) for the uniformity of distributed information $[P_{max} - P_{min}]$ can be written as follows;

$$P_C = P_{min} + \frac{c-1}{C-1}[P_{max} - P_{min}]; \quad c = 1, 2....C. \tag{6.2}$$

It is noteworthy that in this work the transmission power $P_1 = P_{min}$ for binary digit 0 and $P_2 = P_{max}$ for binary digit 1 is assigned, respectively. Therefore, the average power (P_{avg}) selection in IM/DD-OOK modulation technique of an individual UAV followed AWGN noise is written as follows;

$$P_{avg}^{OOK} = \frac{P_{max} + P_{min}}{2}. \tag{6.3}$$

The integration of UAV-based optical communication systems towards existing firefighting and emergency response infrastructure offers a transformative solution to wildfire management. By bridging the capabilities of satellites, ground sensors, and traditional networks, UAVs enhance overall situational awareness and operational efficiency. However, the satellites provide macro-level imagery data, but UAVs capture high-resolution, imaging in real-time views, especially in those sites where satellites face limitations such as clouds and mountains. The ground-based sensors for localization environmental monitoring, benefit from UAVs acting as mobile relays, extending the reach of sensor data to command centers, even when traditional infrastructure is compromised. Furthermore, UAVs can augment and extend traditional communication networks by establishing ad-hoc connections in remote areas, ensuring continuous and reliable communication among firefighting teams. This integration enables a robust, dynamic, and resilient response system, allowing for precise resource allocation, comprehensive monitoring, and adaptive coordination. The synergy between these advanced UAV systems and existing infrastructure ensures a multi-layered defense against wildfires, enhancing both immediate response capabilities and long-term management strategies.

6.2.2 Approximated Path-Loss Channel Coefficient

In this chapter, the optical link is considered directly affected by the atmospheric conditions for fire data collection, the smoke of wildfire events, the capture of critical temperature, and detection activities. Due to harsh atmospheric channel conditions, the optical link severs attenuation in terms of extinction coefficient. Therefore, this study utilizes the channel conditions [72] which are written as follows;

$$\sigma_c^{nm}(\lambda) = \left(\frac{3.912}{V_{nm}}\right)\left(\frac{\lambda}{550}\right)^{-\delta}, \tag{6.4}$$

where the atmospheric extinction coefficient $\sigma_c^{nm}(\lambda)$ totally depends on optical-beam wavelength. The channel parameters as atmospheric visibility V_{nm} (in km), the size distribution coefficient of scattering δ along with the distance L between n and m nodes are considered as in [31]. Furthermore, the path-loss of each optical link in consideration of Beer Lambert law is written as follows [47];

$$I_{nm}^{l} = \exp\left[-\sigma_c^{nm}(\lambda)L\right]. \tag{6.5}$$

6.2.3 The Turbulence Channel Conditions

In this research, the optical turbulence channel conditions are modeled under the GG distribution model which is a significant distribution for irregularities in the terrain, leading to multi-path effects,

and more suitable for optimizing the system performances [58]. The GG distribution is widely acknowledged as the most appropriate model for describing atmospheric turbulence in moderate to strong turbulence regimes [73]. Furthermore, the GG model is attractive from a performance analysis standpoint, particularly for MIMO optical systems, where the distribution of the sum of independent GG variation needs to be determined. The GG distribution can provide more accurate results, especially in moderate to strong turbulence conditions. Additionally, the GG model offers suitability in all types of strong turbulence channels and offers better results [74]. The PDF of atmospheric turbulence channel conditions k^{th} optical links of the proposed system model in terms of the generalized G-Meijer function is given as [75, 76], where k is path links between nm nodes and the PDF for k^{th} layer is written as follows;

$$f_{I_{t_k}}(I_{nm}) = \frac{\prod_{k=1}^{K} \Phi_{(\alpha_k\beta_k)}}{\prod_{k=1}^{K} \Phi_{(\Gamma\alpha_k\Gamma\beta_k)}} G_{0,2K}^{2K,0}\left[\prod_{k=1}^{K} \Phi_{(\alpha_k\beta_k)} I_{nm} \middle| \begin{matrix} \cdots \\ (\alpha_1 - 1), \ldots(\alpha_k - 1), (\beta_1 - 1), \ldots(\beta_k - 1)_{nm} \end{matrix}\right], \tag{6.6}$$

where $f_{I_{t_k}}(I_{nm})$ is the combined vector of nm communication nodes within k^{th} layer, the parameters are used in (6.6) describe which are the product of multiplicative factors of channel conditions as follows;

$$\prod_{k=1}^{K} \Phi_{(\alpha_k\beta_k)} = \left[\prod_{n,m=1}^{N,M} (\alpha)_{k,nm} \prod_{n,m=1}^{N,M} (\beta)_{k,nm}\right]$$

$$\prod_{k=1}^{K} \Phi_{(\Gamma\alpha_k\Gamma\beta_k)} = \left[\prod_{n,m=1}^{N,M} (\Gamma\alpha_k)_{n,m} \prod_{n,m=1}^{N,M} (\Gamma\beta_k)_{n,m}\right]$$

In (6.6), the large (α_k) and small (β_k) scale factors for the optical k^{th} layer can be written as [12],

$$\alpha_k = \left[\exp\left(\frac{0.49\sigma_{I_{tk}}^2}{\left(1 + 0.18d^2 + 0.56\sigma_{I_{tk}}^{\frac{12}{5}}\right)}\right)^{\frac{7}{6}} - 1\right]^{-1}, \beta_k = \left[\exp\left(\frac{0.51\sigma_{I_{tk}}^2}{\left(1 + 0.9d^2 + 0.56\sigma_{I_{tk}}^{\frac{12}{5}}\right)}\right)^{\frac{7}{6}} - 1\right]^{-1}. \tag{6.7}$$

For the optical link as in (6.7), the scintillation index is denoted by $\sigma_{I_{t_k}}^2$, which is known as the Rytov variance and further calculated as $\sigma_{I_{t_k}}^2 = 1.23{C_n}^2(h)\phi^{7/6}L^{11/6}$. However, in the Rytov variance, the number of optical waves is denoted by $\phi = 2\pi/\lambda$ that depends on the wavelength of the transmitted signal λ, and $d = 10D_r\sqrt{\frac{5\pi}{\lambda z}}$ along with the diameter of the receiver aperture D_r. The refraction index is described by ${C_n}^2(h)$ that varies from $10^{-13}m^{-2/3}$ (for strong turbulence regime) to $10^{-17}m^{-2/3}$ (for weak turbulence regime) with uncertainties values at $10^{-15}m^{-2/3}$. Additionally, the Rytov variance is associated with large-scale cells at $\sigma_{I_{t_k}}^2 \gg 1$ while $\sigma_{I_{t_k}}^2 \ll 1$ refers to small-scale cells taken into account by the plane wave model.

Moreover, the refraction index on varying channel conditions and altitude is given as follows [77];

$$C_n{}^2(h) = 0.00594(\frac{\nu}{27})^2(10^5 h)^{10}\exp(-A/1000) + 2.7\times 10^{-16}\exp(-h/1500) + A\exp(-h/100), \tag{6.8}$$

where ν is the wind speed, h represents the level of C_n^2, and A is the altitude of an individual UAV. It is noteworthy that the outage performance is obtained based on varying altitudes for analysis as $h = 25m, 30m, 35m$, and $40m$, respectively. However, in this study, the performance metrics are simulated at different altitudes of UAV in section 3.4.

The instantaneous electrical SNR $\gamma_{sc} = (\eta r_{nm} I_{nm})^2/\sigma^2$ in relation of average electrical SNR could be written as $\overline{\mu} = (\eta|I_{nm}|)^2/\sigma^2$. Further normalizing $|I|= 1$ to utilize the average SNR $(\overline{\mu}) = \gamma/I_{nm}^2$ into (6.6), for equal gain the PDF in terms of instantaneous SNR investigates the CDF is derived according to the Appendix C.

$$f_{\gamma_k}(\gamma) = \frac{\prod_{k=1}^{K}\Phi_{(\alpha_k\beta_k)}}{2\sqrt{\gamma\overline{\mu}}\prod_{k=1}^{K}\Phi_{(\Gamma\alpha_k\Gamma\beta_k)}} G_{0,2K}^{2K,0}\left[\prod_{k=1}^{K}\Phi_{(\alpha_k\beta_k)}\sqrt{\frac{\gamma}{\overline{\mu}}}\middle| \begin{matrix} \cdots \\ (\alpha_1-1),\ldots(\alpha_k-1),(\beta_1-1),\ldots(\beta_k-1)_{nm}\end{matrix}\right]. \tag{6.9}$$

Furthermore, to obtain the CDF of (6.9) as $F_{\gamma_k}(\gamma) = \int_0^{\gamma} f_{\gamma_k}(\gamma)d\gamma$, utilizing the properties of Wolfram Mathematica [56, p. 07.34.21.0084.01] and obtained the expression in (6.10) as follows;

$$F_{\gamma_k}(\gamma) = \frac{2^{\sum_{k=1}^{K}(\alpha_k+\beta_k)-3K}\prod_{k=1}^{K}\Phi_{(\alpha_k\beta_k)}}{(2\pi)^K\prod_{k=1}^{K}\Phi_{(\Gamma\alpha_k\Gamma\beta_k)}}\sqrt{\frac{\gamma}{\overline{\mu}}}G_{1,4K+1}^{4K,1}\left[\prod_{k=1}^{K}\Phi_{(\alpha_k\beta_k)^2}\left(\frac{\gamma}{2^{4K}\overline{\mu}}\right)\middle| \begin{matrix}\frac{1}{2} \\ \mathbf{b}_k,-\frac{1}{2}\end{matrix}\right]. \tag{6.10}$$

6.3 The End-to-End (E2E) Performances

This section includes the BER and outage probability of the proposed MIMO-UAV-assited wildfire optical communication system. The performance metrics are obtained based on the real data given by Meteostat [78] source. However, the outage performances and BER are the main insights to depict the accuracy of the proposed wildfire communication system model.

6.3.1 Outage Probability of the Proposed System

To obtain the outage performance of the system, the instantaneous SNR should be equal to or less than the threshold SNR. Therefore, the outage probability performance could be written as follows;

$$P_{out} = F_{\gamma}(\gamma_{th}) = Pr\{\gamma \leq \gamma_{th}\}. \tag{6.11}$$

Furthermore, substituting (6.10) into (6.11), the outage probability of the proposed system in threshold SNR conditions is derived by (6.11) and the parameters are used mentioned in Appendix C.

$$P_{out} = F_{\gamma}(\gamma_{th}) = \frac{Z_1 \chi}{(2\pi)^K Z_{\Gamma(\alpha)\Gamma(\beta)}} \sqrt{\frac{\gamma_{th}}{\overline{\mu}}} G_{1,4K+1}^{4K,1} \left[\left(\frac{\gamma_{th} \chi^2}{2^{4K} \overline{\mu}} \right) \middle| \begin{matrix} \frac{1}{2} \\ \mathbf{b}_k, -\frac{1}{2} \end{matrix} \right], \tag{6.12}$$

6.3.2 BER Performance Analysis

This subsection summarizes the investigated BER performance analytically of the proposed system and comprises the possible communications as per required MIMO, MISO, SIMO, and SISO system models. It is noteworthy that the proposed system models are designed under consideration of the moderate-to-strong turbulence channel conditions. Moreover, in this work the closed-form expressions are analytically derived by following OOK modulation scheme under the IM/DD technique.

6.3.2.1 Analytical Performance of MIMO-FSO Communication System

To investigate the average BER, the number of UAVs are considered the equal number as at the BS i.e. nm. Therefore, the conditional BER in terms of average SNR ($\overline{\mu}$) for the optical MIMO system can be written as follows [79];

$$\underbrace{P_{I_{nm}}}_{(MIMO)} = \frac{1}{2} erfc \left(\sqrt{\frac{\overline{\mu}}{2(NM)^2} \sum_{m=1}^{M} \left(\sum_{n=1}^{N} I_{nm} \right)^2} \right). \tag{6.13}$$

To form the closed-form expression of average BER within the combined turbulence and path loss conditions the expression can be written by (6.14) by utilizing the PDF expression from (6.6) as follows;

$$\underbrace{\overline{BER}}_{MIMO} = \frac{1}{2} \int_0^{\infty} f_{I_{t_k}}(I_{nm}) erfc \left(\sqrt{\frac{\overline{\mu}}{2(NM)^2} \sum_{m=1}^{M} \left(\sum_{n=1}^{N} I_{nm} \right)^2} \right) dI_{nm}, \tag{6.14}$$

where $f_{I_{t_k}}(I_{nm})$ is the joint PDF of vector I=($I_{11}, I_{12}, ...I_{NM}$). The factors n and m are indicating the transmitted and received power nodes at both communication ends. Furthermore, converting the error function into a generalized G-Meijer function, then we obtained (6.15) which is the complex integration expression.

$$\underbrace{\overline{BER}}_{MIMO} = \frac{\chi}{2\sqrt{\pi} Z_{\Gamma(\alpha)\Gamma(\beta)}} \int_0^{\infty} G_{0,2K}^{2K,0} \left[\chi I_{nm} \middle| \begin{matrix} \cdots \\ \mathbf{a}_{nm} \end{matrix} \right] G_{1,2}^{2,0} \left[\frac{\mu}{2(NM)^2} \sum_{m=1}^{M} \left(\sum_{n=1}^{N} I_{t_{nm}} \right)^2 \middle| \begin{matrix} 1 \\ 0, \frac{1}{2} \end{matrix} \right] dI_{nm}. \tag{6.15}$$

The expression (6.15) is a complex mathematical integration, therefore, utilizing the properties of Wolfarm Mathematica [56, p. 07.34.21.0013.01], and the closed-form expression obtained as

in (6.16) of the proposed optical wildfire MIMO UAV-assisted communication system model as follows;

$$\underbrace{\overline{BER}}_{MIMO} = \frac{2^{\sum_{k=1}^{K}(\alpha_k+\beta_k)-2}}{Z_{\Gamma(\alpha)\Gamma(\beta)\pi^{(\frac{2K+1}{2})}}} G_{4K+1,2}^{2,4K}\left[\frac{2^{4K-1}\mu}{(Z_{\alpha\beta}NM)^2}\middle|\begin{matrix}\Psi, 1\\ 0, \frac{1}{2}\end{matrix}\right]. \tag{6.16}$$

However, in (6.16), the argument[†] is used and can be written as follows;

$$\Psi = \left[\frac{(1-\alpha_1)}{2}, \ldots \frac{(1-\alpha_K)}{2}, \frac{(2-\alpha_1)}{2}, .. \frac{(2-\alpha_K)}{2}, \frac{(1-\beta_1)}{2}, \ldots \frac{(1-\beta_K)}{2}, \frac{(2-\beta_1)}{2}, \ldots \frac{(2-\beta_K)}{2}\right].$$

6.3.2.2 Analytical Performance of Optical MISO Wildfire Communication System

Similarly, in the investigation of the optical MISO communication system, the conditional BER for MISO and SIMO systems can be written by (6.17) according to (6.13). The conditional BER is written as follows;

$$\underbrace{P_{I_{nm}}}_{MISO} = \frac{1}{2} erfc\left(\sqrt{\frac{\overline{\mu}}{2M^2}\left(\sum_{m=1}^{M} I_m\right)^2}\right) \tag{6.17}$$

To obtain the closed-form expression of optical MISO communication system by plugin (6.17) into (6.14) and further integrating by utilizing the properties of Wolfarm Mathematica [56, p. 07.34.21.0013.01]. Therefore, the average BER analytical expression for optical MISO communication system is obtained as in (6.18);

$$\underbrace{\overline{BER}}_{MISO} = \frac{2^{\sum_{k=1}^{K}(\alpha_k+\beta_k)-2}}{Z_{\Gamma(\alpha)\Gamma(\beta)\pi^{(\frac{2K+1}{2})}}} G_{4K+1,2}^{2,4K}\left[\frac{2^{4K-1}\mu}{(Z_{\alpha\beta}M)^2}\middle|\begin{matrix}\Psi, 1\\ 0, \frac{1}{2}\end{matrix}\right] \tag{6.18}$$

6.3.2.3 Analytical Performance of Optical SIMO Communication System

This study follows the same pattern and plugs in the conditional BER (6.19) in (6.14) and further integrates complex expression using [56, p. 07.34.21.0013.01]. The final average BER expression for the SIMO-FSO system is obtained by (6.20) as follows;

$$\underbrace{P_{I_{nm}}}_{SIMO} = \frac{1}{2} erfc\left(\sqrt{\frac{\overline{\mu}}{2N^2}\left(\sum_{n=1}^{N} I_n\right)^2}\right) \tag{6.19}$$

[2†] It is noteworthy that the argument Ψ is modified according to the required system model.

$$\underbrace{\overline{BER}}_{SIMO} = \frac{2^{\sum_{k=1}^{K}(\alpha_k+\beta_k)-2}}{Z_{\Gamma(\alpha)\Gamma(\beta)}\pi^{(\frac{2K+1}{2})}} G_{4K+1,2}^{2,4K}\left[\frac{2^{4K-1}\mu}{(Z_{\alpha\beta}N)^2}\middle| \begin{matrix}\Psi, 1\\ 0, \frac{1}{2}\end{matrix}\right] \tag{6.20}$$

6.3.2.4 Analytical Performance of Optical SISO Communication System

A SISO is a generic communication system model with less complexity. In the SISO wildfire communication system, it is considered a single UAV communicates with a single antenna or $n = m = 1$. Therefore, channel parameters are determined and modeled according to the single path with varying environmental factors. Due to the singularity of the communication nodes, the average BER is analytically derived in (6.21) as follows;

$$\underbrace{\overline{BER}}_{SISO} = \frac{2^{(\alpha+\beta-2)}}{\pi^{3/2}\gamma(\alpha)\Gamma(\beta)} G_{5,2}^{2,4}\left[\frac{4\mu}{(\alpha\beta)^2}\middle| \begin{matrix}\frac{1-\alpha}{2}, \frac{\alpha}{2}, \frac{1-\beta}{2}, \frac{\beta}{2}, 1\\ 0, \frac{1}{2},\end{matrix}\right]. \tag{6.21}$$

6.4 Numerical Evaluation and Simulation Results

In this section, the performance metrics of MIMO, MISO, SIMO, and SISO are simulated according to channel characteristics. However, the distance is between the UAVs and the BSs kept fixed as 30m, which could vary according to the requirements. Additionally, the results are generally depicted at the altitude of 25m to 40m of the UAV above ground level. The altitude can be increased according to the specific purpose or the requirement. However, the RF-enabled UAVs hover on higher altitudes rather than the optical-enabled UAVs. Throughout this research, it has considered the varying altitude of UAVs as 25m, 30m, 35m, and 40m for closely capturing the affected site data. The UAVs are associated with optical links that can be easily affected by sunlight or any other environmental background. Therefore, we have considered the fixed altitude for UAVs for more reliability and extension of this work. The average temperature, humidity, and average pressure of July month in Lisbon, Portugal have been taken for simulation results as $T = 22.56^0$C, average humidity $72.61g/m^2$, and $P = 1.016$bar. The α and β particles are modeled based on the average atmospheric conditions under plan wave modulation and based on the refractive index ${C_n}^2(h)$.

In Fig.6.2, the average BER performances are depicted on varying UAV altitude and BS while the other parameters are fixed as $T = 22.5^0$C and average humidity $72.61g/m^3$. It should be noted that the results are obtained taking into account the equal number of transmitters and receivers. It can be seen that with the increasing altitude of UAVs, the performances are getting poor. It is because of the harsh conditions in the channel on increasing height. However, the best BER performances are depicted at $PSU = 25$m of an individual UAV. If targeting 10^{-5} BER, the performances outperform in the 16dB SNR regimes, while the altitude as $PSU = 40$m the system shows the poorest performance in the high SNR regimes.

Fig.6.3 shows the performance of BER on varying numbers of UAVs and BS. Firstly, the results are obtained on increasing the number of BS while the number of UAVs is kept constant. It can be

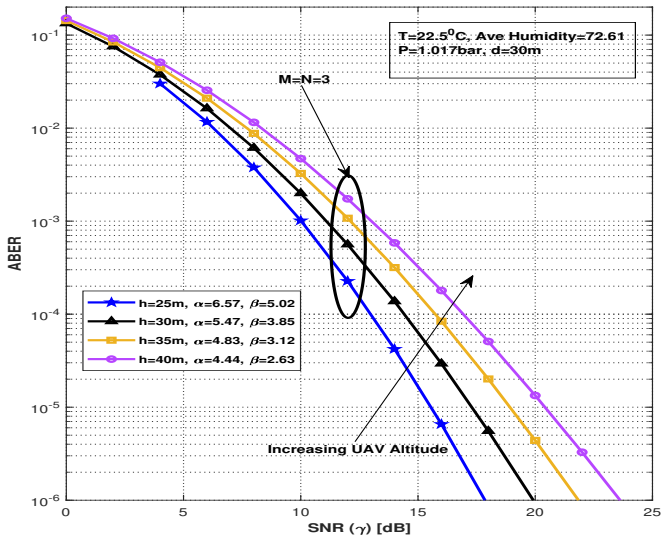

Figure 6.2: The BER performances while varying the altitude of an individual UAV altitude. It is depicted clearly with increasing UAV altitude the performance decreases.

seen that on increasing BS the performance reduces simultaneously while other parameters are fixed as h = 25m and PSU = 20m. On the other hand, if the number of UAVs increases, the performance improves significantly. This is because of the number of source nodes and the high probability of receiving signals from multiple communication nodes. It also includes the performance in equalizing the number of UAVs and the BSs, which could achieve the best performance. However, on concluding these results the BER improves if deploys an equal number of communication nodes. The distance between communication nodes and channel parameters influences the performance metrics. Another sight to obtain these results is the increasing number of BSs the performance reduces in high SNR conditions.

On continuous shifting parameters, Fig.6.4 comprises the BER performance of the proposed system model as MIMO, MISO, SIMO, and SISO wildfire detection. As, in this chapter, the real data has been used to depict the performance of the system. Therefore, the MIMO and MISO systems obtained superior performance compared to those of SIMO and SISO. The reason is discussed in Fig.6.3. Interestingly, the MISO detection system outperforms MIMO. According to Fig.6.3, it is shown that increased UAVs improve performance. The SIMO and SISO have less probability of multiple-node communication. Therefore, MIMO and MISO systems obtain higher BER performance in low SNR conditions rather than SIMO and SISO detection models.

Throughout Fig.6.5, the outage performance of the proposed system is depicted on successive threshold SNR in strong turbulence channel conditions, when other parameters are kept fixed. It could be seen that the threshold SNR γ_{th} increases, the probability of the outage performance shows the poor performance. It should be noted that the best performance is obtained at γ_{th} = 2dB while the average performance is obtained at γ_{th} = 6dB. In this figure, the number of UAVs and BSs are kept equal for simulation results as $n = m = 2$ and the average temperature and humidity

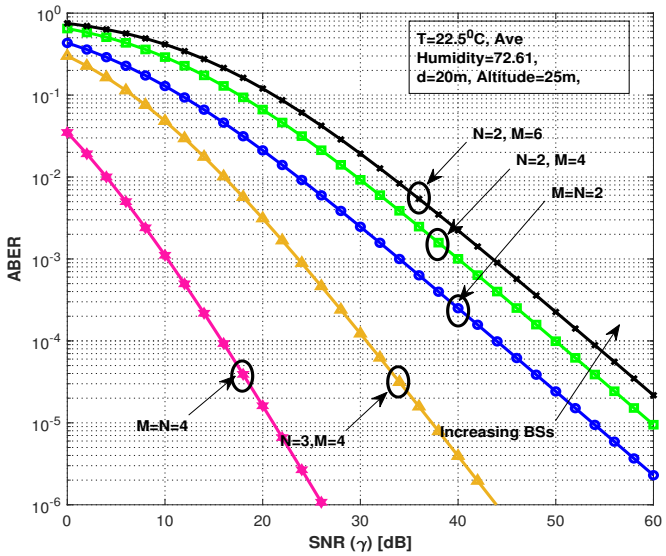

Figure 6.3: The BER performance is obtained and comprised of a fluctuating number of communication nodes. It is depicted that by increasing the number of UAVs, BER performance improves simultaneously.

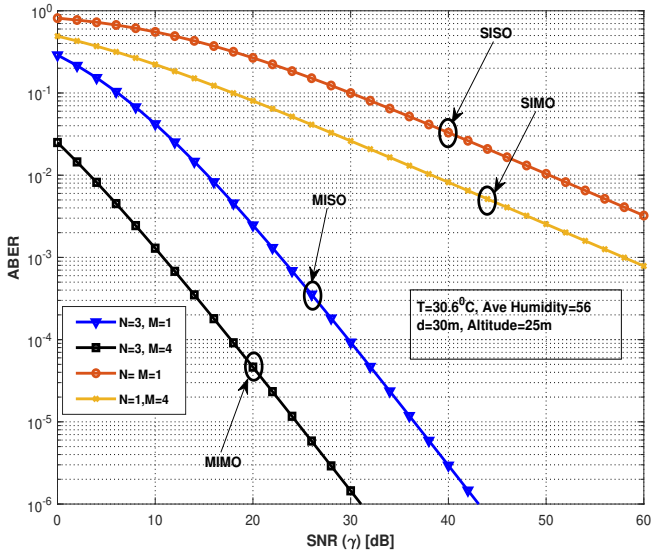

Figure 6.4: The BER performance comparison amongst MIMO, MISO, SIMO, and SISO. When the number of UAVs and BS varies. Moreover, the best BER performance is depicted within MIMO and MISO wildfire detection systems.

have been taken as T = 22.5^{0}C, average humidity 72.61g/m^2. However, the results are obtained at fixed communication distance and UAV altitude of PSU = 30m, h = 30m.

Finally, in Fig.6.6 the outage performance is depicted on varying UAV altitudes which vary from 25m to 40m above ground level. Similarly, increasing UAV altitude reduces the system performance and directly affects it, due to strong turbulence channel conditions. In this figure,

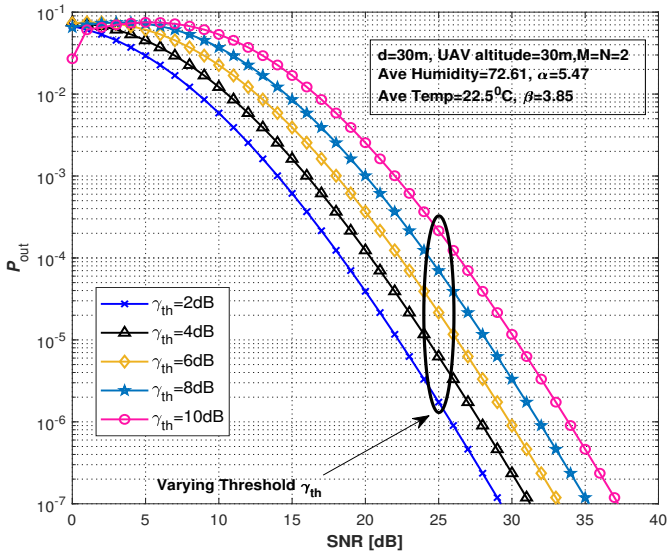

Figure 6.5: The outage performances are depicted on varying threshold SNR while the real-time data is used for July month in Lisbon, Portugal. It is depicted the best performance is obtained at γ_{th} = 2dB.

the results are obtained at average temperature and humidity according to the Fig.6.5. The best performance is obtained at 25m at the lowest SNR regimes because it is the shortest distance than other UAV altitudes.

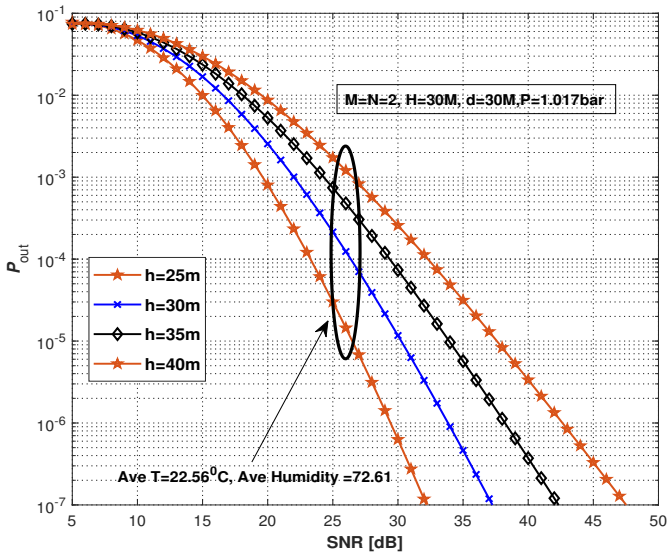

Figure 6.6: The outage probability performance on the successive altitude of UAV from the ground level while the other parameters are kept constant.

6.5 Conclusions

This research provides new insights into wildfire events by enabling UAV communication setups for real-time monitoring within the future wireless system. The MIMO Optical-enabled UAV wildfire communication system represents a cutting-edge and highly efficient approach to early wildfire monitoring and response. In this work, the MIMO optical link among communication nodes is designed using the GG distribution under the IM/DD-OOK modulation scheme. Furthermore, this study explores potential communication approaches in remote areas. The PDF and CDF are derived to obtain the system performance metrics. This work aims to develop a wildfire communication model to save lives and support rescue operations. The results demonstrate improved spatial resolution and accuracy this enables the detection of even small-scale wildfires at its inception stages. The capability of the proposed system is to provide real-time, accurate, and comprehensive wildfire monitoring will not only aid in the prompt observation of fire incidents but also enhance life-saving and rescue operations. The development of this research signifies a revolution in wildfire monitoring and control efforts, substantially impacting the protection of ecosystems, communities, and economies from the devastating effects of wildfires.

The contributed chapter is published in **one Q2** Journal as follows;

1. **Ali Mohammad Furqan**, Dushantha Nalin K. Jayakody†, and P. Muthuchidambaranathan. "Revolutionizing Firefighting: UAV-Based Optical Communication Systems for Wildfires." In Photonics, vol. 11, no. 7, p. 656. MDPI, 2024. doi.org/10.3390/photonics11070656. **Q2, I.F. 2.1**

Chapter 7

Conclusions and Recommendations for Future Studies

7.1 Summary of Contributions

This dissertation analyzed the performance of optical wireless signaling in various wireless communication scenarios, mainly focusing on UAV-assisted networks, underwater based AUV communication systems dealing with the moderate-to-strong turbulence channel conditions. This dissertation provides valuable analytical frameworks and insights to guide the design of optical wireless communications for real-time data streaming, improving the connectivity, and improve the system efficiency under the URLLC methodology in harsh channel conditions.

7.1.1 Chapter 3: SIMO-Underwater Visible Light Communication (UVLC) System

In Chapter 4, the extensive research on optical performance in underwater environment is proposed. This research thoroughly investigates the metrics performances such as average BER and outage probability of the proposed SIMO-UVLC system which is modeled under consideration of GG distribution by following OOK modulation scheme. The channel impairments have taken into accounts for misalignment phenomena of transceivers and strong turbulence conditions in mixed oceanic environment such as the SIO. The performance metrics are simulated based on experimental data collected during 2016 SIO and considering various physio-chemical properties of water at different depths and multiple vertical layers alongside a configuration of (2^M) LEDs at the receiver end. Validating the simulated results, an updated closed-form expression for infinite pointing error is derived and also evaluated within the presence/absence of pointing error conditions. Also, the simulation results are validated by analytically derived mathematical closed-form expressions by utilizing the MC approach. This study demonstrates that the E2E performance of the proposed SIMO-UVLC system is superior in the absence of pointing error and lowest vertical depth, regardless of water type.

7.1.2 Chapter 4: Performance Analysis of Multi-Hop UVLC System: A River-meets-Ocean Scenario

A framework to estimate an AUV-enabled optical communication in diversive underwater environment focusing on multi-hop links in river-meets-ocean scenario is developed which is the extension of Chapter 4. Additionally, this study focuses on the establishment a comprehensive evaluation of the UVLC system in the challenging environment of estuaries, characterized by the interaction of fresh river water and sea salt water. By developing a full-duplex data encryption/decryption model and investigating its performance under various channel conditions including moderate-to-strong turbulence and transceiver misalignment, this research contributes significantly to the field of underwater communication. This research work presented not only offers valuable insights for future UVLC system designs but also lays the groundwork for further exploration of communication technologies in various aquatic environments. Overall, this study paves the way for improved reliability and efficiency in underwater communication, essential for applications such as environmental monitoring and underwater robotics.

An AUV-assisted optical wireless communication system in mixed waters, focuses on multi-hop scenarios is presented in Chapter 5. This chapter made significant contributions to understanding the dynamics of information optical wireless communication within the harsh aqueous channels. A key technical contribution was the derivation of closed-form expressions for optical link in multi-hop scenarios. These expressions grounded in advanced statistical methods including the generalized Meijer-G function that leads to EBGMGF. The EBGMGF function proposes to serve and enhance the efficiency of optical system in terms of key performance metrics such as BER and outage probability of the system. This finding of this chapter underscore the potential of AUV technology to enhance the performance of AUV in challenging deployment scenarios.

7.1.3 Chapter 5: Dual-Hop Mixed FSO-VLC Underwater Wireless Communication Link

This chapter is proposed a new approach to obtain the E2E performance metrics; outage probability and average BER of FSO-UVLC system towards the next generation of advanced networking systems. The proposed system operates in full-duplex mode, where the source communicates with underwater based AUV through the DF-relay protocol. The DF relay protocol is considered as SIM to decode the signals and forwards in different channel. The GG distribution is also used to model moderate-to-strong turbulence channel conditions. The UOT spectrum model is utilized to compute the large and small eddy variances under-consideration of plane wave model. The pointing error effects are also widely summarized and carried out the performances as affecting factors in signal processing per hop. The EBGMGF is used for the accuracy of the proposed work as a new mathematical foundation to obtain the system performance. Furthermore, the MC simulation approach is also used to obtain simulation results to confirm the system accuracy.

7.1.4 Chapter 6: An UAV-based Opitcal Wildfire Communication System

Chapter 3 of the thesis provides new insights into wildfire events by enabling UAV communication setups for real-time monitoring towards the futuristic wireless communication system. The proposed optical enabled MIMO UAV-assisted wildfire communication system exemplifies an innovative and efficient strategy for early detection and response to wildfires. The research investigates various communication modalities suited for remote areas, providing critical insights into the operational viability. The proposed system model facilitates the extensive real-time monitoring and quick response of effective wildfire sites. This development not only promises to improve immediate observational capabilities but also significantly enhances life-saving measures and rescue operations. Additionally this research provides an insight of a transformative shift in wildfire monitoring and control efforts, with profound implications for the protection of ecosystems, communities, and economies from the catastrophic effects of wildfires.

7.2 Recommendations for Future Studies

Based on the results and insights gain from the technical chapters of the dissertation, recommendation for future research are given as:

- *Adaptation of back-scattering and new data gathering techniques within the clusters*

Backscattering techniques can be effectively integrated with UAVs to facilitate sensor observations from Cluster Head (CH)s within the WSN nodes as proposed in Chapter 3. Additionally, emerging multiple access techniques, such as Non-Orthogonal Multiple Access (NOMA), can be employed to efficiently serve a large number of passive backscatter CHs. It is essential to further investigate the optimal interactions between the UAV and backscattering CHs, taking into account various network behaviors and design parameters. Consequently, modifications to the proposed fixed WSN structure illustrated in Fig.6.1 will be necessary. Implementing new modulation schemes into the proposed UWSN architectures for data gathering is expected to enhance performance and support the practical realization of next-generation IoUTs applications.

- *The impact of deployed Reflective Semiconductor Optical Amplifier (RSOA) reflector among divers-to-divers and underwater nodes communication in term of futuristic real-time data streaming in shallow water mediums*

The RSOA offers a promising solution to reduce the extra cost of relay protocol for data transmission. The RSOA can a key solution for UWOC in shallow waters over the moderate distances. In chapter 4, the SIMO-UVLC system model is proposed where the RSOA can play an important role to reflect optical beam to the targeting node and can be manage the light intensity through the shifting optical phase. It is important to highlight that the RSOA demonstrates advantages over existing relayed hybrid communication systems in shallow water, particularly under conditions of weak turbulence. By mitigating the additional costs linked to encoding and decoding optical signals, the RSOA effectively reduces the overall expenses associated with communication setups.

Furthermore, to meet the demands of real-time applications within advanced communication networks, RSOA-enabled systems enhance the performance and reliability of underwater optical communications.

- *An emerging multi-plane-transmit model by characterizing the fluctuating irradiance of optical orbital angular momentum (OAM)*

Being inspired by the proposed work as SIMO-UVLC system in chapter 4, the recent efforts are exemplified to deploy the similar work within different performance metrics, assumptions and fading channel conditions. However, the Optical Orbital Angular Momentum (OAM) is carried by the optical beam helical phases. Generally, the orthogonality of OAM is responsible to increase the spectral efficiency and exploited for multiplexing as well as modulation schemes. In contrast, OAM potentially enhances the information reliability among IoUTs networking structures as futuristic underwater communication. The scintillation is another cause of signal fading due to varying temperature and salinity of water. Therefore, in optical propagation the phase front of OAM beams may suffer from severe distortion and adapting MC approach could be quiet useful to model underwater optical propagation model. Recently, a multiple phase screen underwater optical channel model is proposed where, a number of phase screen are immersed between the transceivers. Due to progression of this proposed chapter 4, a multi-plane-transmit model by characterizing the fluctuating irradiance of optical OAM by using MC simulation in UWOC would be the next-level of underwater communication.

- *An underwater VLC approach in isolated meeting oceans mixing and non-mixing water mediums*

It is challenging to deploy UVLC system in strong turbulence channel conditions where the two different water bodies gathered or mixing waters. In chapter 5, we have developed the UVLC model in highly critical isolated Southern Indian Ocean for the purpose of goods transportation, naval tactical operations, coastal securities, and further underwater exploration activities in vast acrimonious aqueous medium. Hence, the proposed system model could imply for various underwater mixing and non-mixing water mediums all around the globe. This emphasizes the superiority of advance underwater wireless communications. The proposed system model could be deploy for the direct connectivity and real-time monitoring of floating vehicles, observation of marine life, and various underwater applications in any types water meeting bodies existing.

- *Multi-hop links, Network Connectivity, Localization, and Energy Harvesting as Simultaneously Light-Wave Information and Power Transfer (SLIPT) in UVLC*

To connect the underwater environment with the human existence is crucial and could play an ample role of networking connectivity, EH, and localization of UWSNs specially in hybrid underwater communications. However, multi-hop links support to enhance the network connectivity, coverage range, and the QoS. As, multi-hop cooperative communication systems are emphasized for an extensive research to improve the sustainability, efficiency, tracking mechanism, and QoE. In

this regard, the novel localization schemes could be the promising approaches as Received Signal Strength (RSS)-based EH-UOWSNs and EH for hybrid Acoustic-Optical Underwater Wireless Networks (AOUWSNs), which could be the most favorable techniques to strengthen underwater hybrid links.

- *Re-configurable Intelligent Surfaces (RIS) assisted AUV Communications*

The RIS is identified as one of the emerging technology that has the capability of defining new wireless communications by changing propagation patterns and controlling the wireless communications links. The RIS is a meta-surface, which contains electronically controllable low power analog processing elements. Moreover, RIS is the low cost technology, which can be deployed in different environments by attaching to surfaces, i.e., buildings, vehicles, wall, underwater etc. RIS-assisted wireless powered AUV communications has great potential for advancing wireless communications by handling the complexity of wireless channels and providing extended coverage. Further, RIS-assisted wireless powered AUV communication systems can improve the QoS at the end users specially in urban and underwater environments while maintaining the energy efficiency. However, the handshake between these two technologies, RIS and AUV also introduced new set of challenges and opportunities such as channel modelling for underwater RIS, channel estimation between RIS elements, control of RIS elements along with the AUV trajectory, etc. Addressing aforementioned challenges will help to define the role of RIS-assisted AUV communications for future generation of communications and to achieve greater advancements compared to the conventional AUV-assisted communication setups.

In conclusion, optical wireless communication links play a major role in expanding capabilities of IoT applications in next-generation communications. Including optical enabled UAVs and AUVs into the existing infrastructures or communication designs required optimal resource allocation strategies to maintain expected QoS. This dissertation has provided optimal resource allocation strategies for maintaining UAV and AUV user-case scenarios, i.e., AUV as a relay and UAV-assisted data gathering in diverse channel conditions. The results are obtained within the dissertation work provides the required groundwork for future studies mention in section 6.2, which can eventually lead to practical realization of optical wireless information in unguided terrestrial and water mediums through UAV and AUV-assisted communications for the next generations of wireless networking system.

Bibliography

[1] Y.-F. Liu et al. "A survey of recent advances in optimization methods for wireless communications". In: *IEEE Journal on Selected Areas in Communications* (2024) (cit. on p. 1).

[2] M. Shafi et al. "Wireless communications in the twenty-first century: A perspective". In: *Proceedings of the IEEE* 85.10 (1997), pp. 1622–1638 (cit. on p. 1).

[3] Z. Zhu et al. "Overview of demand management in smart grid and enabling wireless communication technologies". In: *IEEE Wireless Communications* 19.3 (2012), pp. 48–56 (cit. on p. 1).

[4] Y. Zhang et al. "Challenges and opportunities of future rural wireless communications". In: *IEEE Communications Magazine* 59.12 (2021), pp. 16–22 (cit. on p. 1).

[5] X. Ke. "Optical wireless communication". In: *Handbook of Optical Wireless Communication*. Springer, 2024, pp. 1–20 (cit. on p. 1).

[6] C.-W. Chow. "Recent advances and future perspectives in optical wireless communication, free space optical communication and sensing for 6G". In: *Journal of Lightwave Technology* 42.11 (2024), pp. 3972–3980 (cit. on pp. 1, 2, 9).

[7] M. H. Khoshafa et al. "RIS-Assisted Physical Layer Security in Emerging RF and Optical Wireless Communication Systems: A Comprehensive Survey". In: *arXiv preprint arXiv:2403.10412* (2024) (cit. on p. 1).

[8] X. Ke. *Handbook of Optical Wireless Communication*. Springer Nature, 2024 (cit. on p. 1).

[9] B. K. Levidala, P. N. Ramavath, and P. Krishnan. "Performance enhancement using multiple input multiple output in dual-hop convergent underwater wireless optical communication–free-space optical communication system under strong turbulence with pointing errors". In: *Optical Engineering* 60.10 (2021), p. 106106 (cit. on pp. 1, 19).

[10] M. F. Ali, D. N. K. Jayakody, and P. Muthuchidambaranathan. "Revolutionizing Firefighting: UAV-Based Optical Communication Systems for Wildfires". In: *Photonics*. Vol. 11. 7. MDPI. 2024, p. 656 (cit. on p. 1).

[11] M. F. Ali and D. N. K. Jayakody. "SIMO-underwater visible light communication (UVLC) system". In: *Computer Networks* 232 (2023), p. 109750 (cit. on p. 1).

[12] M. F. Ali, D. N. K. Jayakody, and M. V. Ribeiro. "A Hybrid UVLC-RF and Optical Cooperative Relay Communication System". In: *2021 10th International Conference on Information and Automation for Sustainability (ICIAfS)*. IEEE. 2021, pp. 13–18 (cit. on pp. 2, 14, 23, 59).

[13] Z. Qu and M. Lai. "A Review on Electromagnetic, Acoustic and New Emerging Technologies for Submarine Communication". In: *IEEE Access* (2024) (cit. on p. 2).

[14] M. F. Ali et al. "Recent advances and future directions on underwater wireless communications". In: *Archives of Computational Methods in Engineering* 27 (2020), pp. 1379–1412 (cit. on pp. 2, 14).

[15] A. Wibisono et al. "A survey on underwater wireless power and data transfer system". In: *IEEE Access* (2024) (cit. on p. 2).

[16] A. I. Al-Shamma'a, A. Shaw, and S. Saman. "Propagation of electromagnetic waves at MHz frequencies through seawater". In: *IEEE Transactions on antennas and propagation* 52.11 (2004), pp. 2843–2849 (cit. on p. 2).

[17] A. Bouguettaya et al. "A review on early wildfire detection from unmanned aerial vehicles using deep learning-based computer vision algorithms". In: *Signal Processing* 190 (2022), p. 108309 (cit. on pp. 2, 55).

[18] M. Elamassie et al. "Effect of eddy diffusivity ratio on underwater optical scintillation index". In: *JOSA A* 34.11 (2017), pp. 1969–1973 (cit. on pp. 6, 21, 45, 83, 84).

[19] S. Shi et al. "Energy-efficient UAV-enabled computation offloading for industrial internet of things: a deep reinforcement learning approach". In: *Wireless Networks* 30.5 (2024), pp. 3921–3934 (cit. on p. 9).

[20] Q. Zhang, D.-W. Yue, and X.-Y. Xu. "Performance Analysis of Reconfigurable Intelligent Surface-Assisted Underwater Wireless Optical Communication Systems". In: *IEEE Photonics Journal* (2024) (cit. on p. 9).

[21] A. Wibisono et al. "An Autonomous Underwater Vehicle Navigation Technique for Inspection and Data Acquisition in UWSNs". In: *IEEE Access* (2024) (cit. on p. 9).

[22] G. K. Pandey et al. "UAV-Assisted Communications With RF Energy Harvesting: A Comprehensive Survey". In: *IEEE Communications Surveys & Tutorials* (2024) (cit. on p. 9).

[23] R. S. Allison et al. "Airborne optical and thermal remote sensing for wildfire detection and monitoring". In: *Sensors* 16.8 (2016), p. 1310 (cit. on p. 9).

[24] L. Zhu et al. "3-D beamforming for flexible coverage in millimeter-wave UAV communications". In: *IEEE Wireless Communications Letters* 8.3 (2019), pp. 837–840 (cit. on p. 10).

[25] P. Yi et al. "3-D Positioning and Resource Allocation for Multi-UAV Base Stations Under Blockage-Aware Channel Model". In: *IEEE Transactions on Wireless Communications* (2023) (cit. on p. 10).

[26] L. Zhu et al. “Multi-UAV aided millimeter-wave networks: Positioning, clustering, and beamforming”. In: *IEEE Transactions on Wireless Communications* 21.7 (2021), pp. 4637–4653 (cit. on p. 10).

[27] L. Zhu et al. “Millimeter-wave full-duplex UAV relay: Joint positioning, beamforming, and power control”. In: *IEEE Journal on Selected Areas in Communications* 38.9 (2020), pp. 2057–2073 (cit. on p. 10).

[28] P. Liu et al. “MI-Based Cross-Medium Communication for Multi-Auv-Assisted Underwater Data Acquisition”. In: *2024 IEEE 99th Vehicular Technology Conference (VTC2024-Spring)*. IEEE. 2024, pp. 1–6 (cit. on p. 10).

[29] X. Wang, Y. Guo, and Y. Gao. “Unmanned Autonomous Intelligent System in 6G Non-Terrestrial Network”. In: *Information* 15.1 (2024), p. 38 (cit. on p. 10).

[30] H. Kaushal and G. Kaddoum. “Underwater optical wireless communication”. In: *IEEE access* 4 (2016), pp. 1518–1547 (cit. on p. 11).

[31] R. Miglani and J. S. Malhotra. “Performance enhancement of high-capacity coherent DWDM free-space optical communication link using digital signal processing”. In: *Photonic Network Communications* 38 (2019), pp. 326–342 (cit. on pp. 11, 58).

[32] A. A. Farid and S. Hranilovic. “Outage capacity optimization for free-space optical links with pointing errors”. In: *Journal of Lightwave technology* 25.7 (2007), pp. 1702–1710 (cit. on pp. 12, 13, 20, 35).

[33] M. Elamassie and M. Uysal. “Performance characterization of vertical underwater VLC links in the presence of turbulence”. In: *2018 11th International Symposium on Communication Systems, Networks & Digital Signal Processing (CSNDSP)*. IEEE. 2018, pp. 1–6 (cit. on pp. 12, 39).

[34] M. Elamassie and M. Uysal. “Vertical underwater VLC links over cascaded gamma-gamma turbulence channels with pointing errors”. In: *2019 IEEE International Black Sea Conference on Communications and Networking (BlackSeaCom)*. IEEE. 2019, pp. 1–5 (cit. on pp. 12, 17, 19–21, 50).

[35] M. Elamassie, S. M. Sait, and M. Uysal. “Underwater visible light communications in cascaded Gamma-Gamma turbulence”. In: *2018 IEEE Globecom Workshops (GC Wkshps)*. IEEE. 2018, pp. 1–6 (cit. on pp. 12, 13, 21, 50).

[36] G. K. Varotsos et al. “DF relayed FSO communication systems with time dispersion over Gamma Gamma turbulence and misalignment”. In: *2017 6th International Conference on Modern Circuits and Systems Technologies (MOCAST)*. IEEE. 2017, pp. 1–4 (cit. on p. 13).

[37] T. G. Waduge, B.-C. Seet, and K. Vopel. “Modeling Ambient Light in Stratified Waters for Underwater Optical Wireless Communication”. In: *2024 IEEE 99th Vehicular Technology Conference (VTC2024-Spring)*. IEEE. 2024, pp. 1–6 (cit. on p. 14).

[38] N. Saeed et al. “Underwater optical wireless communications, networking, and localization: A survey”. In: *Ad Hoc Networks* 94 (2019), p. 101935 (cit. on pp. 14, 45).

[39] S. Khan, M. Usman, and S. Ali. "Perspective on light-fidelity and visible light communication". In: *Journal of Laser Applications* 34.1 (2022), p. 011202 (cit. on p. 14).

[40] A. M. Ibrahimy et al. "Performance of Underwater Audio Transmission Based on Underwater Visible Light Communication (UVLC)." In: *Engineering Letters* 30.1 (2022) (cit. on p. 14).

[41] C. Chen. "Special Issue on "Visible Light Communication (VLC)"". In: *Photonics*. Vol. 9. 5. MDPI. 2022, p. 284 (cit. on p. 14).

[42] A. Gunasekar et al. "All-Optical UAV-Based Triple-Hop FSO-FSO-VLC Cooperative System for High-Speed Broadband Internet Access in High-Speed Trains". In: *IEEE Access* (2023) (cit. on p. 14).

[43] S. Arya and Y. H. Chung. "A Comprehensive Survey on Optical Scattering Communications: Current Research, New Trends, and Future Vision". In: *IEEE Communications Surveys & Tutorials* (2023) (cit. on p. 15).

[44] S. Javaid et al. "Communication and control in collaborative UAVs: Recent advances and future trends". In: *IEEE Transactions on Intelligent Transportation Systems* 24.6 (2023), pp. 5719–5739 (cit. on p. 15).

[45] A. Alshehry and I. Darwazeh. "Harmonic Suppression for Electro-Optic Communication Systems". In: *2024 IEEE 30th International Conference on Telecommunications (ICT)*. IEEE. 2024, pp. 1–5 (cit. on p. 15).

[46] M. Ismail et al. "Line-of-Sight-Based Coordinated Channel Resource Allocation Management in UAV-Assisted Vehicular Ad Hoc Networks". In: *IEEE Access* (2024) (cit. on p. 15).

[47] M. Elamassie, F. Miramirkhani, and M. Uysal. "Channel modeling and performance characterization of underwater visible light communications". In: *2018 IEEE International Conference on Communications Workshops (ICC Workshops)*. IEEE. 2018, pp. 1–5 (cit. on pp. 17, 19, 58).

[48] M. Furqan Ali et al. "Selection Relay-Based RF-VLC Underwater Communication System". In: *Machine Learning, Deep Learning and Computational Intelligence for Wireless Communication*. Springer, 2021, pp. 177–192 (cit. on p. 17).

[49] C. Wang, H.-Y. Yu, and Y.-J. Zhu. "A long distance underwater visible light communication system with single photon avalanche diode". In: *IEEE Photonics Journal* 8.5 (2016), pp. 1–11 (cit. on p. 17).

[50] M. V. Jamali et al. "Statistical studies of fading in underwater wireless optical channels in the presence of air bubble, temperature, and salinity random variations". In: *IEEE Transactions on Communications* 66.10 (2018), pp. 4706–4723 (cit. on p. 17).

[51] M. Shin, K.-H. Park, and M.-S. Alouini. "Statistical modeling of the impact of underwater bubbles on an optical wireless channel". In: *IEEE Open Journal of the Communications Society* 1 (2020), pp. 808–818 (cit. on p. 17).

[52] M. Elamassie and M. Uysal. "Vertical underwater visible light communication links: Channel modeling and performance analysis". In: *IEEE Transactions on Wireless Communications* 19.10 (2020), pp. 6948–6959 (cit. on p. 19).

[53] R. Bansal. *A textbook of fluid mechanics and hydraulic machines*. Laxmi publications, 2004 (cit. on p. 20).

[54] Y. Baykal, M. C. Gökçe, and Y. Ata. "Anisotropy effect on performance of subcarrier intensity modulated binary phase shift keying optical wireless communication links in weakly turbulent underwater channel". In: *Journal of Modern Optics* 66.19 (2019), pp. 1871–1875 (cit. on p. 21).

[55] F. Roquet et al. "Accurate polynomial expressions for the density and specific volume of seawater using the TEOS-10 standard". In: *Ocean Modelling* 90 (2015), pp. 29–43 (cit. on p. 22).

[56] W. Mathematica. "http://functions.wolfram.com/01.06.02.0001.01". In: *online* (Online Available in September 2023) (cit. on pp. 24, 36, 39, 48–50, 60–62, 86, 88).

[57] M. O. Hasna and M.-S. Alouini. "Outage probability of multihop transmission over Nakagami fading channels". In: *IEEE Communications Letters* 7.5 (2003), pp. 216–218 (cit. on p. 35).

[58] M. F. Ali et al. "Dual-Hop Mixed FSO-VLC Underwater Wireless Communication Link". In: *IEEE Transactions on Network and Service Management* (2022) (cit. on pp. 36, 59).

[59] K. O. Odeyemi, P. A. Owolawi, and O. O. Olakanmi. "Performance analysis of reconfigurable intelligent surface assisted underwater optical communication system". In: *Progress In Electromagnetics Research M* 98 (2020), pp. 101–111 (cit. on p. 37).

[60] I. S. Ansari et al. "A new formula for the BER of binary modulations with dual-branch selection over generalized-K composite fading channels". In: *IEEE Transactions on Communications* 59.10 (2011), pp. 2654–2658 (cit. on pp. 39, 49, 85, 86).

[61] H. Lei et al. "Performance analysis of dual-hop RF-UWOC systems". In: *IEEE photonics journal* 12.2 (2020), pp. 1–15 (cit. on p. 39).

[62] S. Yahia et al. "A Survey of Channel Modeling Techniques for Visible Light Communications". In: *Journal of Network and Computer Applications* 194 (2021), p. 103206 (cit. on p. 45).

[63] T. V. Nguyen et al. "Link availability of satellite-based FSO communications in the presence of clouds and turbulence". In: *IEICE Communications Express* 10.5 (2021), pp. 206–211 (cit. on p. 45).

[64] F. A. Miranda et al. "An overview of key optical communications technologies under development at the NASA Glenn Research Center". In: *Optical Interconnects XXI* 11692 (2021), pp. 130–144 (cit. on p. 45).

[65] S. A. H. Mohsan and H. Amjad. "A comprehensive survey on hybrid wireless networks: practical considerations, challenges, applications and research directions". In: *Optical and Quantum Electronics* 53.9 (2021), pp. 1–56 (cit. on p. 45).

[66] M. F. Ali, D. N. K. Jayakody, and Y. Li. "Recent Trends in Underwater Visible Light Communication (UVLC) Systems". In: *IEEE Access* 10 (2022), pp. 22169–22225 (cit. on p. 45).

[67] I. S. Ansari, F. Yilmaz, and M.-S. Alouini. "Impact of pointing errors on the performance of mixed RF/FSO dual-hop transmission systems". In: *IEEE Wireless Communications Letters* 2.3 (2013), pp. 351–354 (cit. on p. 47).

[68] V. Adamchik and O. Marichev. "The algorithm for calculating integrals of hypergeometric type functions and its realization in REDUCE system". In: *Proceedings of the international symposium on Symbolic and algebraic computation*. ACM. 1990, pp. 212–224 (cit. on p. 48).

[69] Z. Liao et al. "Physical layer security for dual-hop VLC/RF communication systems". In: *IEEE Communications Letters* 22.12 (2018), pp. 2603–2606 (cit. on p. 48).

[70] M. Shah. "On generalizations of some results and their applications". In: *Collectanea Mathematica* (1973), pp. 249–266 (cit. on pp. 49, 85).

[71] B. Sharma and R. Abiodun. "Generating function for generalized function of two variables". In: *Proceedings of the American Mathematical Society* 46.1 (1974), pp. 69–72 (cit. on pp. 49, 85).

[72] M. Aggarwal, P. Garg, and P. Puri. "Analysis of subcarrier intensity modulation-based optical wireless DF relaying over turbulence channels with path loss and pointing error impairments". In: *IET Communications* 8.17 (2014), pp. 3170–3178 (cit. on p. 58).

[73] E. Zedini, Y. Ata, and M.-S. Alouini. "Improving Performance of Integrated Ground-HAPS FSO Communication Links with MIMO Application". In: *IEEE Photonics Journal* (2024) (cit. on p. 59).

[74] M. N. Elahee and M. Faisal. "Performance Analysis of Terrestrial FSO Communication Under Typical Rain-Affected Environment of Bangladesh". In: *2024 International Conference on Advances in Computing, Communication, Electrical, and Smart Systems (iCACCESS), Dhaka, Bangladesh*. IEEE. 8–9 March, 2024, pp. 1–6 (cit. on p. 59).

[75] G. Xu et al. "Outage probability and average BER of UAV-assisted dual-hop FSO communication with amplify-and-forward relaying". In: *IEEE Transactions on Vehicular Technology* 72.7 (2023), pp. 8287–8302 (cit. on p. 59).

[76] Z. Xu, G. Xu, and Z. Zheng. "BER and channel capacity performance of an FSO communication system over atmospheric turbulence with different types of noise". In: *Sensors* 21.10 (2021), p. 3454 (cit. on p. 59).

[77] A. Lionis et al. "Supervised Machine Learning for Refractive Index Structure Parameter Modeling". In: *Quantum Beam Science* 7.2 (2023), p. 18 (cit. on p. 60).

[78] P. Meteosta The Weather's Record Keeper. "https://meteostat.net/en/place/pt/alfragide?s=08535&t=2023-07-22/2023-07-29". In: *online* (Online Available in July 2023) (cit. on p. 60).

[79] T. A. Tsiftsis et al. “Optical wireless links with spatial diversity over strong atmospheric turbulence channels”. In: *IEEE transactions on wireless communications* 8.2 (2009), pp. 951–957 (cit. on pp. 61, 88).

Appendix A

Proof of Lemmma A

According to Nikishov underwater optical turbulence UOT, the spatial power spectrum of turbulent fluctuation of the seawater refraction index is given as follows [18];

$$E_n(\kappa) = \frac{1}{4\pi\kappa^2\sqrt[3]{\epsilon\kappa^5}}\chi_n C_0\left[1 + C_1(\eta\kappa)^{2/3}\right]\phi(\kappa,\omega) \tag{A.1}$$

where the parameter $\phi(\kappa,\omega)$ is defined as;

$$\begin{aligned}\phi(\kappa,\omega) &= \frac{1}{\omega^2 - (1-d_r)\omega + d_r} \\ &\times\left(\omega^2\exp\left(\frac{-C_0\delta}{P_T C_1^2}\right) + d_r\exp\left(\frac{-C_0\delta}{P_S C_1^2}\right) - \omega(d_r+1)\exp\left(\frac{-C_0\delta}{2P_{TS}C_1^2}\right)\right)\end{aligned} \tag{A.2}$$

The Prandtl numbers for temperature and salinity in terms of kinematic viscosity ν and the molecular diffusivity of temperature (D_T) and salinity (D_S) are defined as $P_T = \nu/D_T$, and $P_S = \nu/D_S$. While, the δ coefficient is expressed as;

$$\delta = 1.5C_1^2(\kappa\eta)^{4/3} + C_1^3(\kappa\eta)^2 \tag{A.3}$$

However, the dissipation rate of mean-squared refractive index χ_T can be written as,

$$\chi_T = \alpha^2\chi_T + \beta^2\chi_S - 2\alpha\beta\chi_{TS} \tag{A.4}$$

The dissipation rate of mean-squared temperature χ_T, salinity χ_T, and correlation coefficient χ_{TS} are also given as;

$$\chi_T = K_T\left(\frac{dT_0}{dz}\right)^2 \tag{A.5}$$

$$\chi_S = K_S\left(\frac{dS_0}{dz}\right)^2 \tag{A.6}$$

$$\chi_{TS} = \frac{K_T + K_S}{2}\left(\frac{dT_0}{dz}\right)\left(\frac{dS_0}{dz}\right) \tag{A.7}$$

By using (A.5) and (A.6) further replacing in to (A.7), to obtain (A.8) as;

$$\chi_{TS} = \frac{1}{2}\left[\left(\frac{dS_0/ds}{dT_0/dz}\right)\chi_T + \left(\frac{dT_0/ds}{dS_0/dz}\right)\chi_S\right] \tag{A.8}$$

It is noteworthy that the relative strength of temperature and salinity fluctuation ω is depending on the temperature and salinity gradient as;

$$\omega = \frac{\alpha(dT_0/dz)}{\beta(dS_0/dz)} \tag{A.9}$$

To obtain the dissipation rate of mean-squared refractive index χ_T, replacing the diffusivity ratio $d_r = K_s/K_T$ in (A.5), (A.6), and (A.8), we obtain χ_T as follows;

$$\chi_n = \frac{\alpha^2\chi_T}{\omega^2}\left[\omega^2 - (1+d_r)\omega + d_r\right] \tag{A.10}$$

Further, replacing (A.2) and (A.10) into (A.1) through some mathematical manipulation, the fluctuation of the seawater refraction index obtains as;

$$\begin{aligned} E_n(\kappa) &= \frac{C_0}{4\pi\kappa^2}\left(\frac{\alpha^2\chi_T}{\omega^2\sqrt[3]{\epsilon\kappa^5}}\right)\left[1 + C_1\sqrt[3]{\kappa\eta}\right] \\ &\times\left(\omega^2\exp\left(A_T\delta\right) + d_r\exp\left(A_S\delta\right) - \omega(d_r+1)\exp\left(A_{TS}\delta\right)\right). \end{aligned} \tag{A.11}$$

For the spherical waves assumption the scintillation index (Rytov variance) can be calculated as [18] as;

$$\chi^2_{I_t^k} = 8\pi^2k_0^2d_0\int_0^1\int_0^\infty \kappa E_n(\kappa)\left\{1 - cos\left[\frac{d_0\kappa^2}{k_0}(\xi - \xi^2)\right]\right\}d\kappa d\xi \tag{A.12}$$

The final expression of Rytov variance could be written by replacing (A.11) into (A.12) as follows;

$$\begin{aligned} \chi^2_{I_t^k} &= \frac{2\pi^2k_0^2d_0C_0\alpha^2\chi_T}{\omega^2\sqrt[3]{\epsilon}}\int_0^1\int_0^\infty \frac{1}{\sqrt[3]{\kappa^8}}\left\{1 - cos\left[\frac{d_0\kappa^2}{k_0}(\xi - \xi^2)\right]\right\} \\ &\times 1 + C_1(\kappa\eta)^{\frac{2}{3}}]\left(\omega^2\exp(-A_T\delta) + d_r\exp(-A_S\delta) - \omega(d_r+1)\exp(-A_{TS}\delta)\right)d\kappa d\xi. \end{aligned} \tag{A.13}$$

Appendix B

Proof of Lemmma B

To formulate the EBGMGF for outage probability for the proposed system in (5.10), we use to follow the steps as mentioned in [60, 70, 71]. Firstly, we write the product of two CDFs into EBGMGF as in (B.1), where $S(\cdot)$ is denoted an EBGMGF as given in [60, Table I]. We could write $S(\cdot)$ function in G-Meijer function by utilizing (B.2). Furthermore, following the expressions in (B.1) and (B.2), we are formulated EBGMGF which is given by (B.3) as well as in (B.4).

$$\prod_{k=1}^{2} F_{\gamma_k} = F_{\gamma_{sr}}(\gamma_{sr}) F_{\gamma_{rd}}(\gamma_{rd}) = S\left[\begin{array}{c|c|c} \begin{bmatrix} 0,0 \\ 0,0 \end{bmatrix} & -,- & \left(\frac{B_{sr}\gamma_{th}}{\overline{\gamma}_{sr}}\right), \left(\frac{B_{rd}\gamma_{th}}{\overline{\gamma}_{rd}}\right) \\ \begin{pmatrix} 6,1 \\ 3,7 \end{pmatrix} & \phi_{sr}, \kappa_{sr} & \\ \begin{pmatrix} 6,1 \\ 3,7 \end{pmatrix} & \phi_{rd}, \kappa_{rd} & \end{array}\right] \tag{B.1}$$

$$\begin{aligned} S\begin{bmatrix} x \\ y \end{bmatrix} &\equiv S\left[x, y \middle| \begin{bmatrix} m_1, n_1 \\ p_1, q_1 \end{bmatrix} a_{p_1} \middle| \begin{pmatrix} m_2, n_2 \\ p_2, q_2 \end{pmatrix} c_{p_2} \middle| \begin{pmatrix} m_3, n_3 \\ p_3, q_3 \end{pmatrix} e_{p_3}\right] \\ &\equiv G^{m_1,0:m_2,n_2:m_3,n_3}_{p_1,q_1:p_2,q_2:p_3,q_3}\left[\begin{matrix} a_1, ..., a_{p_1} \\ b_1, ..., b_{q_1} \end{matrix} \middle| \begin{matrix} c_1, ..., c_{p_2} \\ d_1, ..., d_{q_2} \end{matrix} \middle| \begin{matrix} e_1, ..., e_{p_3} \\ f_1, ..., f_{q_3} \end{matrix} \middle| x, y\right] \end{aligned} \tag{B.2}$$

$$\begin{aligned} S\left[\begin{matrix} B_{sr}\left(\frac{\gamma_{th}}{\overline{\gamma}_{sr}}\right) \\ B_{sr}\left(\frac{\gamma_{th}}{\overline{\gamma}_{sr}}\right) \end{matrix} \middle| \begin{bmatrix} 0,0 \\ 0,0 \end{bmatrix} - \middle| \begin{pmatrix} 6,1 \\ 3,7 \end{pmatrix} \phi_{sr} \middle| \begin{pmatrix} 6,1 \\ 3,7 \end{pmatrix} \phi_{rd} \right] \\ \equiv G^{0,0:6,1:6,1}_{0,0:3,7:3,7}\left[\begin{matrix} - \\ - \end{matrix} \middle| \begin{matrix} \phi_{sr} \\ \kappa_{sr} \end{matrix} \middle| \begin{matrix} \phi_{rd} \\ \kappa_{rd} \end{matrix} \middle| \left(\frac{B_{sr}\gamma_{th}}{\overline{\gamma}_{sr}}\right), \left(\frac{B_{rd}\gamma_{th}}{\overline{\gamma}_{rd}}\right)\right] \end{aligned} \tag{B.3}$$

In (5.14), using [56, Eq. 07.34.21.0081.01] and replacing the values from (5.4), then we get (5.18). Furthermore the product of G-meijer function is solved by the representation of EBGMGF in [60] as follows,

$$\begin{aligned} S\begin{bmatrix} X \\ Y \end{bmatrix}\Bigg\| \begin{bmatrix} 0,0 \\ 0,0 \end{bmatrix} - \Bigg| \begin{pmatrix} 2,5 \\ 6,3 \end{pmatrix} \phi_{I_{sr}} \Bigg| \begin{pmatrix} 2,5 \\ 6,3 \end{pmatrix} \phi_{I_{rd}} \end{bmatrix} \\ \equiv G^{0,0:2,5:2,4J+1}_{0,0:6,3:4J+2,3} \begin{bmatrix} - \\ - \end{bmatrix} \Bigg| \begin{matrix} \phi_{I_{sr}} \\ \kappa_X \end{matrix} \Bigg| \begin{matrix} \phi_{I_{rd}} \\ \kappa_Y \end{matrix} \Bigg| X, Y \Bigg]. \end{aligned} \tag{B.4}$$

Additionally, the parameters X and Y are described as,

$$X = \left(\frac{16A^2 D\bar{\gamma}_{sr}}{P^2_{\alpha_{sr}\beta_{sr}}} \right),$$

$$Y = \left(A^2 C_{rd} D\bar{\gamma}_{rd} \right),$$

$$\kappa_X = \left[0, \frac{1}{2}, \frac{-\zeta_{sr}}{2} \right],$$

$$\kappa_Y = \left[0, \frac{1}{2}, \frac{-\zeta_{rd}}{2} \right].$$

Appendix C

Proof of Lemmma C

Plugin the instantaneous SNR $\gamma = \bar{\gamma} I^2$ in (6.6) in the terms of average SNR and further integrating for obtaining CDF and analytical outage performance of the system as follows;

$$P_{out} = Pr\{\gamma \leq \gamma_{th}\} = F_{\gamma}(\gamma_{th}) \tag{C.1}$$

$$f_{\gamma_k}(\gamma_{th}) = \frac{\prod_{k=1}^{K} \Phi_{(\alpha_k \beta_k)}}{2\sqrt{\gamma_{th}\overline{\mu}} \prod_{k=1}^{K} \Phi_{(\Gamma \alpha_k \Gamma \beta_k)}} G_{0,2K}^{2K,0} \left[\prod_{k=1}^{K} \Phi_{(\alpha_k \beta_k)} \sqrt{\frac{\gamma}{\overline{\mu}}} \middle| \begin{matrix} \cdots \\ (\alpha_1 - 1), \ldots (\alpha_k - 1), (\beta_1 - 1), \ldots (\beta_k - 1)_{nm} \end{matrix} \right]. \tag{C.2}$$

The variables Z_1, $Z_{\Gamma(\alpha)\Gamma(\beta)}$, χ_T, and $Z_{\alpha\beta}$ in (C.2) are used as follows;

$$Z_1 = 2^{\sum_{k=1}^{K} (\alpha_k + \beta_k) - 3K}, \quad \text{and} \quad \chi = \prod_{k=1}^{K} \Phi_{(\alpha_k \beta_k)}$$

$$Z_{\Gamma(\alpha)\Gamma(\beta)} = \prod_{k=1}^{K} \Phi_{(\Gamma \alpha_k \Gamma \beta_k)}, \quad \text{and} \quad Z_{\alpha\beta} = \prod_{k=1}^{K} \Phi_{\alpha_k \beta_k)}.$$

The BER of the IM/DD within the OOK scheme in the presence of perfect CSI, at the receiver end it is given as $P_{error} = P(1)_{e|0} + P(0)_{e|0}$. The parameters $P(1)$ and $P(0)$ are associated with the probabilities of transmitting bits as 1 and 0. Therefore, the symmetrical problem and the probabilities can be written as $P(0) = P(1) = 0.5$ or $P(e|1) = P(e|0)$. The error probability for conditional irradiance I_{nm} is given [79] as follows;

$$P(e|I_{nm}) = P(e|1, I_{nm}) = P(e|0, I_{nm}) = \frac{1}{2} erfc\left(\frac{\eta I_{nm}}{\sqrt{2N_0}}\right) \tag{C.3}$$

Therefore, the average BER can be written as follows;

$$\underbrace{\overline{BER}}_{MIMO} = \frac{1}{2}\int_0^{\infty} erfc\left(\frac{\eta I_{nm}}{\sqrt{2N_0}}\right) f_{I_{nm}} dI_{nm} \tag{C.4}$$

Furthermore, plugin the PDF from (C.2) as follows;

$$\underbrace{\overline{BER}}_{MIMO} = \frac{1}{2}\int_0^{\infty} f_{I_{t_k}}(I_{nm}) erfc\left(\sqrt{\frac{\overline{\mu}}{2(NM)^2}\sum_{m=1}^{M}\left(\sum_{n=1}^{N} I_{nm}\right)^2}\right) dI_{nm}. \tag{C.5}$$

However, the above integration is complex to integrate. Therefore, utilizing the properties of the G-Meijer function from integral table [56, p. 07.34.21.0013.01], we obtain the final closed-form expression for BER as follows;

$$\underbrace{\overline{BER}}_{MIMO} = \frac{2^{\sum_{k=1}^{K}(\alpha_k+\beta_k)-2}}{Z_{\Gamma(\alpha)\Gamma(\beta)}\pi^{\left(\frac{2K+1}{2}\right)}} G_{4K+1,2}^{2,4K}\left[\frac{2^{4K-1}\mu}{(Z_{\alpha\beta}NM)^2}\middle| \begin{matrix}\Psi, 1\\ 0, \frac{1}{2}\end{matrix}\right]. \tag{C.6}$$